NODE LOCALIZATION VIA ANALYZING MULTI-PATH SIGNALS IN ULTRASONIC SENSOR NETWORKS

By

William J. Tomlinson Jr.

A THESIS

Submitted to
Michigan State University
in partial fulfillment of the requirements
for the degree of

Electrical Engineering – Master of Science

2013

ABSTRACT

NODE LOCALIZATION VIA ANALYZING MULTI-PATH SIGNALS IN ULTRASONIC SENSOR NETWORKS

By

William J. Tomlinson Jr.

This thesis proposes a novel signal analysis based node localization strategy for sensor networks used in structural health monitoring (SHM) applications. The key idea is to analyze location-dependent multipath signal patterns in inter-node ultrasonic signals, and use machine-learning mechanisms to detect such patterns for accurate node localization on metal substrates on target structures. Majority of the traditional mechanisms rely on radio based Time Delay of Arrival (TDOA), coupled with multilateration, and multiple reference nodes. The proposed mechanism attempts to solve the localization problem in an ultrasonic sensor network (USN), avoiding the use of multiple reference beacon nodes. Instead, it relies on signal analysis and multipath signature classification from a single reference node that periodically transmits ultrasonic localization beacons. The approach relies on a key observation that the ultrasonic signal received at any point on the structure from the reference node, is a superposition of the signals received on the direct path and through all possible multi-paths. It is hypothesized that if the location of the reference node and the substrate properties are known a-priori, it should be possible to train a receiver (source node), to identify its own location by observing the exact signature of the received signal. To validate this hypothesis, steps were taken to develop a TI MSP430 based module for implementing a run-time system from a proposed architecture. Through extensive experimentation within an USN on the 2024 Aluminum substrate, it was demonstrated that localization accuracies up to 92% were achieved in the presence of varying spatial resolutions.

In Loving Memory of:

Arthur P. Thomas II
Kenneth D. Thomas
Joe C. Tomlinson
Laurine E. Thomas
And
Martella A. Tomlinson

For all of their positive values instilled

ACKNOWLEDGEMENTS

I would like to grant a special thank you to all of those involved throughout the process of completing my Master of Science Degree. I would first like to thank my advisor, Dr. Subir K. Biswas for all of his invested time, resources, effort and motivational push, which contributed to nurturing me to become a better researcher, graduate student and professional. Secondly, I would like thank my lab mates, Bo Dong and Stephan Lorenz for their constructive feedback, input and technical expertise provided during the multiple implementation phases of this thesis. Additionally, I would like to thank Dr. Percy Pierre and those involved within the Sloan Program for their guidance and support in giving me the opportunity to attend graduate school at Michigan State University. A special thank you also goes to my family and friends, specifically my parents, William and Karen for their continuous love and encouragement, and my sister Telecia, for inspiring me to set a positive example for her to follow. Lastly, but certainly not least, a very heartfelt thank you goes out to Kego Chima-Emenyonu for putting up with my crazy schedule and work habits, and never leaving my side during the process; for that I love her dearly.

TABLE OF CONTENTS

LIST OF TABLES

LIST OF FIGURES

CHAPTER 1: INTRODUCTION

Determining the location of an entity holds usefulness in many applications. To cope with the increasing number of possible applications that exist, a wide variety of localization techniques have been developed to meet these demands. Today, technology has afforded society with the opportunity to make use of localization in areas that include, but are not limited to health care, non-destructive evaluation (NDE) and even human and animal tracking. This thesis introduces another form of localization in an ultrasonic sensor network (USN), by adopting a system similar to [1], in which an energy efficient ultrasonic pulse based WSN is used for binary information exchange. By utilizing ultrasound and propagation of mechanical carrier waves (lamb waves) in substrates, a 2024 aluminum plate has been chosen as the medium in which the waves will propagate. With the addition of an intelligent ultrasound pulse transmitter and receiver system, it is possible to create energy efficient and accurate system of ultrasound localization, using the geometry of the aluminum plate in a cell based distribution.

1.1. Traditional Localization

The most common forms of localization invoke the principles of received signal strength intensity (RSSI), time of arrival (TOA), time difference of arrival (TDOA), and angle of arrival (AOA). RSSI takes advantage of the attenuation that occurs when the signal from the transmitting node to the receiving node propagates through the medium being utilized. Empirical mathematical formulas are modeled according to signal propagation and localization environment in order to calculate the distance between the transmitting node and receiving node. Deemed as ranged based location estimation techniques, TOA and TDOA have been known to yield the best accuracy in terms of positioning in a 2D or 3D localization environment [2]. These techniques are based on the measurement of the difference in distance between the nodes within a localization environment. TOA uses the time delay introduced when a signal travels from a reference node (known location) to the source node (unknown location), relying on the speed of the signal to assist in providing a distance measurement. TDOA uses two different types of signals and calculates the difference in each signal's arrival time in order to calculate the distance between reference and source node. The use of these two methods implies that an accurate timing mechanism needs to be present in order for accurate estimation to be achieved. In order to ensure proper functionality of TOA and TDOA methods, a minimum of two reference nodes (TOA) and a minimum of three reference nodes (TDOA) are required in order to estimate the location of at least one source node within the localization environment. Angle of arrival based localization techniques allow the reference nodes to have the competences needed to measure the angle of arrival based on information obtained during the localization process. Directional antennas are commonly used to facilitate the process of direction finding and angle measurement. In conjunction with the difference of the arrival times of an incoming signal, a known geometry of antenna arrays is responsible for determining the angle information needed to provide accurate localization results. These different forms of localization invoke commonly known positioning algorithms to perform reliable localization. Trilateration of a source node is based upon the physical coordinates of the reference nodes and each of their respective distances from the source node. The Euclidean distance equation is the most common method used in trilateration algorithms. Triangulation, another frequently used positioning algorithm, can only be implemented where AOA measurements are available. The position of the source node is determined by the intersection of several pairs of angled direction lines [3].

1.2. Localization Application

A wide variety of applications are available if accurate localization is realized. Some of these applications even have capability to enhance the long-term quality of human life. Recent research has afforded society with the opportunities to make use of various structures that are interacted with on a daily basis. Such structures include but are not limited to aircrafts, bridges and buildings. With these structures, comes the need to monitor their physical condition and make repair under situations where the structures performance is questionable. Current research in the realm of Structural Health Monitoring (SHM), an area of Non-Destructive Evaluation (NDE), has made this evaluation process simpler by introducing wireless sensor networks (WSN), which have the capability to perform advanced data acquisition techniques in respect to any structure, in order to diagnose damage over a long period of time. Due to the usefulness' of WSNs, the physical integrity of a structure can now be determined without any external breaking or tapping into its internal infrastructure. Many important aspects of the damage diagnosing need to be assessed. One of which includes localizing the position of damage in the form of structural faults. In order for wireless sensor networks to achieve such a goal, other factors in addition to performing accurate position estimation need to be taken into consideration [4]. The sensor networks need to be able to send data and communicate reliably, operate efficiently under limited amounts of battery power, be equipped with sufficient computational capability and even be somewhat resistant to information being compromised.

1.3. Limitations of Traditional Localization in the context of WSN

Localization limitations are highly dependent upon the context in which localization is sought to be achieved. In respect to WSNs, numerous factors need to be taken into account in order to ensure optimal performance of a specific localization application.

1.3.1. Time Synchronization

Localization techniques that utilize time of flight and/or time of arrival techniques require a heavy demand of reliable clock synchronization [3]. Without accurate timing information, the distance between reference node and source node cannot be determined. By calculating the round trip time between reference node and source node, this issue can be mitigated. However there exists an underlying cost of potentially losing localization precision, as well as adding additional communication overhead.

1.3.2. Computational Complexity

Each node within a localization environment, whether its position is known or unknown, must be able to process and store a certain amount of data. In traditional localization, time measurements, distance parameters (known locations and estimations) have to be stored, in addition to the algorithm being used to perform the localization. Depending on the complexity of the application and the amount of data to be processed, real-time localization can be infeasible when dealing large amounts of data and large network topologies.

1.3.3. Presence of Reference Nodes

Without the presence of reference nodes, the most commonly used position estimation algorithms become infeasible to implement. Ignoring the use of reference nodes limits the number of localization techniques accessible. RSSI do not make use of reference nodes but there are several factors that increase the complexity of localization when modeling the effects of signal attenuation during propagation [3]. Such factors include the number of obstacles present in the environment and the attenuation factors of each respective obstacle.

1.3.4. Security

Most localization schemes were not designed with security in mind. Localization methods that use radio communication are subject to even the most basic forms of network security attacks. A common attack such as eavesdropping, can easily compromise data within a localization network and unveil the location of important entities of interest.

1.4. Research Issues Addressed in this Thesis

Ultrasound localization yields many benefits in contrast to traditional radio and packet based forms of communication. Sound as a source for localization requires less elaborate techniques to drive its implementation, since sound is unable to interfere with other RF signals. Thus, in the context of performing ultrasound localization on an aluminum substrate, any means of ultrasound communication are not detectable outside the medium. This thesis also demonstrates that it is possible to estimate the position of an unknown source node without using traditional techniques mentioned in an earlier section of this work. The work introduced uses only one reference node and one source node, whose location is unknown. Taking advantage of the structural geometry of the 2024 aluminum plate, in conjunction with key properties of ultrasound communication, no time synchronization is required during the localization process. In fact, by using pattern classification techniques, multipath reflections (a feature normally deemed as problematic), are chosen to perform position estimation in a cell based distribution. The elimination of additional resources such as reference nodes, time synchronization and on-board data processing allows for this method to not only present a novel approach in position estimation, also reduces the complexity of the network and the overall energy consumption.

CHAPTER 2: RELATED WORK

This chapter provides a literature review of various signal processing and localization techniques that utilize ultrasound in relation to plate structures and indoor environments, ultrasound signal classification and even structural health monitoring. The work presented here will be useful in determining the best approach to ultrasound signal classification for the purpose of localization.

2.1. Localization in Plate Structures and Indoor Environments using Ultrasound

The work conducted in [5], involves the creation, experimentation and characterization of a wavenumber frequency-steerable acoustic transducer (WS-FSAT). This approach allows for directional acoustic waves to be generated and also enables the sensing of guided waves via simultaneous activation of large arrays of transducers that arranged in a particular fashion. The transducers are employed for applications in the realm of structural health monitoring. More specifically, the transducers are adopted for the purpose of localizing broadband acoustic events that correspond to the propagation of guided waves in plate structures. The latter is achieved by conducting a time-frequency analysis of the signal received by single and multiple sources through the use of a centralized measuring device. The plate structure under inspection is a .75 mm thick 6061 aluminum plate of size 915 mm x 915 mm. The diameter of the piezo-electric transducers (PZT) used to produce the guided waves is 5 mm in diameter. The location of the piezo-electric transducers are to be determined by the SMH apparatus. Single source imaging is first tested by activating a single PZT, out of the 17 bonded to the substrate of interest. The accuracy of the localization is determined by how well the method of computing the difference between the estimated energy maximum position and the actual location of each source is calculated. For single source imaging, results indicated that coordinate based localization error lies below 2 cm. Multisource imaging, or simultaneously activating two acoustic sources, can also have their locations distinguishable from one another. However, this result depends on the angular separation and distance between the two sources. Results also indicate that localization error shows an increase due to the coupling (coupling gel). Inconsistencies in coupling can attribute to an increase in noise levels and signal strength, ultimately effecting the capabilities of an imagining based localization system.

Parametric modeling and estimation of ultrasonic backscattering and echoes are analyzed in [6], providing significant advantages in terms of estimating parameters that require a high-resolution, such as time of arrival information. Acoustic waves are generated through pulse excitation, using piezo-electric transducers. Here, closely spaced and overlapping echoes that contain noise are modeled and represented by Gaussian Chirplet or Gaussian Echo. The echo models represented are generalized and from this generalization, an efficient supervised learning algorithm is fashioned in a way to estimate model parameters, subject to constraints known prior to its implementation. Results show that the Gaussian echo and Gaussian Chirplet models provide the ability to decompose signals in sparse conditions and will be likely to improve ultrasound based echo estimation techniques in the future, and likely to improve the performance of model-based ultrasonic echo estimation techniques.

Ultrasound Localization is also being utilized in 3-D environments, as seen by [7], where an indoor 3-D positioning system is proposed using a single source and reference node. It makes use of time-of-flight information and the characteristic that ultrasonic waves do not propagate through walls and other obstacles, as a means to remove the additional reference nodes. As a result, two methods are studied. The first method uses the reflections to its advantage, be leveraging them in a way to find the time-of-flight information in relation to the origin of the reflection. The second method, utilized an array of transducers used to produce the ultrasonic waves. The primary method that is deemed as related work involves the use of acoustic reflections. Three sounds are transmitted from the base station or reference node, one line of sight; the remaining two originate from a reflected source, such as a wall or the floor. However, before communication can begin, a thorough model of the acoustic channel has to be present. A room is chosen that takes on the shape of a box, allowing for consistent measuring of the acoustic reflections. From this model, a pattern of acoustic reflections, is created on a grid system for the layout of the room. A matching procedure known as signature matching is then used to compare all the observed patterns to the predicted patterns created. The best match is chosen and used to localize the source node's position. The accuracy of the position estimates ranges from 0.01 meters to 0.79 meters, depending on the mobile-device position (source node). A possible solution that is proposed as future work is a combination of the acoustic reflections method and the array method. This approach can mitigate both the line-of-sight path occlusion problem and the multiple-matches problem, thereby improving the accuracy of position estimates.

2.2. Classification of Ultrasound Signals

Ultrasonic signal classification was conducted on artificial insertion of defects on a composite substrate of carbon fiber and epoxy makeup in [8]. Numerous classification schemes were evaluated and assessed to determine which would yield the best performance in order to define an upper bound on the error rate achieved when ultrasound signals of similar visual appearance are processed. In the case of similar signals, the feature space chosen heavily impacts performance and problem complexity. Ultrasonic signals are excited at a center frequency of 5MHz and digitized with a sampling frequency of 100MHz A/D board. The composite substrate consists of 15 artificially inserted defects and 16 amplitude modulation scans were taken at each of the 15 defects. Each measurement consists of 2048 data points of signal measurement, including those of captured echoes. The signals captured, though originating from many different types of defects, appear similar in appearance. To reduce the amount of visual similarity, pre-processing in the form of the FFT and auto-correlation were applied to each ultrasound signal. From three domains, time, frequency and auto-correlation, many descriptors (features) were extracted. Using supervised learning as a training approach, conventional pattern recognition and classification algorithms were implemented to evaluate the usefulness of the descriptor values computed in the pre-processing stage. From this work it can be seen that representing a signal in a different form is a popular means of extracting useful information and that the use of signal processing to accomplish the goal of feature extraction is a useful tool in solving signal processing problems.

In [9], initial phases also include pre-processing an ultrasound signal, in an attempt to minimize the effects of noise and variation from experimental testing. Extracting informative features from the pre-processing stage gives the basis needed to solve complex classification problems with ultrasonic signals. Pre-processing in the form of time-scaling and normalization were used to map signals with different frequencies into a single reference frequency. The effect of such pre-processing resulted in either the stretching or compression of each signal. Expanding on the concept that the frequency component of a signal holds more useful information, which is easily distinguishable. As a result of such, the FFT coefficients of each ultrasonic signal are used as a feature. Both the magnitude and phase components are kept for analysis. Phase is deemed an important feature. When examining the entire duration of the ultrasound signal, the echoes that are present normally exhibit a change in phase. Therefore, the phase coefficients are also deemed an import feature and are used in classification. However, when using only FFT for analysis, timing information is loss and it is impossible to tell when an actual event took place in respect to how the signal may change. Therefore, the discrete wavelet transform (DWT) of the ultrasonic signals are also computed. It was concluded that using DWT as a feature, out performs the FFT and yields substantial data reduction, directly reducing the computation complexity during feature extraction.

2.3. Localization for Applications in SHM via Ultrasound

The research presented here focuses on using ultrasonic guided waves to perform structural health monitoring on various structures such as the skin of an aircraft wing. In the work presented in [10], inspection experimentation is conducted on an actual wing, composed of aluminum material and under the insertion of real defects. Preliminary testing and results were done to characterize the wave propagation on the aluminum substrate. A system is achieved to perform damage inspection (cracks, corrosions, etc.) via the use of monitoring the transmission and reception of guided waves, produced by piezo-electric transducers (PZT), placed in arrays throughout the surface of the aircraft wing. Collection of received ultrasonic waves under normal conditions (i.e., no faults), served as a baselines for comparing subsequent measurements under conditions where faults existed. By use of a novel correlation algorithm deemed RAPID (reconstruction algorithm for probabilistic inspection of defects), the presence of damage and its location can be determined with good performance. Analysis of cracks and corrosions using guided waves are produced by 8 PZT in the form of a circular array. The method of detecting a change in signal characteristics between an undamaged (reference signal) and damaged signal uses the basic concept of signal correlation. The signals collected after damage has taken place are compared with the reference signal, and their correlation coefficients are computed in addition to an estimate of their area of occurrence by use of the RAPID algorithm. Vv the wave propagation approach,

Additional work in this area also focusses on the propagation of ultrasonic waves, particularly broadband signals [11]. These signals that propagate through the structure of the material are suitable for detecting defects. The approximate whereabouts and harshness of an unknown defect is determined using a damage correlation index, which is derived from a frequency response function of the structure. This index becomes a metric whose value relies on the differences in the comparison between the undamaged structure and damaged structure. The method is applied to components consisting of a makeup which has aluminum beams and plates with reduced local stiffness. The experimental setup consists of several transducers to produce the broadband ultrasonic signals, operated at a center frequency of 5 MHz. Coupled with ultrasonic coupling gel, and combined with variable signal attenuators, the amplitude of the signal can be controlled up to an optimal point. Data is sampled at a high rate through a data acquisition device, to be used on a personal computer for post-processing. Composite plates are also evaluated under the same guidelines, but will not be discussed in detail. Another method, using vibrational data is used to provide information on existing defects, while the wave propagation method mentioned above is more suitable for determining smaller defects and discovering their location. Within this work however, a major limitation exists in the form of the localization accuracy, a drawback that is deemed to be handled in future research.

In this work, [12], a steel cantilever beam is used to study damage detection that is simulated through the use of smart sensor networks (128 nodes total), lumping mass to particular node in the network. The Damage Location Assurance Criterion (DLAC) methodology based on previous work cited in this paper was selected as the foundation of SHM monitoring algorithms used in this work as well as others. This, correlation-based health monitoring technique is used to compute a direct correlation between experimental and analytical test cases, attempting to evaluate the validity of the latter mentioned item. With the addition of the spatially quantized surface area of the beam, the reduction of the near infinite degrees of freedom on the surface of the beam is mapped to finite degrees of freedom. This change does not significantly alter the performance for localization, and removes the sensitivity of the original method of the DLAC operations. Ultimately, the work presented here deems it possible for sensor networks to be capable of implementing a system of localization of material defects even in the presence of their limited resources. Future work includes transitioning from an offline model to an online model, making use of an experimental lab setting.

.

CHAPTER 3: PROBLEM FORMULATION

In this chapter, the framework for implementing ultrasound node localization on a metal substrate is introduced. Localization is achieved by taking advantage of the multipath reflections generated by the physical substrate boundaries to classify the node's location based on a cellular distribution of the aluminum plate structure.

3.1. Motivation

The use of localization in wireless sensor networks is an important piece in their overall functionality of localization in ultrasonic sensor networks. The ability to have an awareness of the position of all nodes, or simply one node present, can yield great benefits across many diverse applications. Many methods of communication are also used to facilitate a process of localizing the unknown position of a node. Common methods utilize radio, light and acoustics to perform localization. Acoustic localization makes use of such techniques as beamforming and time-delay estimation to achieve desirable results in terms of accuracy and precision [13]. Localization can also be achievable in many different environments, through many different mediums, in which a signal must propagate. Sonar, a common and widely used form of acoustic localization, uses water as a medium in many applications. Recently, there have been numerous works done with plate structures, where substrates of many single and multiple materials such as aluminum and carbon fiber reinforced plastic, are used as mediums to achieve some form of localization [14-15]. This form of substrate localization, in conjunction with using acoustics as the method of communication, has many advantageous methods over traditional localization. Therefore, the purpose of this work is to implement a system of ultrasound node localization that is capable of accurately estimating the position of a node without the use the traditional methods that are commonly known.

3.2. Problem Formulation

3.2.1. Substrate geometry

The problem formulation first begins with defining the environment for which localization will take place. The environmental factors play a heavy role in the way ultrasonic signals behave and propagate in the form of lamb waves [16]. For example, the plate thickness is one parameter that dictates how the many modes of the signal are generated. In addition to this, the physical boundaries and properties of any plate structure will also cause multi-path reflections to occur. In this thesis, 2024 aluminum (material commonly used in aircraft skin construction) is used with a thickness of 1mm, and a length and width of 3.6m and 1.2m respectively.

3.2.2. Ultrasound communication link

In order to transmit ultrasonic waves and successfully receive them, a robust ultrasound communication link is formed on the surface of the aluminum medium. The receiver portion of this link shall act as the source node, while the transmitter shall be fixed in one position on the plate and act as a reference for ultrasound localization. The overall functionality of the transmitter and receiver will be explained in greater detail in a later section of this thesis. Figure 3-1 depicts the metal plate and the position of the transmitter that will be fixed throughout the course of this thesis. To fully utilize the effect of multipath reflections while creating a simple, energy efficient infrastructure for localization, an ultrasound communication link was created using one transmitter and receiver. All localization will be done in the presence of only these two entities.

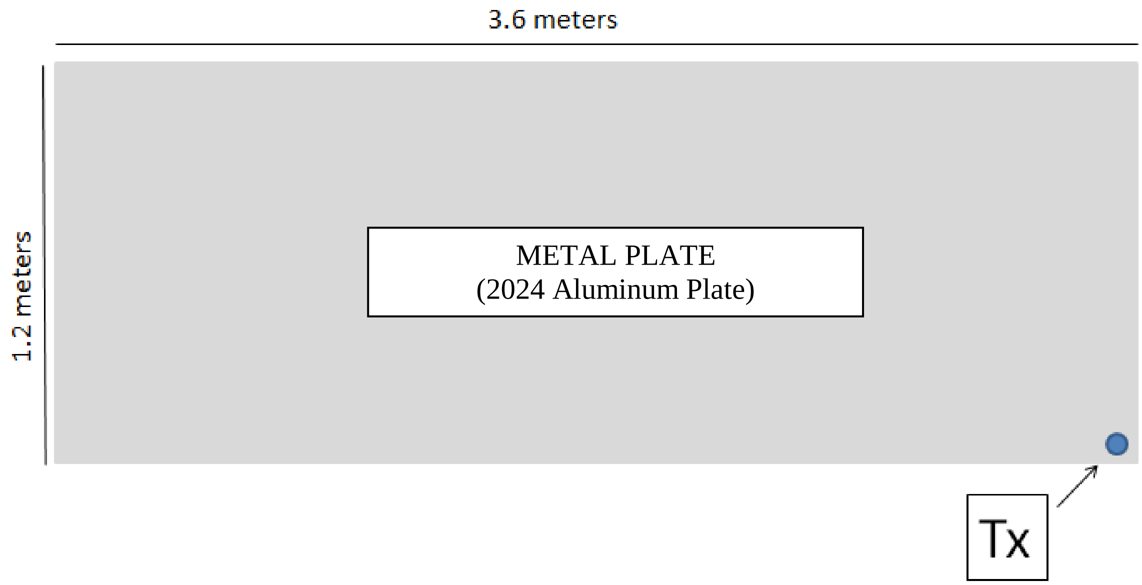

FIGURE 3-1: TRANSMITTER FIXED POSITION

For interpretation of the references to color in this and all other figures, the reader is referred to the electronic version of this thesis.

3.2.3. Multipath Reflections

Examining the characteristics of the raw signal received through ultrasound transmission, certain observations were discovered that can be used to create a localization framework using the appearance of multipath reflections that exist in every signal measured. In the work done by [1], multipath reflections were not of interest. The dominant lamb wave modes, Symmetric (S) and Asymmetric (A) modes are the only parts of the signal that carry useful information in the form of such parameters as wave velocity and wave dispersion. Based on the dispersion curve diagrams for the aluminum plate [17], it can be determined that the frequency at which the ultrasound is transmitted (245 kHz), and the thickness of the plate, allow for only the first incident of the S and A waves to propagate [18]. For the analysis in this thesis, these waves will use the notation S0 and A0 wave. Further examination, has led to the conclusion that the patterns of multipath reflections at random positions on the aluminum plate, yielded an almost unique multipath spread from a visual prospective. Figure 3-2 shows a raw received signal, how the multipath reflections appear, and distinguishes the S0 and A0 wave from the rest of the signal.

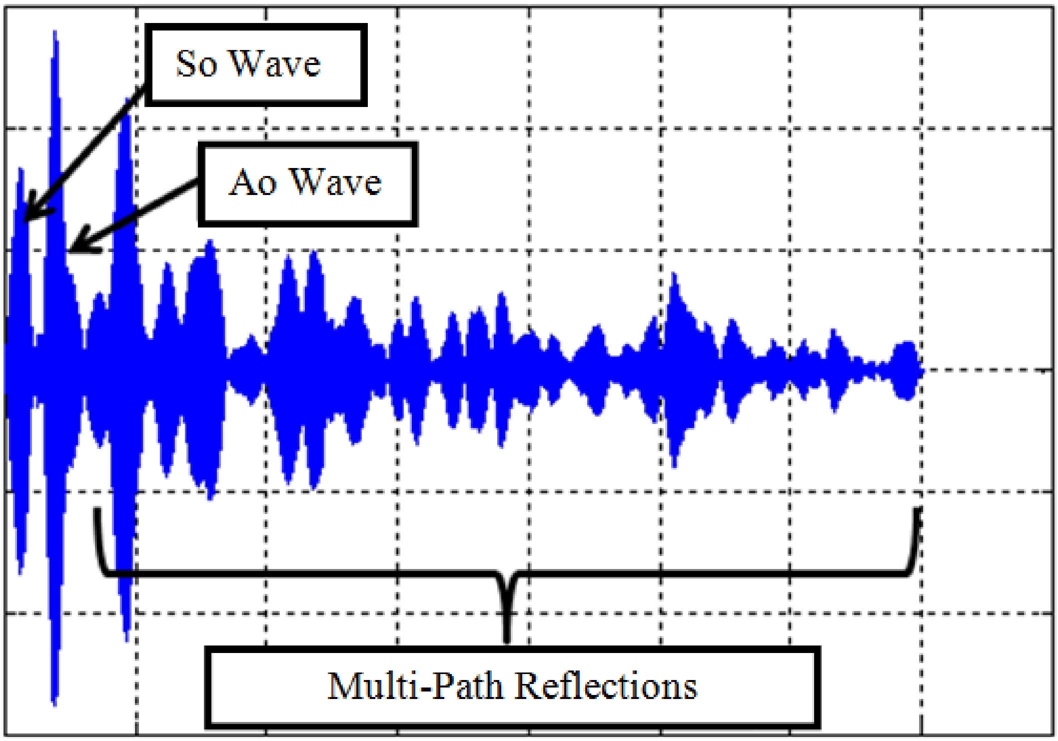

FIGURE 3-2: MULTIPATH REFLECTIONS

3.2.4. Signal Differentiation

Visually noting that a direct correlation existed between changes in the location on the plate and the raw signal observed, prompted a brief study to verify this concept. A zinc plate (Length: 457.2mm, Width: 304.8 mm, Thickness: 1mm) is used to observed the raw received signal at 6 random positions on its surface, using the same ultrasound communication link developed for the experiments that will be discussed later in this thesis. Figure 3-3 shows the layout of where each signal was visually noted and captured. Initial results show that even though it is difficult to find distinguishing factors in each signal, a clear difference does exist and can be exploited.

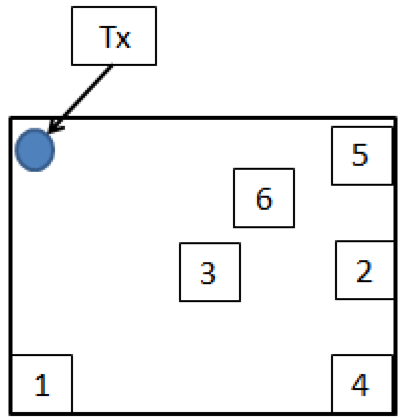

FIGURE 3-3: LOCATIONS OF RANDOM RAW RECEIVED SIGNAL OBSERVATIONS

3.2.5. Cell based localization

Attempting to characterize the entire behavior of the multipath present with the substrate to yield precise coordinate based localization was deemed too infeasible for achieving a localization system with the criteria that this thesis aims to meet .MATLAB software entitled SoundSim 2D Elastic Wave, was used to simulate the wave propagation for the substrate being used in this thesis. This script generated a simulation to help with visualizing the way lamb waves propagate with respect to an aluminum medium. It also allowed for the control of variables such as wave speed, plate dimension and transmitter location. Simulation results show that the lamb waves move all along the boundary positions of the plate and take no dedicated and precise path. However, preliminary studies done for the sake of this thesis have shown that the appearance of the raw signal is indeed location dependent. Thus, to be able to achieve control over the granularity of localization, the resolution of localization is mapped to a cell based distribution. Resolution of localization will be varied from low to high, increasing the number of cells, while also decreasing the area on the plate that each cell governs. Thus, the overall goal is to determine the correct cell location of the unknown node, whether the position lies in the cell center or near its boundary.

CHAPTER 4: EXPERIMENTAL SETUP

The purpose of this chapter is to describe in detail, the structure and setup used for the purpose of conducting experimental tests, in order to assess the potential methods needed to be able to identify the differences in raw received signals from cell to cell.

4.1. Ultrasound Receiver

To evaluate the lamb waves that propagate through the aluminum medium, a formal and consistent method of receiving the acoustic waves must be present. For the experimental portion of this thesis, a standalone piezo-electric transducer (PZT) disc from APC International (D-9.55mm-1.00mm-850 WFB) is used as a receiver. The general functionality of the PZT from a receiver perspective is as follows: (1) The lamb waves received create a mechanical vibration at the transducer; (2) The mechanical vibrations facilitate a process that coverts the mechanical waves into a readable voltage from the wires soldered to the PZT. It is also important to note that this PZT is the same model used in [1]. Results from this work indicate that the resonance frequency is approximately 245 kHz; therefore at this frequency, the PZT is most sensitive and has the ability to yield the highest received signal strength.

4.2. Ultrasound Transmitter

In order initiate the communication process using ultrasonic pulses, an ultrasonic transmitter is designed and implemented, and is used in conjunction with the Mica2 sensor platform. The transmitter designed is based strongly off of the work done in [1], with a few slight modifications. The Mica2 controls the transmitter's ability to inject ultrasonic pulses every 30 milliseconds into the medium using a PZT. From a transmitting perspective, the PZT functions in the following manner: (1) An induced voltage generates small mechanical vibrations at the transducer disc and (2) The mechanical vibrations produce the lamb waves that propagate through the medium for the signal to be detected by a receiving PZT. The interval in which pulses are sent plays an important role in the number of multipath reflections that may occur. If pulses are sent more frequently, more pulses occur and overlap with pulses from previous transmissions also occurs. In contrast to this, if pulses are sent too infrequently, fewer reflections exist and results may yield a signal lower with amplitude, resulting in less distinct peaks in the signal. Additionally, the entire transmitter is designed to function at 245 kHz, since the PZT has a resonance at roughly this frequency. The transmission voltage is kept constant at 6V, as opposed to the option to select 3V or 6V from the work presented in [1]. Transmission voltage is kept at a level of 6V in order to successfully reach the entire span of the aluminum plate (i.e., receive a signal strong enough to be detected). Figure 4-1 depicts a block diagram of the ultrasound transmitter.

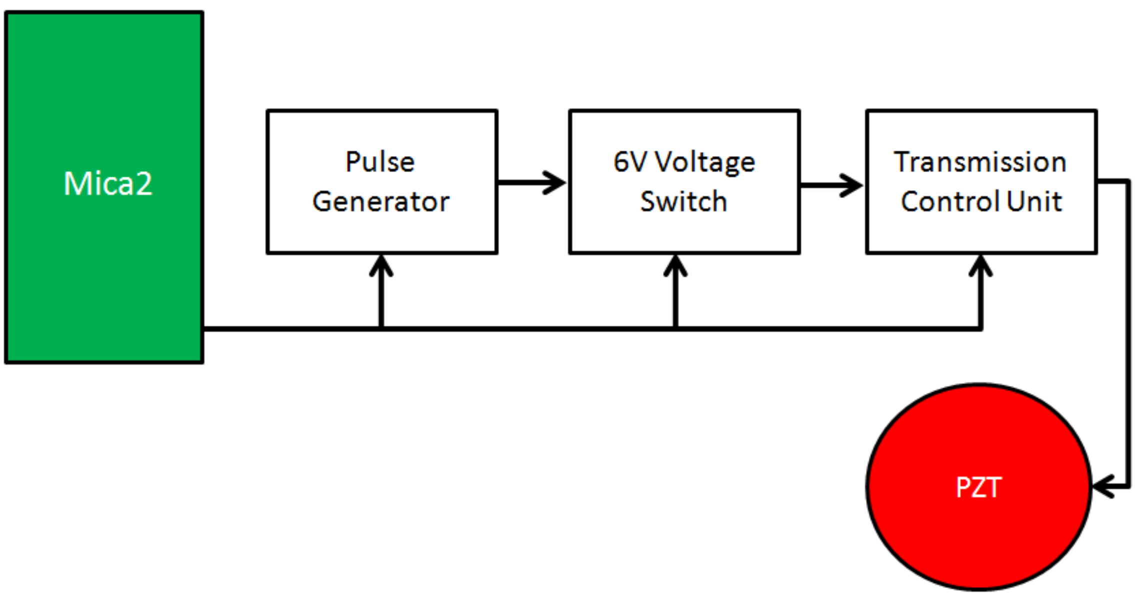

FIGURE 4-1: ULTRASOUND TRANSMITTER BLOCK DIAGRAM

4.3. Coupling

Coupling inconsistencies can have a huge impact on received signal strength. Many coupling methods exist in the form of thermo bonding tape, epoxy, coupling gel and more [19]. A coupling method was devised and tested in this thesis to ensure the most consistent data was obtained from the aluminum plate. Figure 4-2 depicts the design of the coupling method used. An earth disc magnet is bonded to the PZT using epoxy glue. The layer of glue forms an even layer that is attached to the magnet. This ensures that the soldering points from the wires attached to the PZT do not provide any unevenness when the magnet is placed on top of the PZT. A magnet of reverse polarity is attached to the opposite side of the plate, to allow the PZT to be fixed to the surface. Figure 4-3 shows the variability of coupling as a result of the method used in this thesis. Although results are pretty consistent, variability is clearly shown due to no waveform being completely overlapped by another.

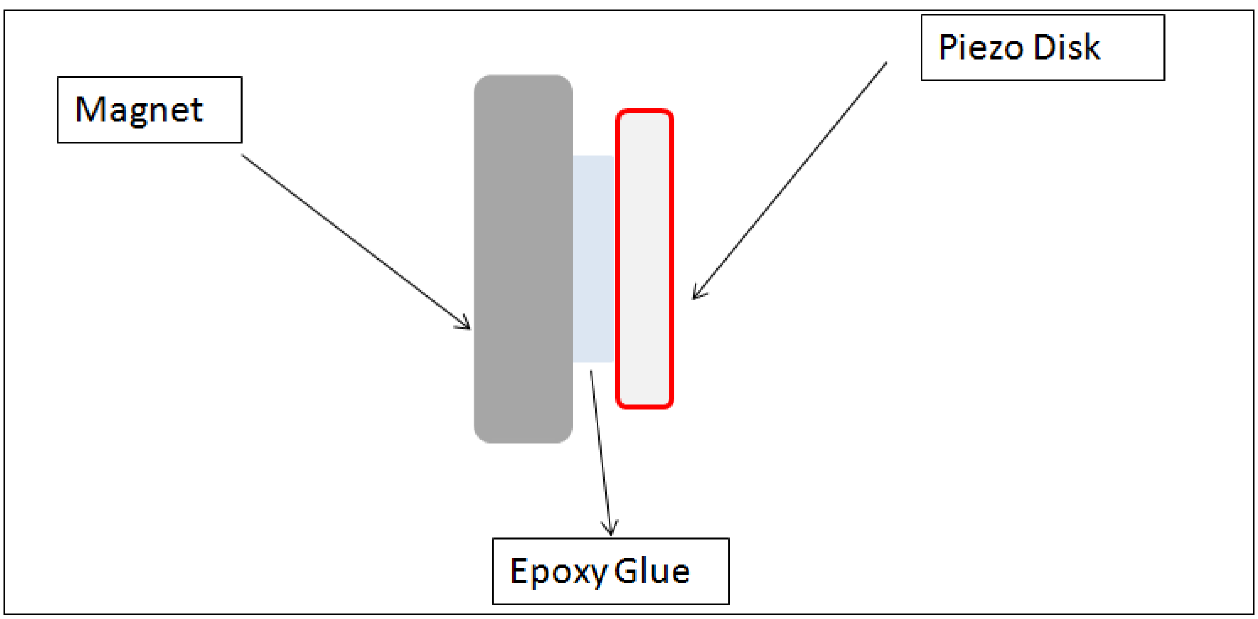

FIGURE 4-2: COUPLING CONFIGURATION USING A MAGNET BONDING APPROACH

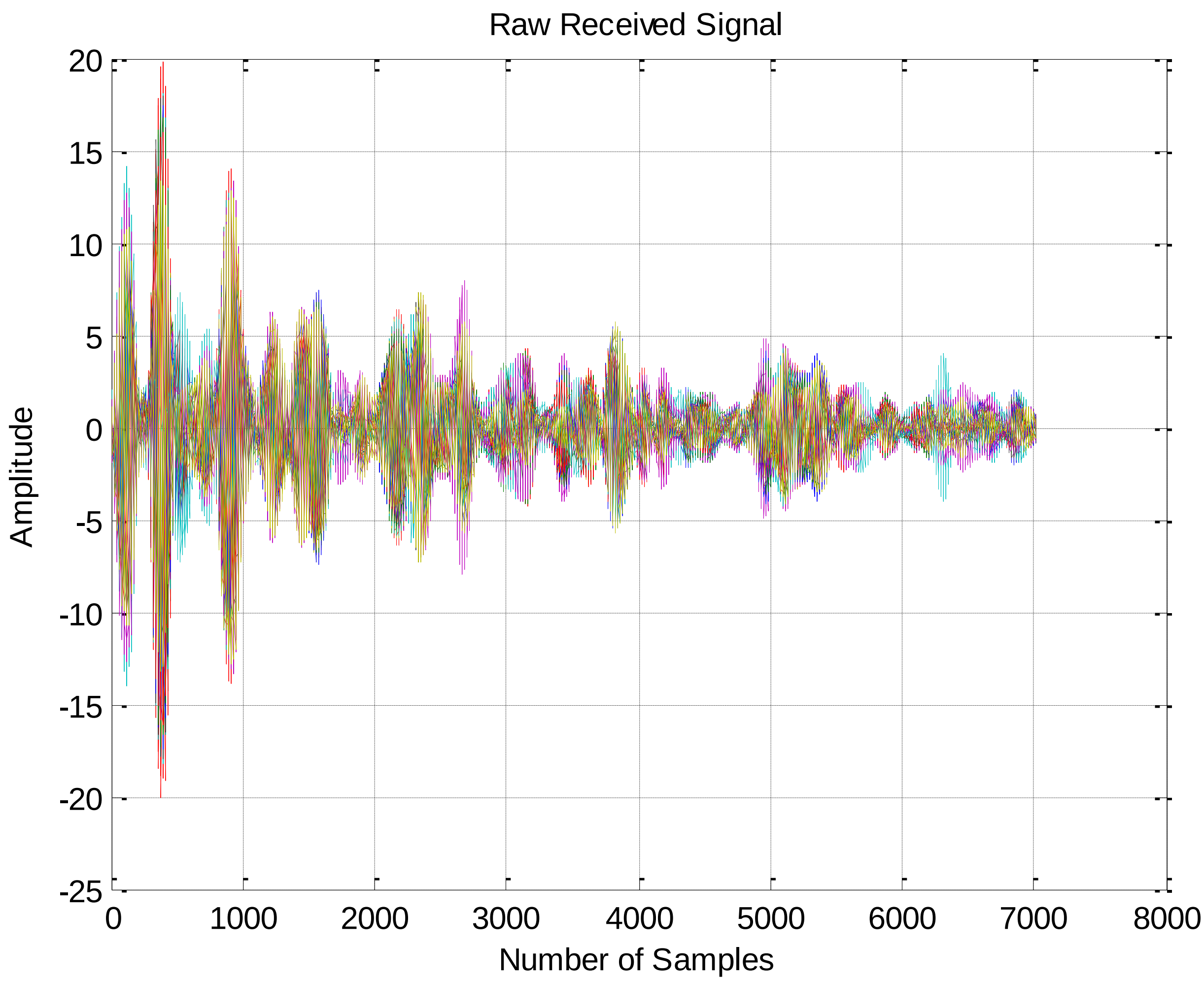

FIGURE 4-3: VARIABILITY IN COUPLING INSTANCES OF RECEIVED SIGNAL

4.4. Data Collection Method

In order to utilize pattern classification techniques, where training and testing data must be generated, a large amount of data must be collected as an initial stage. Therefore, data is collected from the aluminum plate using the Ultrasound transmitter to send the pulses and the stand alone PZT to observe the signal. To sample, view and collect data, the Picoscope 2204 version is used, which has a varying maximum sampling rate in the range of 50 to 100 Mega samples per second. In all experiments, data is sampled at a rate of 3.965 MHz. Proceeding the sampling and storing of a raw received signal, the PZT is re-coupled to the aluminum plate. This is done multiple times, in order to account for amount of viability mentioned in the previous section.

4.5. Cell Based Localization Resolution

As stated in Chapter 3, it is important to be able to determine how accurate of a localization resolution can be achieved. The aluminum plate has been divided into several cells, based on the limits of its physical dimensions. The cells will all be of equal size and the number of cells will vary from 3, to 12 to 24. Data collection of raw received signals will take place at the center of each cell, in addition to at least two positions that lie outside the center of each cell and lie close to the boundaries of another cell. Each cell centered measurement and non-centered location measurement will be a product of data collected from twenty coupling trials. The purpose of data collection outside the center is to be able to assess the amount of confusion that may exist when a position is close to a neighboring cell.

4.5.1. Center of Cell

Figures 4-4, 4-5 and 4-6 show depictions of 3, 12, and 24 cell distributions respectively. Analysis will be conducted in the attempt to first achieve a reasonable level of accuracy for center of cell classification, before performing experiments on non-centered cell locations.

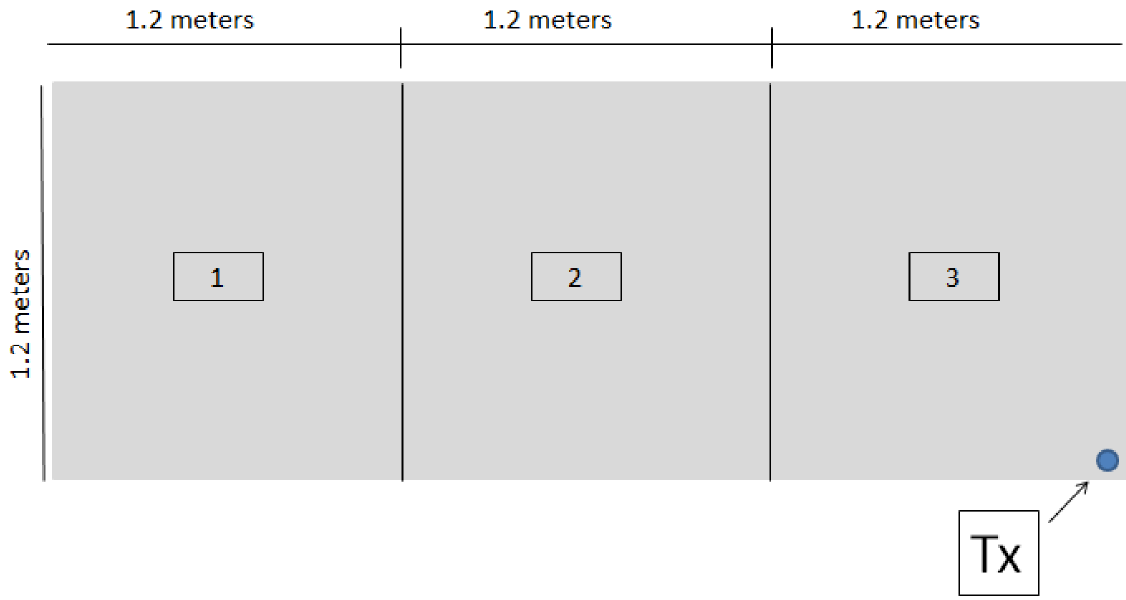

FIGURE 4-4: 3-CELL LOCALIZATION RESOLUTION

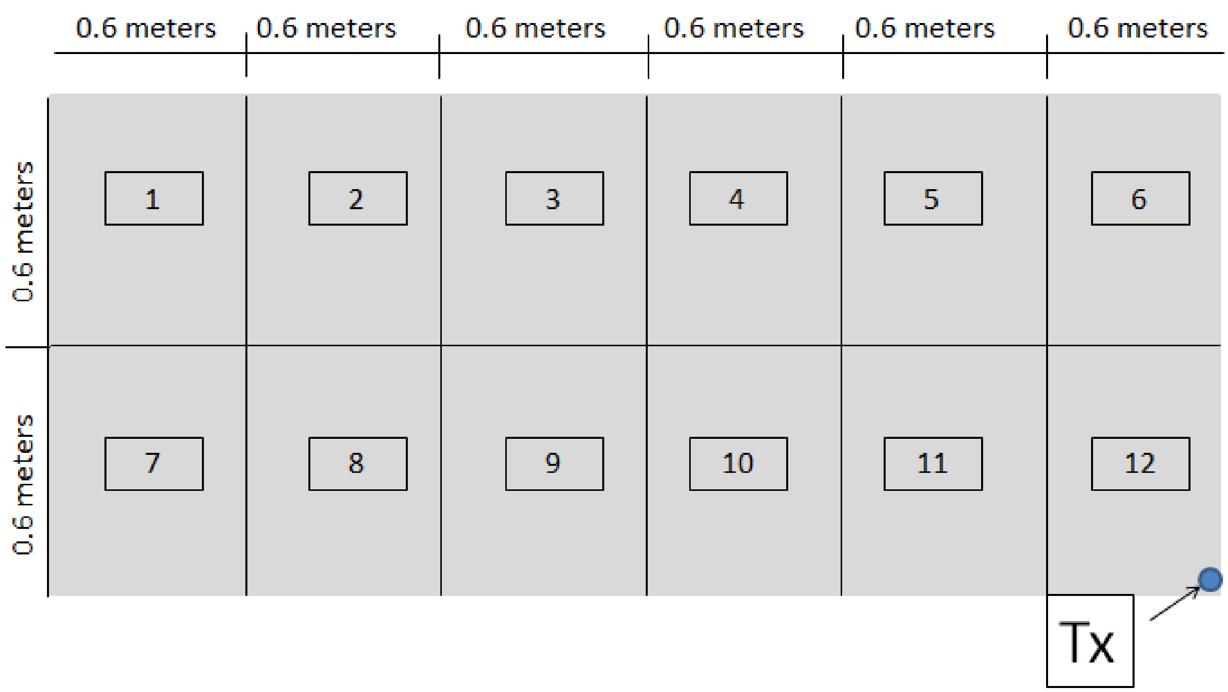

FIGURE 4-5: 12-CELL LOCALIZATION RESOLUTION

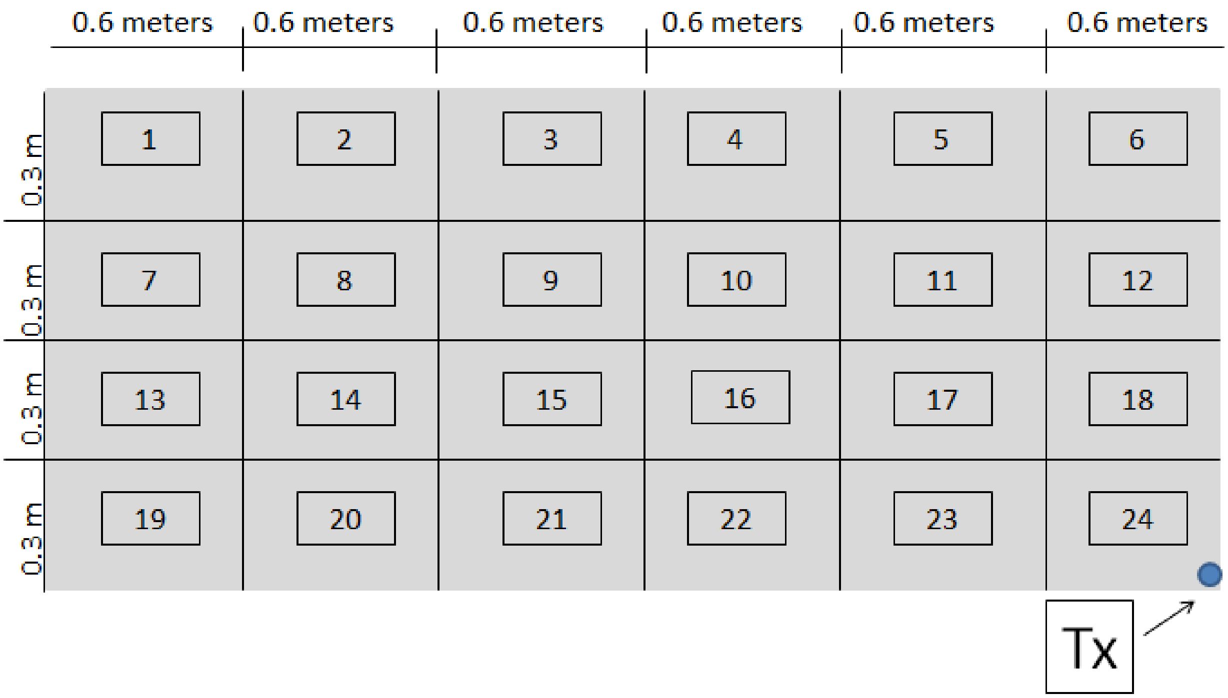

FIGURE 4-6: 24-CELL LOCALIZATION RESOLUTION

4.5.2. Non-Centered Locations

For each cell localization resolution, non-centered locations are placed under the same steps for data collection. For 3-Cell Localization Resolution (3CLR), there exist a total of 4 non-centered locations in each cell. For 12-Cell Localization Resolution (12CLR), there exist a total of 2 non-centered locations in each cell, and the same applies to 24-Cell Localization Resolution (24CLR). Each cell mapping is featured in figures 4-7, 4-8 and 4-9 where 3, 12, and 24 cell distributions for data collection have their non-centered locations depicted respectively. Locations with lettered nomenclature represent the center of each cell, while numbered representations exist for labeling non-centered locations.

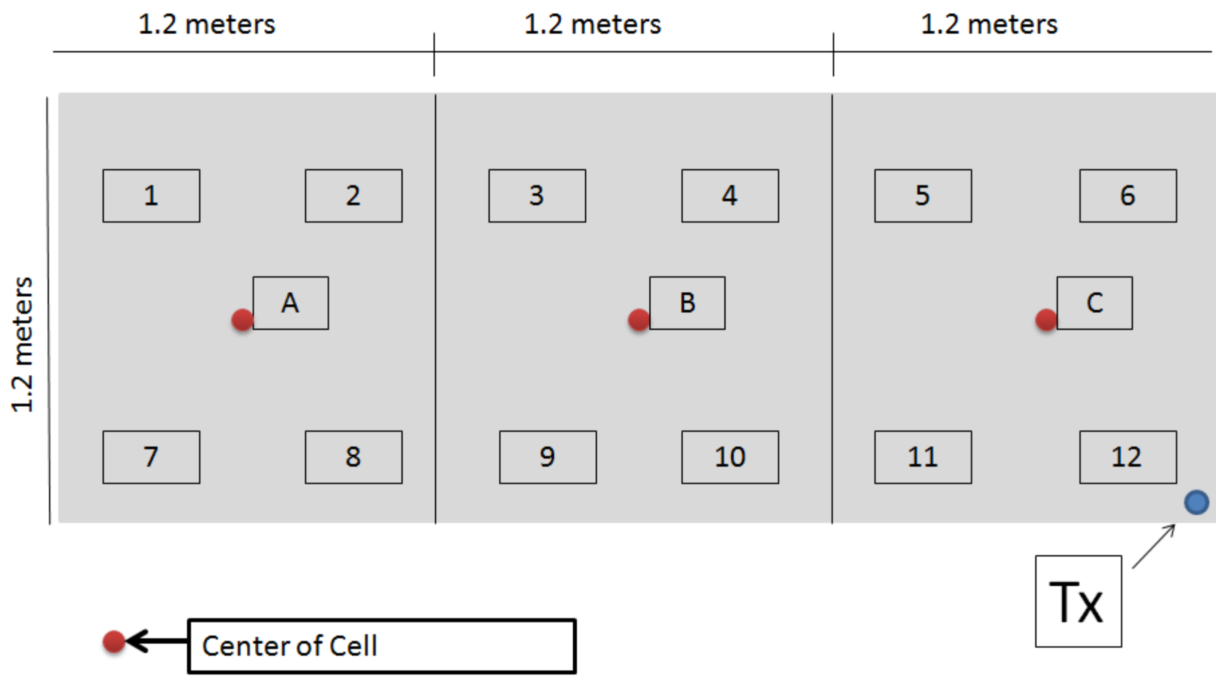

FIGURE 4-7: 3CLR, NON-CENTERED LOCATIONS

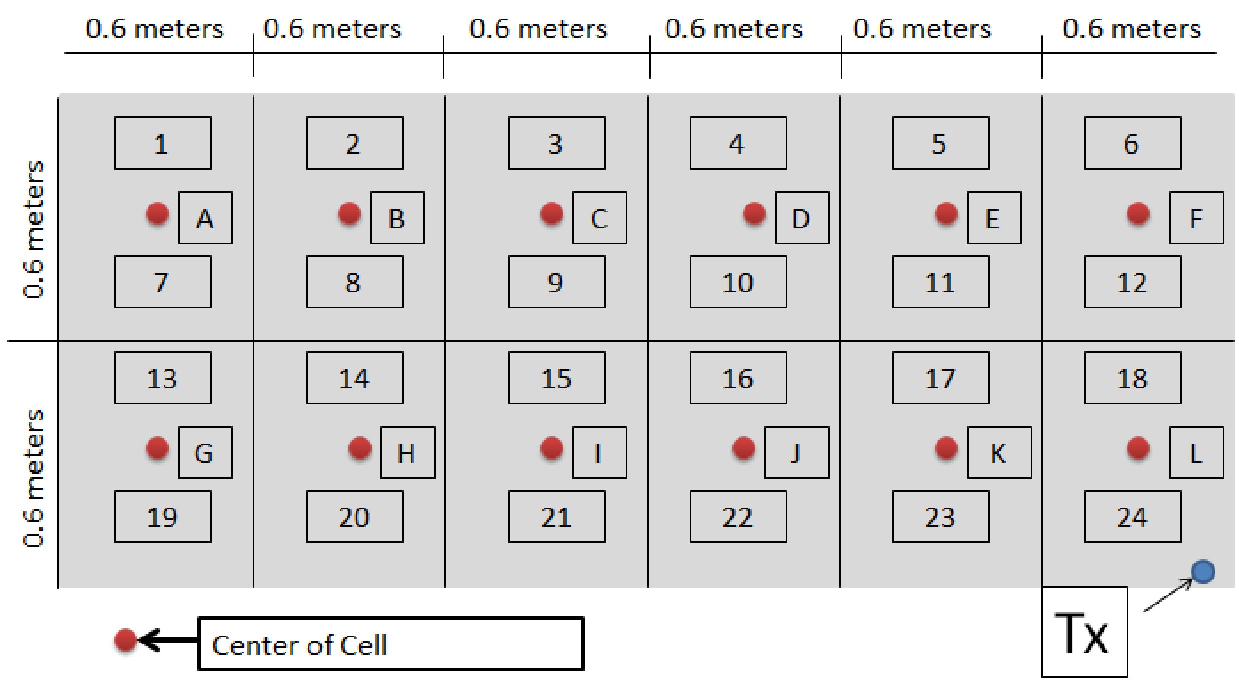

FIGURE 4-8: 12CLR, NON-CENTERED LOCATIONS

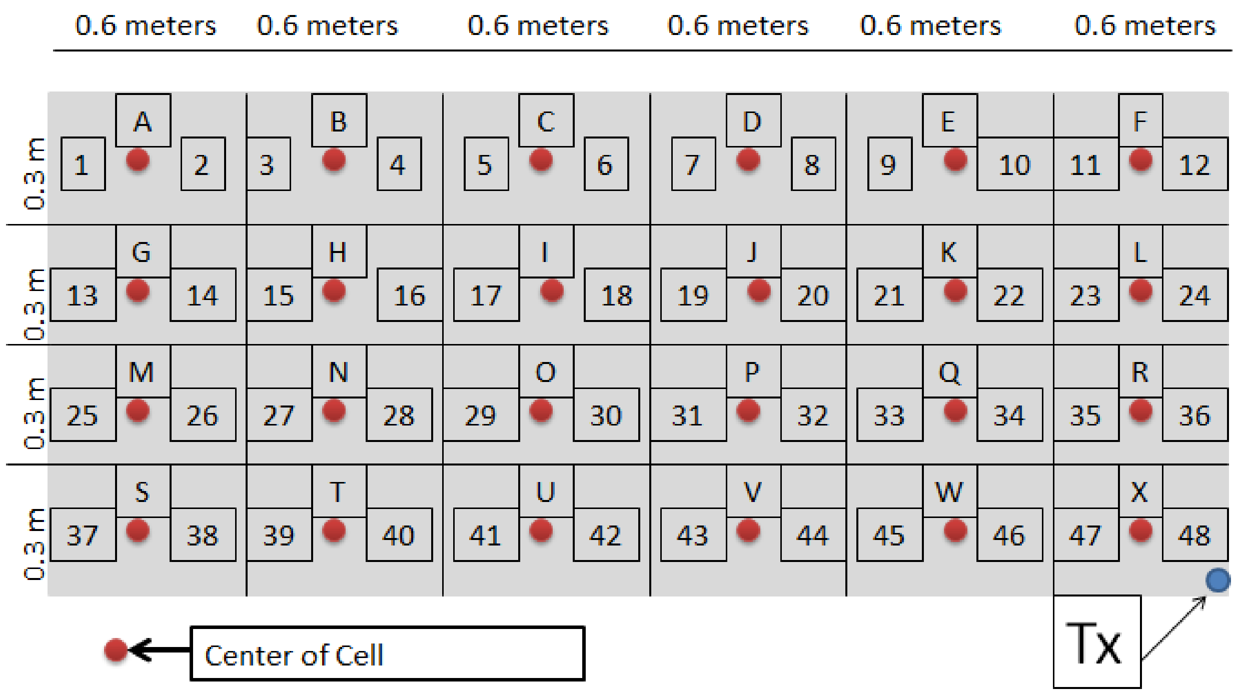

FIGURE 4-9: 24CLR, NON-CENTERED LOCATIONS

CHAPTER 5: FEATURE DETERMINATION AND EXTRACTION

This chapter outlines the techniques used in the pre-processing of raw signals, and the determination of what features could be extracted that grant the highest degree of distinguishability when examining received waveforms on a cell-to-cell basis.

5.1. Pre-Processing

Pre-processing is a commonly used step in signal processing before extracting useful information from a signal. The benefits of pre-processing include data size reduction, and the elimination of noise and variability in signals that originate from the same conditions in which data was collected. In this thesis, a number of pre-processing techniques were implemented in MATLAB, which also provide the benefits mentioned above. Figure 5-1 depicts the block diagram for the pre-processing system implemented in software. The overall goal of the pre-processing techniques that will be discussed below is to obtain the signal envelope. From the envelope, features will be extracted to obtain and improve classification results.

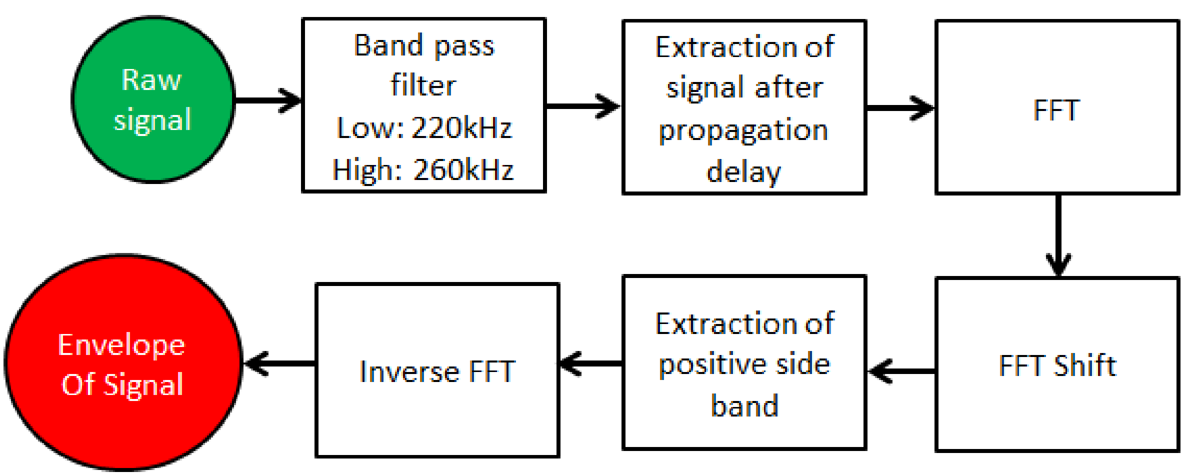

FIGURE 5-1: PRE-PROCESSING BLOCK DIAGRAM

5.1.1. Band pass filter

The effects generated by the use of a band pass filter were necessary in the removal of various sources of noise present within the raw signal. From the power supply connected near the plate (used to provide power to the ultrasound transmitter), a 60 Hz noise was present in almost every position close to the transmitter. In addition, noise from the battery charger of the laptop used to collect data introduced high frequency noise into the raw signals. It was also determined that the probes used in conjunction with the Picoscope, leaked noise into the received signal from the ultrasound transmitter pulse also being measured by the same scope. The signal, whose dominant frequency at 245 kHz, also contained harmonics that were dominant enough to be observed by the oscilloscope. However, it was determined that the he only signal of interest was that in which the 245 kHz frequency component was present. To account for both the low and high frequencies mentioned previously in this section, and to extract the dominant frequency component of the raw signal, a band pass filter was deemed as the best choice. The MATLAB Signal Processing Toolbox was used to implement a 10^{th} order Butterworth band pass filter, with a pass band of 40 kHz, passing frequencies in the range of 220 kHz to 260 kHz. These frequencies represent the high pass filter cutoff and low pass filter cutoff respectively. The initial performance of these cutoff frequencies was determined to be suitable enough for the application presented in this thesis, requiring no need to find tune the pass band through additional experimentation with different cutoff values. Figures 5-2 and 5-3 correspond to the raw received signal and the band pass filtered raw received signal respectively.

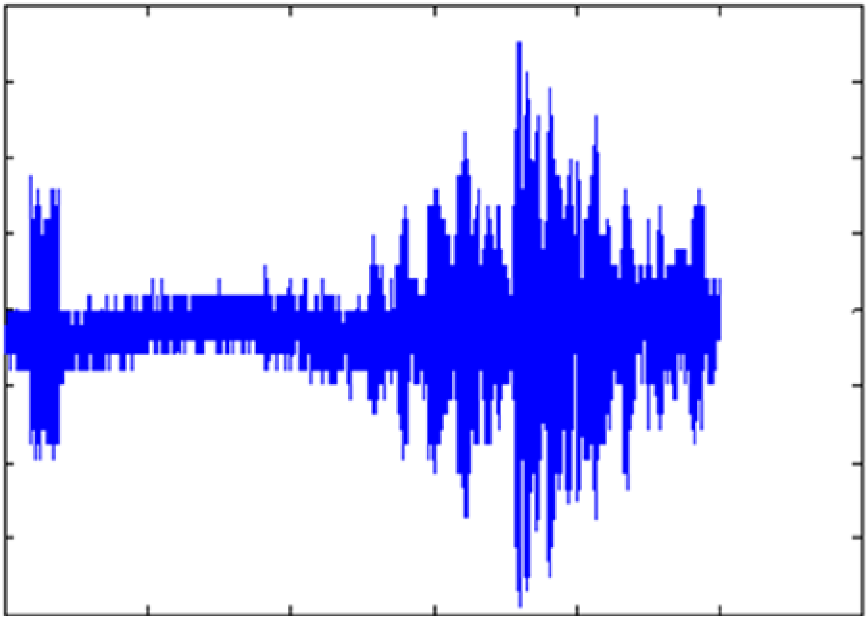

FIGURE 5-2: RAW RECEIVED SIGNAL

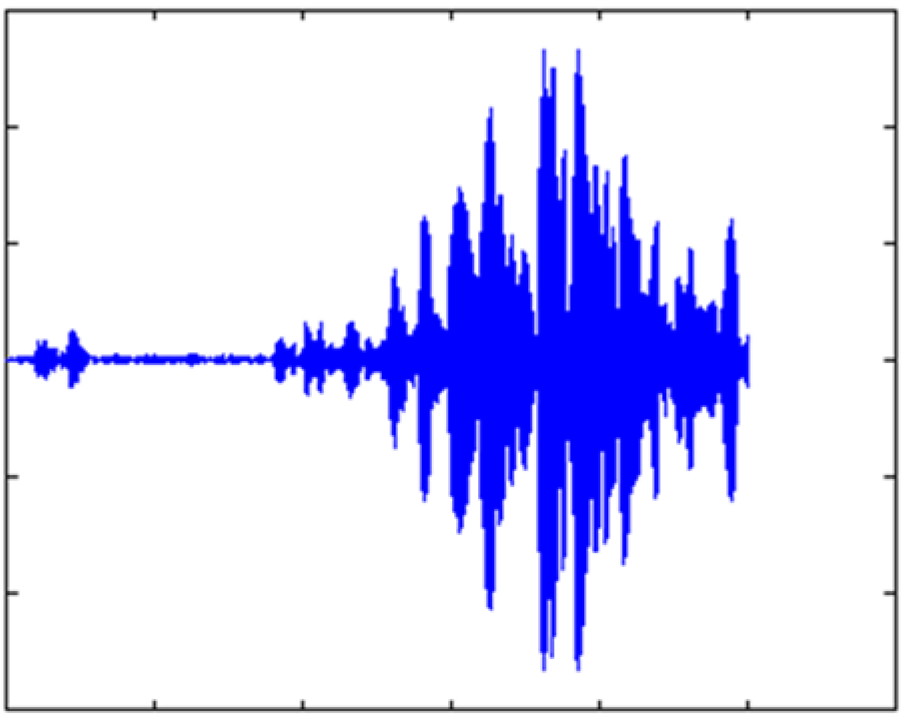

FIGURE 5-3: RAW SIGNAL AFTER BAND PASS FILTER

5.1.2. Extraction of signal minus prop delay

Based on the work studied in [20], the frequency component of ultrasound signals can provide useful information when utilizing applications that involve some form of machine learning and pattern recognition. Thus, eventual steps will lead to analyzing the Fourier transform of the band pass filtered signal. However, data collected in the form of the raw signal does not only include the signal itself. After the signal is filtered, in some cases there exist remnants of the noise leaked from the Picoscope probe from the ultrasound transmission. In addition to this, the signal itself has a propagation delay. This delay (distance dependent), causes the actual signal to occur later in the set of data and not at the start of when the data is collected. These samples that are not the actual signal, in addition to the noise from the probe, can alter the appearance of the signal in the frequency domain. To remove the effect of such uncertainties, a manual extraction of the signal is done based on its position on the aluminum plate, which corresponds to a certain propagation delay. From each position in which data was collected in 20 instances of coupling, the index in the data in which the signal began and ended was taken as the new data set for the raw signal. The start of the signal was chosen from the observance of the first dominant wave after the propagation delay. The end of the signal was determined by observing the point at which the last dominant reflection occurred before an interval of inactivity became visible. This stage of inactivity happens during the phase in which there is no pulse being transmitted. This indexing process was done for 5 random coupling instances. After averaging the results among the randomly chosen 5 instances, this indexing was applied to all 20 coupling instances belonging to each particular cell. Figure 5-4 depicts the raw band pass filtered signal, with the manual extraction of the signal minus samples from the effects of propagation delay and period of signal inactivity.

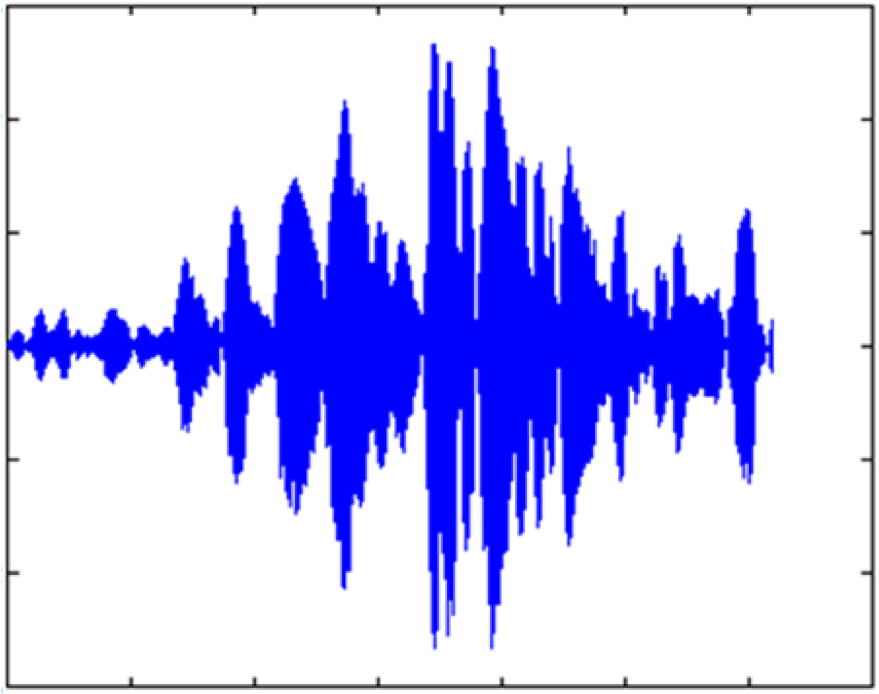

FIGURE 5-4: RAW SIGNAL AFTER MANUAL EXTRACTION

5.1.3. Fourier Transform

In order to successfully begin the process for attempting to produce an envelope signal, a discrete Fourier transform of the raw signal data is computed using the Fast Fourier Transform (FFT) MATLAB algorithm. From a generic standpoint, the frequency components of signal, achieved through the complex decomposition of the signal into complex exponential representation, is very useful in analyzing data. The result of this transform is an important step needed in the fulfilling the ultimate goal of obtaining the signal envelope.

5.1.4. Fast Fourier Transform Shift

Upon the successful acquisition of the FFT, succeeding this step is the FFT Shift. The output of the FFT is shifted such that it rearranges the FFT by moving the zero-frequency component to the center of the array. This step is useful for visualization purposes.

5.1.5. Extract positive side band

The symmetric nature of the FFT MATLAB algorithm allows for the signal to appear to have a mirror representation of itself in the negative frequency portion of the axis. Both the positive and negative representations of the signal in the frequency domain hold the same information. Thus, when extracting the signal for the purpose of performing the Inverse Fourier transform, it is presumed that only the positive side band of the signal is needed. Any additional information would just add more redundancy to the data set. This reasoning leads to the assumption that the envelope should be able to be properly constructed from using only the positive side of the signal. To actually extract the positive side band, manual determination of the bands start and endpoint are determined in the same process applied in the extraction of the band pass filtered raw signal.

5.1.6. Inverse Fourier Transform

The reasoning presented in the previous sub-section, leads to the final step in the pre-processing chain, the Discrete Inverse Fourier Transform. This computation is made possible through the Inverse Fast Fourier Transform (IFFT) MATLAB Algorithm. Taking a look at Figure 5-5, a comparison between the raw band pass filtered signal (right) and the constructed envelope (left), it can be seen that indeed it is possible to generate an envelope by taking the IFFT of the positive side band only. It was observed at the end of the envelope, some of the signal may be cut off in comparison to the raw band pass filtered signal. This can be attributed to the human error introduced from the manual method of extracting the positive side band. It is also important to note that the data set length of the side band becomes the data set length for the envelope. This concept will become important in sections to come, and will also be explained in more detail.

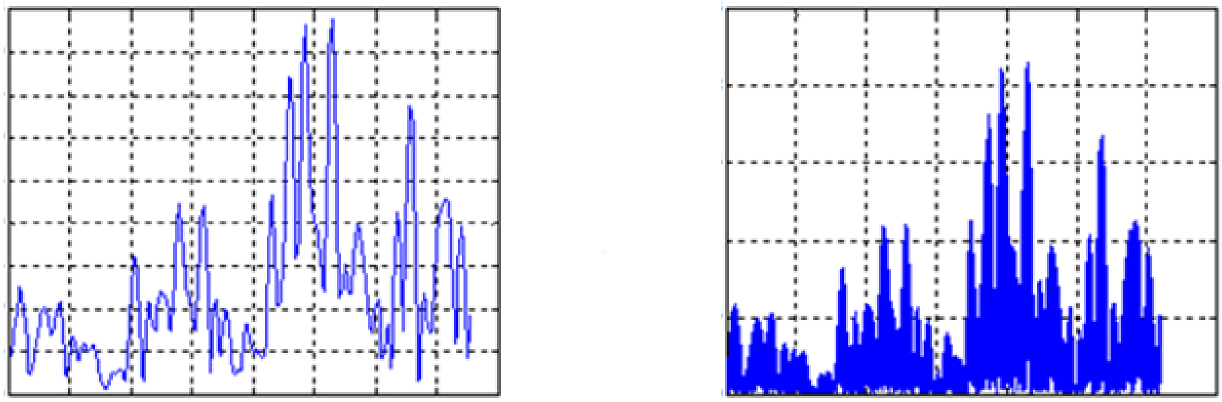

FIGURE 5- 5: COMPARISON BETWEEN ENVELOPE AND RAW SIGNAL

5.2. Feature Determination and Extraction

To be able to confidently asses what distinguishable features may be present in the envelope, extensive study was conducted on the physical appearance and attributes of the signal. This study was combined with the knowledge gained in relation to lamb wave propagation and the signal’s envelope shape dependence on the proximity to the ultrasound transmitter. Once a suitable set of features was determined, the implementation of methods to extract the features was created.

5.2.1. Correlation coefficient

Computing the correlation between two signals is a common statistical method used for applications in signal processing. Associated with the concept of correlation are the techniques for auto and cross correlation, where the statistical measure of similarly it computed against the signal itself and against a different signal, respectively. The cross correlation computes a correlation coefficient (whose absolute value lies between 0 and 1) that represents how similar the two waveforms are in comparison to one another, where one signal normally has some time lag applied to it. The Auto correlation is simply the cross correlation of the signal with itself. Once again MATLAB is used to provide the algorithm for the cross correlation (XCORR) coefficients computed in this work. To examine whether computing the XCORR coefficients would be a suitable feature, a set of computations were done for the 3CLR Case for proof of concept, and then extended to the higher cell localization resolutions. The XCORR coefficient was computed and a distribution was plotted for all permutations (with no repetitions) of coupling instances within each cell and all permutations against neighboring cells. The within cell XCORR, or intra-cell correlation, was expected to yield a distribution containing higher values of the XCORR coefficient, while the inter-cell correlation (neighboring cell correlation), was expected to yield lower values within the plotted distributions. Figure 5-6 shows an example of the inter-cell and intra-cell correlation with respect to cell 1, for 3CLR. From the figure it can clearly be shown that the expected results match the results obtained. The first graph on the far left depicts the intra-cell correlation (auto-correlation) from all the instances within cell 1. The middle graph and the graph on the far right depict the correlation between cell 1 and cell 2 and cell 1 and cell 3 respectively. It can be clearly seen that the distribution for these two graphs does not lie in the entire range seen in the graph that represents the intra-cell correlation. It can also be seen that there exists a greater correlation between cell 1 and cell 2 than the correlation between cell 1 and cell 3. This is due to the fact that cell 2 is a direct neighbor to cell 1. Plots for the remaining cells, as well as other resolutions follow a similar trend. To explain how a tangible numeric feature was produced from using the XCORR coefficient, let $L_i^m \; for \; i = 1 \ldots 12 \; and \; m = 1 \ldots 20$, represent the waveforms for the non-centered locations (3CLR) and let $C_j^k \; for \; j = A, B \; and \; C \; and \; k = 1 \ldots 20$, represent the waveforms for centered locations (3CLR). Thus, the correlation coefficient feature is represented by Equation 1.

$$Xcorrf_j = \frac{\sum_{all\;k} Xcorr({L^m}_i, {C^k}_j)}{20} \qquad (1)$$

When expanding this experiment to consider the data for non-centered locations, results exhibit a different trend. Figure 5-7 depicts the intra-cell correlation between Cell A and all of its respective non-centered locations. It can be shown that there exist correlation coefficients within the same range of values for the correlation between the center of Cell A (noted as cell 1 for center of cell experiments) and the center of Cell B (noted as cell 2 for center of cell experiments), as well as other non-centered locations within Cell A. Therefore, the ability to distinguish a non-centered location within Cell A from neighboring locations (in and out of the cell), has been reduced substantially. It is here that the necessity of other discriminating features becomes evident.

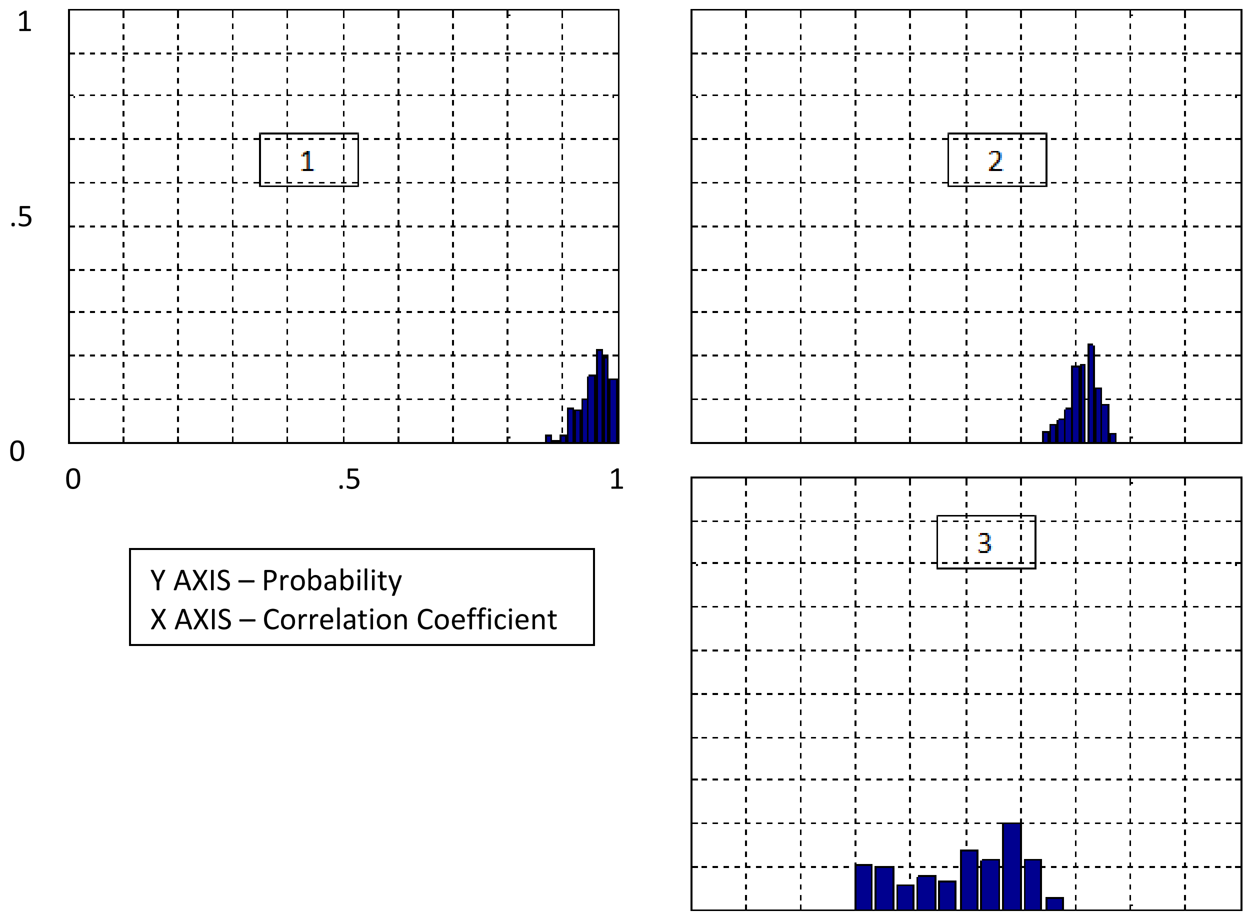

FIGURE 5-6: CROSS CORRELATION WITH RESPECT TO CELL 1 (3CLR)

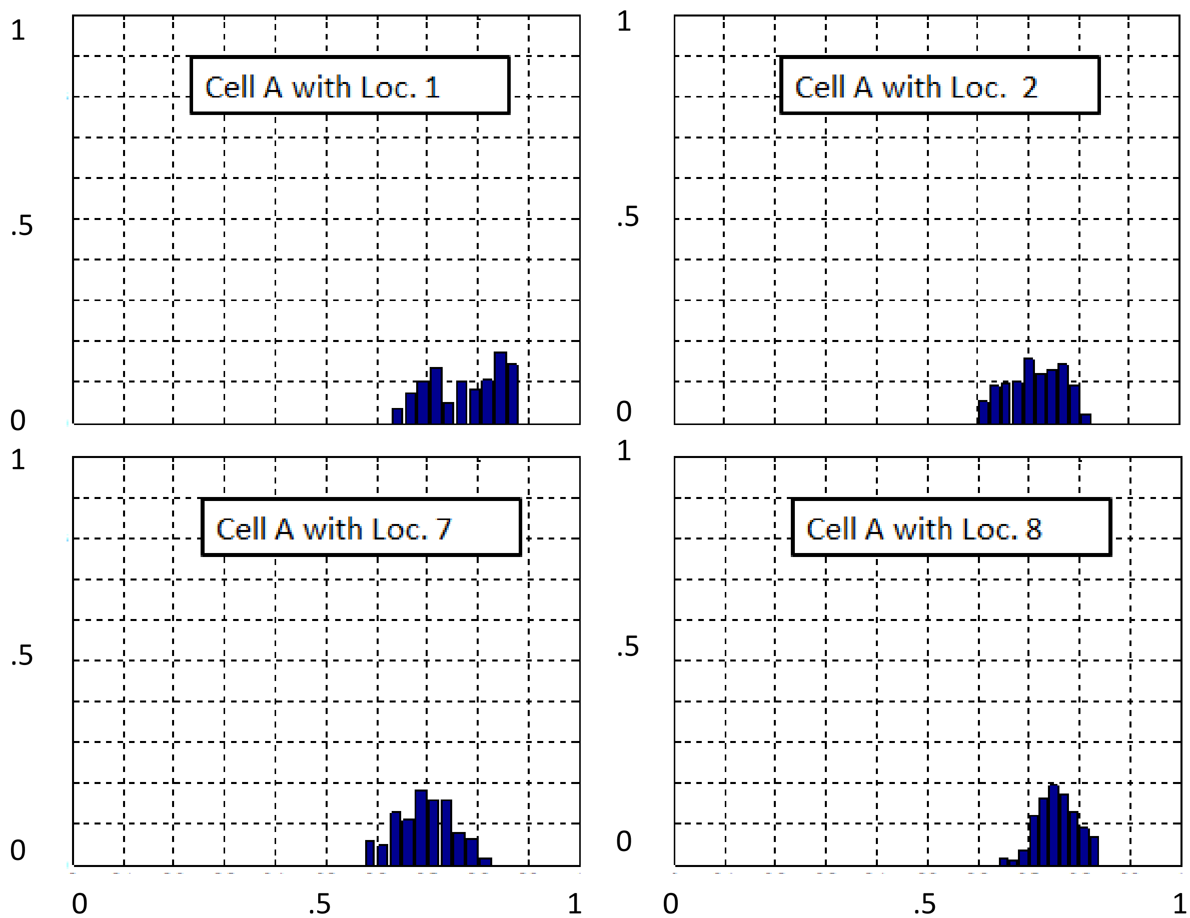

FIGURE 5-7: NON-CENTERED CROSS CORRELATION WITH RESPECT TO CELL 1 (3CLR)

5.2.2. Signal Length

Mentioned previously in this chapter, the raw signal was manually extracted, removing data that did not contain the signal from effects generated by the propagation delay and the period of inactivity before another pulse is transmitted. When examining the non-centered locations for 3CLR, a relationship was observed between the center of cell locations and the non-centered locations that belong to it. Figure 5-8 shows a bar graph representing this relationship. The signal length (i.e., the number of samples representing the signal), for each non-centered location has a value that is closest to the cell that it belongs in. For example, cell A's signal length is closest to the lengths of non-centered locations 1, 2, 7 and 8. To be able to make use of such a feature, the manual method of extracting the signal must be eliminated and replaced with an autonomous process. Therefore, a simple script file was written in MATLAB to automatically extract the signal length from each coupling instance in each center of cell and non-centered location. Through intense observation of the behavior of the start of the raw signals and the end of the signals (i.e., the signal delay spread), it was noted that the lamb wave modes at the beginning were higher in amplitude than those towards the end of the delay spread. Therefore, a threshold was place on the signal to detect the beginning and endpoint of the signal envelope. The first occurrence of a signal that is 20% of the amplitude of the max peak in the envelope is used as a starting point while the last occurrence of 10% of the amplitude of the max peak in the envelope is used to detect the end point. Following the same notation for the center and non-centered locations in the previous sub section, the feature for the signal length is represented in Equation 2.

$$Lengthf_j = \left| length\left(L_i^m - \frac{\sum_{all\ k} C_j^k}{20} \right) \right| \quad (2)$$

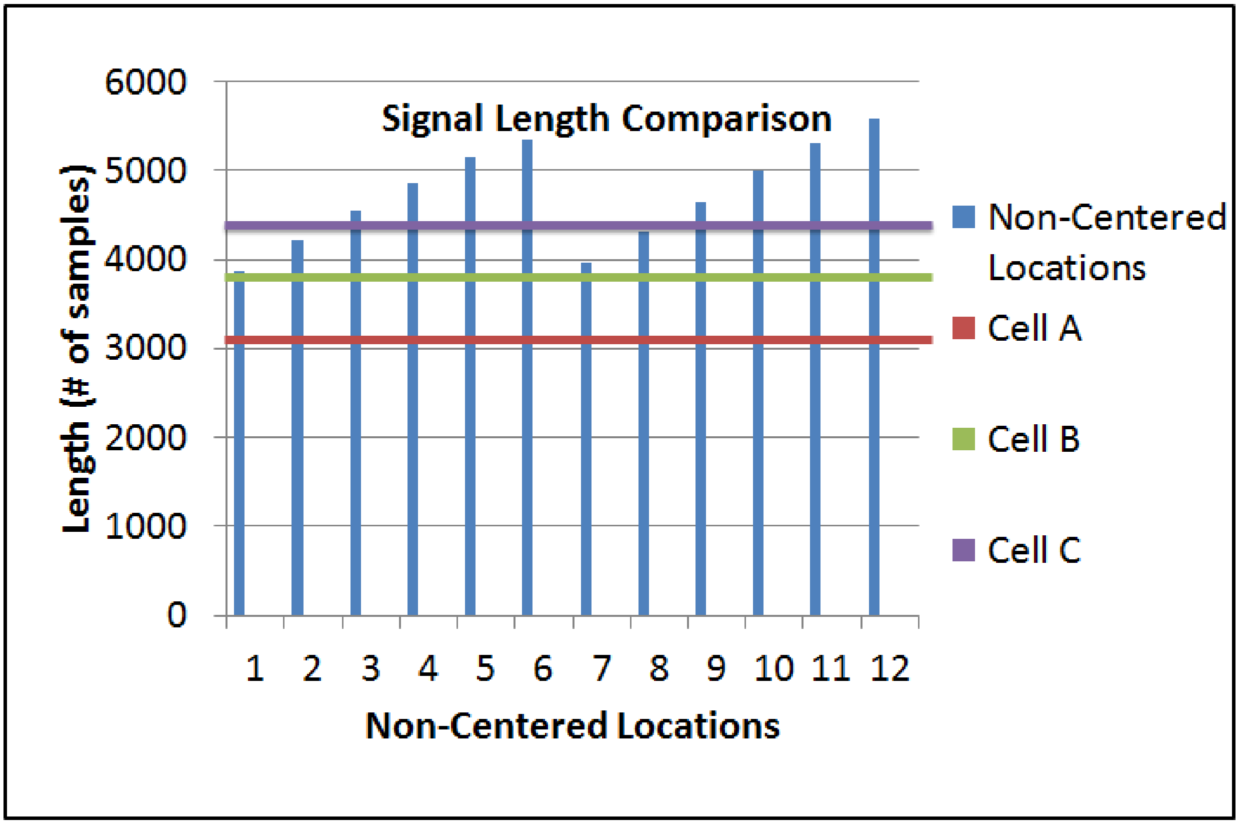

FIGURE 5-8: SIGNAL LENGTH COMPARISON FOR NON-CENTERED LOCATIONS (3CLR)

5.2.3. Number of Peaks above Threshold

Examining the characteristics of each envelope, a small relationship was discovered between the number of peaks present in the signal and the ultrasound receiver's location in relation to its proximity to the edges of the aluminum plate. For some positions close to the boundary of the plate, the presence of peaks becomes more dominant. This is also slightly intuitive, for the reason that one would expect more reflections to occur close to the edges of the plate, thus creating more noticeable peaks. Figure 5-9 shows an example of this concept for 3CLR and its 12 non-centered locations. However, the definition of what actually classifies as a peak is needed to be formally set. To mitigate this issue, a threshold is used as a baseline for peak detection. Data points that lie above the threshold are evaluated for their relative maximum peaks. Therefore, for some waveform, $w(n)$, a peak exists at a point n', if the following is satisfied:

$$If\ there\ exists\ some\ value(\alpha) > THR(threshold\ value)$$

$$if\ w(n') > w(n), when\ |n - n'| < \alpha$$

$$Where\ THR = \beta\ x\ Global\ Maximum\ Peak \qquad (3)$$

$$And\ \beta = \{.10, \quad .20, \quad .30, \quad .40, \quad .50, \quad .60, \quad .70, \quad .80, \quad .90\}$$

Using MATLAB, a script is created that varies the value of β in order to find the optimal threshold value that will be evaluated later for the purposes of finding which threshold yields higher inter-class distinguishability. This concept will be revisited when the performance of these features is examined.

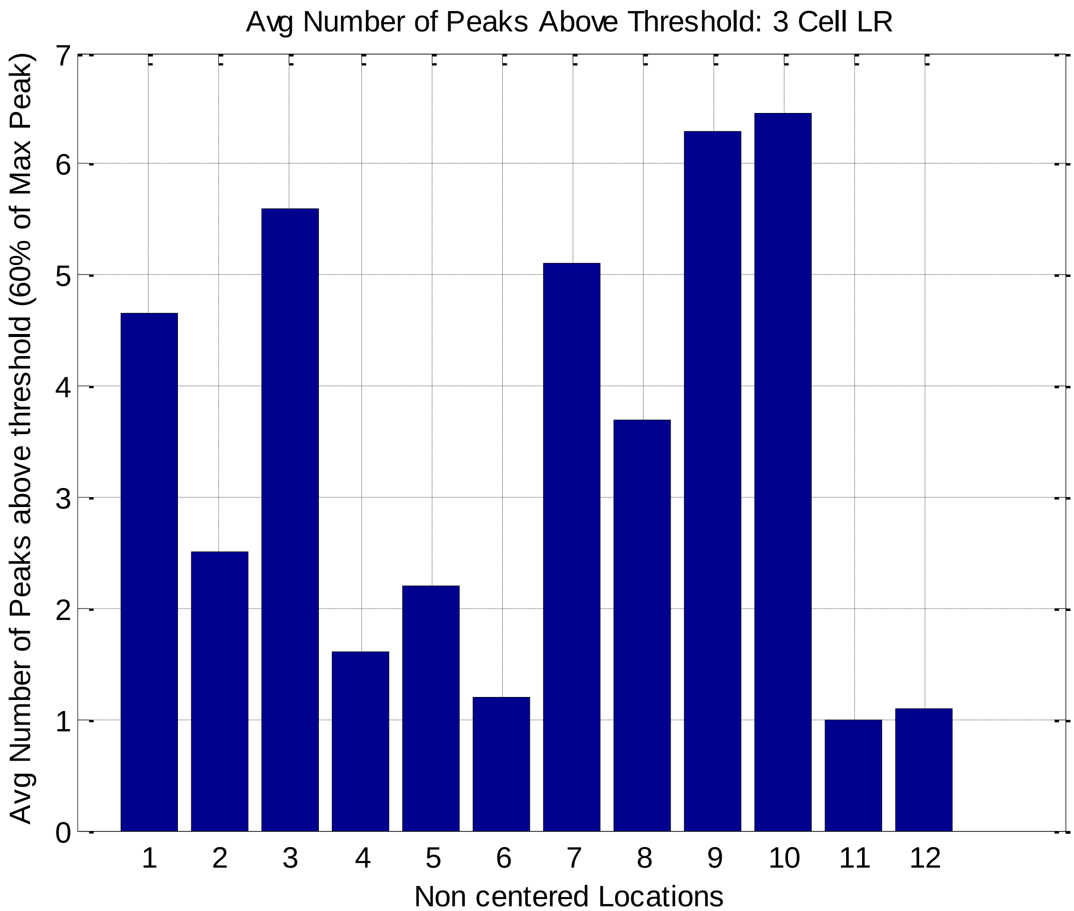

FIGURE 5-9: AVERAGE NUMBER OF PEAKS ABOVE THRESHOLD (3CLR)

5.2.4. Number of samples from start of the waveform to its max peak

Upon further examination, another location dependent observation was made. It was discovered that on average, locations close to the ultrasound transmitter will have a lower amount of samples from the start of the envelope to the location of its maximum peak value. In contrast, on average, locations that are further away from the transmitter have a larger amount of samples present between the start of the envelope and the index of its maximum peak value. Figure 5-10 depicts two graphs for 3CLR representing non-centered location point 1(left) and non-centered location 12 (right). The graphs are plotted for values for all 20 coupling instances. Notice that the stem plot represents the number of samples from the start of the waveform to the location of its max peak of the location of interest. The line plots represent the same quantity, but are fixed for all three cell centers A, B and C. To utilize this information in the form of the feature, the following notation is used to form Equations 4. Let μ be the number of samples from the index of start of the envelope (ε), to the index of the first max peak. Using the additions of these two notations, the following is defined:

$$[maxpoint, location] = GlobalMAX(L^{m}{}_{i}) \qquad (4)$$
$$\text{where } \mu = location - \varepsilon$$

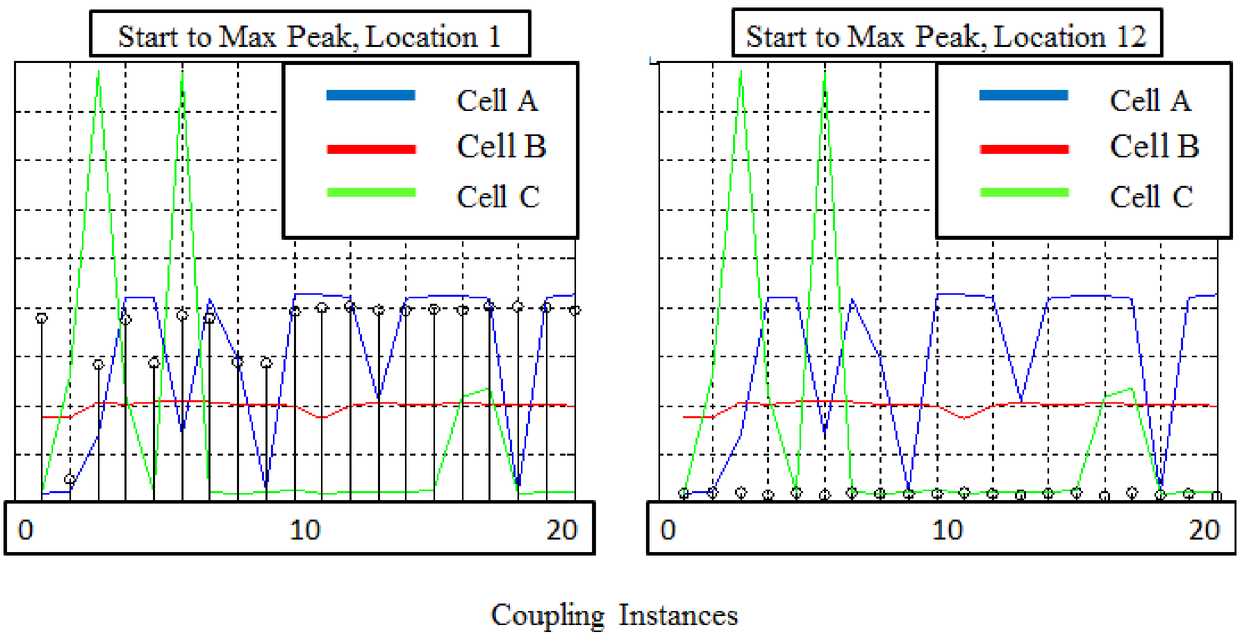

FIGURE 5-10: NUMBER OF SAMPLES FROM START OF WAVEFORM TO MAXIMUM PEAK

5.2.5. Standard deviation

Using the standard deviation as a feature is common practice in applications using pattern classification [8]. The standard deviation shows how much variation is present from the average envelope value. The standard deviation was added as feature to increase the feature space in which classification will be performed. The intent is to increase the overall classification accuracy. However, its usefulness will be evaluated in a later chapter of this thesis.

5.2.6. Kurtosis

The Kurtosis value, also used in [8] as a feature, seemed plausible due to its relationship with probability distributions. By using the correlation coefficient distributions generated, the kurtosis value can be used to characterize its behavior in accordance to the shape of the distribution. High kurtosis valued distributions have sharper peaks and longer and fatter tails. Low valued kurtosis distributions have more rounded peaks and shorter and thinner tails. By observing the XCORR coefficient distributions, it can be seen that the distributions that yield higher values of correlation, for the center of cell cases, have higher kurtosis values. Though this case is not entirely consistent, it was chosen with the notion of being able to add some measure of differentiability between determining the location of the ultrasound receiver in terms of center of cell locations. Using the kurtosis value as a feature will be fully analyzed in the chapter that discusses classification results.

5.2.7. Skewness

The value of Skewness, also based on the shape of a probability distribution, is also evaluated for the use of providing similar benefits to that of using the kurtosis value. The skewness can take on positive or negative values. Negative skew indicates that the tail on the left side of the distribution is longer or fatter than the right side. Positive skew indicates that the tail on the right side is longer or fatter than the left side. Distributions that have higher values of correlation with a particular cell or non-centered location tend to skew towards the right, while the contrast case skews to the left. In some cases, using the skewness as feature can provide evidence as to which cell the ultrasound receiver may belong to.

5.2.8. Summary

The results outlined in this chapter show that it is possible to pre-process the raw signal in such a way that allowed successful production of an envelope signal. From the envelope signal, the behavior of the effects of multipath is studied to determine distinguishable features. Each feature has a distinct relationship with either the shape of the signal or the position in which the signal is collected. It is hypothesized that those that are location dependent will be able to provide the most useful data to aid in the classification of the cell position in which the signal originated.

CHAPTER 6: CLASSIFICATION METHODS AND ALGORITHMS

The learning and evaluating procedures done during pattern classification prove very useful when attempting to generalize and represent data sets. Generalization of the data would allow the system to perform well under data instances that have not yet been seen or processed by the system. Achieving generalization will be discussed in a later section of this thesis. Representing the data has been achieved through the data collected from the aluminum plate. Therefore, in this chapter, classification algorithms used to evaluate the data represented in the localization system are introduced. One approach taken at classification is a rather simplistic method, while the remainder of the algorithms are utilized via the popular machine learning software, Weka (Waikato Environment for Knowledge Analysis), developed at the University of Waikato, New Zealand.

6.1. Maximum Average Correlation Coefficient

The XCORR coefficient, explained in Chapter 5, was able to provide good distinguishability for classes of data that represent that center of each cell. To properly evaluate the performance of this stand-alone feature, for the case of strictly center of cell classification, a classification algorithm was developed that utilizes a rather simple decision rule. The Maximum Average Correlation Coefficient (MACC) Algorithm is used to classify the center of cell positions on the aluminum plate and it is implemented via MATLAB. Figure 6-1 outlines the steps involved in the algorithms decision making process, where Equation 5 in this chapter stems from Equation 1, first introduced in Chapter 5. Step (1) is used as a training phase, in order to simulate the functionality of the localization system if it were implemented in real time. The selection of a random waveform is chosen from the pool of data collected from each cell and all 20 instances, totaling 60 envelopes for 3CLR, 240 envelopes for 12CLR and 480 envelopes for

24CLR. Step (2), removes the random waveform from the pool of collected data as well as one random waveform in the form of one instance of coupling from every other cell. This allows for the averaging result that takes place in Step (3), to not be affected by one value of the variable *Xcorr* that will have a correlation coefficient of 1, due to the comparing of the randomly selected waveform with itself at some point in the summation. The other cells not containing the randomly selected waveform also have one instance removed to account for the removal of the waveform from the cell of origin. Finally, in Step (4), Equation 6 is used to classify the cell of origin of each randomly selected waveform. Once an array of averaged correlation coefficients is computed, index belonging to the cell with the maximum XCORR coefficient is chosen to be the cell of origin of the random waveform previously selected. The algorithm continues to select random waveforms until the entire pool of collected envelope data has been selected, thus depleting the entire set of data.

- Step 1
  - Select random waveform envelope "*w*" from collection of envelopes, to use as a test waveform
- Step 2
  - To make the data from each cell the same size, remove "*w*" from envelope matrix and also remove a random waveform instance from every other cell that "*w*" is not present in
- Step 3
  - Compute the cross correlation of "*w*" with every instance in every cell and average the results using Equation 5 :

$$C_i = \frac{\sum_{j=1}^{j=19} Xcorr(w, {w^j}_i)}{19} \; for\ i = 1 \ldots (3\ or\ 12\ or\ 24) \qquad (5)$$

- Step 4
  - To Classify the waveform, "*w*":

$$C_{est} = \max(C_i), for\ i = 1 \ldots (3\ or\ 12\ or\ 24) \qquad (6)$$

FIGURE 6-1: STEP-BY-STEP IMPLEMENTATION OF THE MAXIMUM AVERAGE CORRELATION COEFFICIENT ALGORITHM

6.2. Weka

It is important to note that the overall goal of thesis was not to develop novel algorithms for the purpose of creating a pattern classification approach to ultrasound localization, but rather to assess whether such a system was possible with a high degree of accuracy. Thus, Weka was sought out for the purpose of obtaining diversity in classification accuracy by taking advantage of the many classifiers available through Weka's infrastructure. Weka is used to classify the non-centered locations, due to the fact that the XCORR coefficient does not provide similar results as the center of cell cases. The training set for this system is composed of all the features mentioned in Chapter 5, with each center of cell location as the reference for generating the features for the non-centered case. To test each class, 10-Fold Cross Validation is used. Using Weka, the performance of eight (8) common classifiers was evaluated for the same set of training and testing environments. A brief description of each will be given as a form of background and introductory information.

6.2.1. Multilayer perceptron

A Multilayer Perceptron (MLP) is a feedforward artificial neural network. It generates multiple layers of nodes (neurons) that are fully connected and that are used to model and map sets of input data onto a set of outputs. It also used a concept known as backpropagation for training purposes.

6.2.2. Meta Bagging

Meta Bagging is a form of ensemble learning, also called bootstrap aggregating. It involves having each model in the ensemble vote with equal weight. Meta bagging trains each model in the ensemble using a randomly drawn subset of the training set in order to reduce the variance between attributes in the model. Decision trees are used as a base classifier to provide higher classification results. In this thesis, the J48 decision tree is used for all results pertaining to Meta Bagging.

6.2.3. Radial Basis Function Network

Radial Basis Function (RBF) is another type of artificial neural network classifier that implements a normalized Gaussian radial basis function network. The algorithm utilizes the k-means clustering algorithm to produce the basis functions needed to generate predictive models via logistic regression or linear regression.

6.2.4. J48 Decision Tree

This classifier is derived from the C4.5 statistical classier. It uses decision tree based learning to develop a predictive model, and performs a mapping from an observation about an item to generate a conclusion about what result the item of interest may lead to. In Weka, a pruned or unpruned decision tree can be utilized.

6.2.5. Logistic Regression

This classifier is used to construct regression models used to predict the outcome of the occurrence of some form of dependent variables.

6.2.6. Simple Logistic Regression

Simple Logistic Regression is a branch of Logistic Regression. It is used to build linear logistic regression models to perform the same modeling and estimation done in traditional regression techniques.

6.2.7. Sequential Minimal Optimization

Sequential Minimal Optimization (SMO) is implemented using John Platt's sequential minimal optimization algorithm for training a support vector machine classifier. The version used within Weka globally replaces all missing values for attributes and transforms nominal values for attributes into a binary representation.

6.2.8. Naïve Bayes

A simple classifier that uses probabilistic methods based off Bayes Decision Rule. Very strong assumptions of independence among features exist within this classifier.

6.3. Summary

The information presented in this chapter discusses the two approaches taken in the classification of the cell positions for the purpose of localization. The first approach, for the center of cell case, involves the use of MATLAB to invoke the Maximum Average Correlation Coefficient Algorithm for offline data localization. This algorithm utilizes the distinguishing power of the correlation coefficient for the intra-cell and inter-cell cases, comparing each coupling trial from every cell to a randomly selected waveform from another. The second approach, for the non-centered locations, uses the offline data in conjunction with Weka, and the classifiers at its disposal. The features discussed in Chapter 5 are extracted and uploaded into Weka for training and testing for all cell resolutions. The next chapter will discuss the results of adopting both approaches for both cases of cell localization.

CHAPTER 7: LOCALIZATION PERFORMANCE

In this chapter, the purpose of creating distinguishable features is realized. Here, the performance of the classification algorithms implemented in MATLAB and utilized within Weka is presented. Results of the localization accuracy for the current system are categorized by cell resolution, containing the performance results for center of cell classification and non-centered location classification under the MACC algorithm and the Weka in-house classifiers.

7.1. Cell Localization Resolution Performance

Before any tangible results were obtained, an initial hypothesis is made, generalizing the results of localization performance as the resolution of the localization increases. For example, for 3CLR, it is hypothesized that the localization accuracy will be higher than 12CLR and 24CLR, with 12CLR consisting of the higher performance accuracy out of the two. This can be contributed to the fact that there are fewer neighboring cells to provide confusion in the three cell case, in addition to each cell covering a larger area of the plate. It is important to note that this assumption is valid for the use of the MACC algorithm only. The classifiers in Weka all have different methods of evaluating discriminating features, and thus may yield different relationships for different cell resolutions.

7.2. Center-of-Cell Performance

The performance of the MACC algorithm under 3CLR, 12CLR and 24CLR yield promising results for future analysis of the non-centered locations. Figure 7-1 through 7-3 (a&b) gives the confusion matrix for the classification of center of cell data for each resolution. The results for 3CLR show that there was no confusion between neighboring cells and that the classification accuracy was 100%. For the 12CLR case, the accuracy obtained was 98.75%, with confusion existing with Cell 2 being misclassified as Cell 7 in two instances and Cell 3 as Cell 5 in one instance. The case for 24CLR also shows a similar trend. Accuracy for this case lies slightly below the 12CLR case, at roughly 98.54%, with confusion present among four cells, with Cell 5 being classified as Cells 8, 10, 11 and 17 (ordered from highest to lowest confusion). From these results it can be seen that the MACC algorithm is a sufficient as a stand-alone classifier, needed to correctly assign randomly chosen waveforms to their proper cell center.

Cell 1	Cell 2	Cell 3	
20	0	0	Cell A – Accuracy = 100%
0	20	0	Cell B – Accuracy = 100%
0	0	20	Cell C – Accuracy = 100%
Percent Accurate = 100%			

FIGURE 7-1: CONFUSION MATRIX FOR 3-CELL LOCALIZATION RESOLUTION

C1	C2	C3	C4	C5	C6	C7	C8	C9	C10	C11	C12
20	0	0	0	0	0	0	0	0	0	0	0
0	18	0	0	0	0	0	2	0	0	0	0
0	0	20	0	0	0	0	0	0	0	0	0
0	0	0	20	0	0	0	0	0	0	0	0
0	0	1	0	19	0	0	0	0	0	0	0
0	0	0	0	0	20	0	0	0	0	0	0
0	0	0	0	0	0	20	0	0	0	0	0
0	0	0	0	0	0	0	20	0	0	0	0
0	0	0	0	0	0	0	0	20	0	0	0
0	0	0	0	0	0	0	0	0	20	0	0
0	0	0	0	0	0	0	0	0	0	20	0
0	0	0	0	0	0	0	0	0	0	0	20

Cell 1 -100.0% accuracy
Cell 2 -0.900.0% accuracy
Cell 3 -100.0% accuracy
Cell 4 -100.0% accuracy
Cell 5 -95.0% accuracy
Cell 6 -100.0% accuracy
Cell 7 -100.0% accuracy
Cell 8 -100.0% accuracy
Cell 9 -100.0% accuracy
Cell 10 -100.0% accuracy
Cell 11 -100.0% accuracy
Cell 12 -100.0% accuracy

Percent Accurate
98.75%

FIGURE 7-2: CONFUSION MATRIX FOR 12-CELL LOCALIZATION RESOLUTION

C1	C2	C3	C4	C5	C6	C7	C8	C9	C10	C11	C12
20	0	0	0	0	0	0	0	0	0	0	0
0	20	0	0	0	0	0	2	0	0	0	0
0	0	20	0	0	0	0	0	0	0	0	0
0	0	0	20	0	0	0	0	0	0	0	0
0	0	0	0	16	0	0	1	0	1	1	0
0	0	0	0	0	20	0	0	0	0	0	0
0	0	0	0	0	0	20	0	0	0	0	0
0	0	0	0	0	0	0	19	1	0	0	0
0	0	0	0	0	0	0	0	20	0	0	0
0	0	0	0	0	0	0	0	0	20	0	0
0	0	0	0	0	0	0	0	0	0	20	0
0	0	0	0	0	0	0	0	0	0	0	20

Cell 1 -100.0% accuracy
Cell 2 -100.0% accuracy
Cell 3 -100.0% accuracy
Cell 4 -100.0% accuracy
Cell 5 -80.0% accuracy
Cell 6 -100.0% accuracy
Cell 7 -100.0% accuracy
Cell 8 -95.0% accuracy
Cell 9 -100.0% accuracy
Cell 10 -100.0% accuracy
Cell 11 -100.0% accuracy
Cell 12 -100.0% accuracy

Percent Accurate
=98.5417%

FIGURE 7-3: (A) CONFUSION MATRIX FOR 24-CELL LOCALIZATION RESOLUTION, CELLS 1-12

C13	C14	C15	C16	C17	C18	C19	C20	C21	C22	C23	C24
0	0	0	0	0	0	0	0	0	0	0	0
0	0	0	0	0	0	0	0	0	0	0	0
0	0	0	0	0	0	0	0	0	0	0	0
0	0	0	0	0	0	0	0	0	0	0	0
0	0	0	0	1	0	0	0	0	0	0	0
0	0	0	0	0	0	0	0	0	0	0	0
0	0	0	0	0	0	0	0	0	0	0	0
0	0	0	0	0	0	0	0	0	0	0	0
0	0	0	0	0	0	0	0	0	0	0	0
0	0	0	0	0	0	0	0	0	0	0	0
0	0	0	0	0	0	0	0	0	0	0	0
0	0	0	0	0	0	0	0	0	0	0	0
20	0	0	0	0	0	0	0	0	0	0	0
0	20	0	0	0	0	0	2	0	0	0	0
0	0	20	0	0	0	0	0	0	0	0	0
0	0	0	20	0	0	0	0	0	0	0	0
0	0	0	0	16	0	0	1	0	1	1	0
0	0	0	0	0	20	0	0	0	0	0	0
0	0	0	0	0	1	19	0	0	0	0	0
0	0	0	0	0	0	0	20	1	0	0	0
0	0	0	0	0	0	0	0	20	0	0	0
0	0	0	0	0	0	0	0	0	20	0	0
0	0	0	0	0	1	0	0	0	0	19	0
0	0	0	0	0	0	0	0	0	0	0	20

Cell 13 -100.0% accuracy
Cell 14 -100.0% accuracy
Cell 15 -100.0% accuracy
Cell 16 -100.0% accuracy
Cell 17 -100.0% accuracy
Cell 18 -100.0% accuracy
Cell 19 -95.0% accuracy
Cell 20 -100.0% accuracy
Cell 21 -100.0% accuracy
Cell 22 -100.0% accuracy
Cell 19 -95.0% accuracy
Cell 24 -100.0% accuracy

Percent Accurate
98.5417%

FIGURE 7-3: (B) CONFUSION MATRIX FOR 24-CELL LOCALIZATION RESOLUTION, CELLS 13-24

7.3. Non-Centered Location Performance

Applying the MACC algorithm for the following experiments: (1) the 12 non-centered locations compared with each cell center for the case of 3CLR, (2) the 24 non-centered locations compared with each cell center for the case of 12CLR, and (3) the 48 non-centered locations compared with each cell center for the case of 24CLR, it's performance will again be evaluated to see if it can be solely applied for classifying cell positions outside of the center, until the need to use Weka presents itself. Figures 7-4 through 7-6 (a&b) show the confusion matrix for 3CLR, 12CLR and 24CLR, in the case where 12, 24 and 48 non-centered locations are being mapped to their proper cell of origin respectively. The results differ greatly from the center of cell case. The overall accuracy of the 3CLR case was roughly 58.08%, where most of the confusion stemmed from Cell B, which turns out to be quite intuitive since Cell B has two neighboring cells while Cells A and C do not. For 12CLR, the accuracy obtained was 27.92% and for the last case (24CLR), 18.13%. This also holds true to the hypothesis generated in the beginning of this chapter. In an attempt to study or determine a pattern of confusion, the data collected during classification was used to generate more informative means of presenting the confusion that is present within this set of classification results. Figure 7-7 illustrates three bar graphs that represent the number of times each individual non-centered location is classified into respective cell centers A, B and C for 3CLR. Again, this figure also depicts the same trend amongst the other cell resolutions. The results show that most confusion lies in Cell B, hence the distribution of non-centered locations classified into Cell B is more widespread in comparison to the other cells. Results from these bar graphs also show that on some occasions, there were higher instances of classification from non-centered locations that do not belong to that particular cell of interest. This can be easily justified again through the reiteration of an important concept mentioned in Chapter 6, regarding the overlapping of the correlation coefficient distribution. Figure 7-8 shows a case that is consistent among multiple cells for 3CLR. For a given non-centered location (non-centered location 2 in figure 7-4), there is plenty of overlap with the correlation coefficient distributions between cells A, B and C. Based on these observations, and the observance that each cell resolution exhibits more confusion as the number of cells increase, it has been concluded that the other resolutions will be equally as bad in terms of overlap. Therefore, features that were previously extracted need to be evaluated, in an attempt to improve the accuracy that has been achieved thus far.

Cell A	Cell B	Cell C	
40	37	3	Cell A – Accuracy = 50.00%
18	30	32	Cell B – Accuracy = 37.50%
0	25	25	Cell C – Accuracy = 68.75%
Percent Accurate = 52.08%			

FIGURE 7-4: CONFUSION MATRIX FOR 3-CELL LOCALIZATION RESOLUTION, NON-CENTERED LOCATIONS

A	B	C	D	E	F	G	H	I	J	K	L	
20	0	0	0	0	0	6	14	0	0	0	0	Cell A -50.00% accuracy
5	1	5	0	13	0	2	0	13	0	0	1	Cell B -02.50% accuracy
0	0	0	0	0	1	0	0	0	0	3	36	Cell C -00.00% accuracy
0	1	0	0	0	0	0	0	0	0	1	38	Cell D -00.00% accuracy
1	5	0	0	23	7	0	0	0	0	3	1	Cell E -57.50% accuracy
0	0	0	1	2	7	0	0	0	0	0	30	Cell F -17.50% accuracy
0	2	0	0	0	0	11	21	0	0	0	6	Cell G -27.50% accuracy
0	3	0	1	0	0	2	18	1	6	8	1	Cell H -45.00% accuracy
0	2	0	10	5	0	0	16	0	0	7	0	Cell I -00.00% accuracy
3	0	0	1	0	0	15	2	0	13	2	4	Cell J -32.50% accuracy
0	1	0	0	1	0	2	13	0	1	1	21	Cell K -02.50% accuracy
0	0	0	0	0	0	0	0	0	0	0	40	Cell L -100.00% accuracy
Percent Accurate = 27.9167%												

FIGURE 7-5: CONFUSION MATRIX FOR 12-CELL LOCALIZATION RESOLUTION, NON-CENTERED LOCATIONS

A	B	C	D	E	F	G	H	I	J	K	L
0	0	0	0	0	0	39	0	0	0	0	0
0	0	0	0	0	0	2	0	14	0	0	0
0	0	0	0	0	0	0	0	0	0	0	0
0	0	0	0	0	1	0	0	1	0	2	0
0	0	0	0	0	0	0	0	2	3	1	0
0	0	0	0	0	0	0	0	0	0	0	26
0	1	0	0	0	0	26	0	0	0	0	0
0	0	0	0	0	0	14	0	0	0	0	0
0	0	0	0	0	0	0	0	14	0	0	0
0	0	0	0	0	0	0	0	0	21	0	0
0	0	0	0	0	0	0	0	0	0	0	0
0	0	0	0	0	0	0	0	0	0	0	0

Percent Accurate = 18.1250%

Cell A -00.00% accuracy
Cell B -00.00% accuracy
Cell C -00.00% accuracy
Cell D -00.00% accuracy
Cell E -00.00% accuracy
Cell F -00.00% accuracy
Cell G -65.00% accuracy
Cell H -00.00% accuracy
Cell I -35.00% accuracy
Cell J -52.50% accuracy
Cell K -00.00% accuracy
Cell L -72.50% accuracy

FIGURE 7-6: (A) CONFUSION MATRIX 24-CELL LOCALIZATION RESOLUTION, NON-CENTERED LOCATIONS

M	N	O	P	Q	R	S	T	U	V	W	X
1	0	0	0	0	0	0	0	0	0	0	0
4	0	0	0	0	0	0	3	17	0	0	0
9	9	0	0	12	0	5	5	0	0	0	0
7	0	0	1	0	0	0	24	0	0	0	4
6	12	0	0	4	0	0	0	1	0	0	11
0	0	0	0	0	0	0	0	0	0	0	14
10	0	0	0	0	0	2	2	0	0	0	0
19	4	0	0	0	0	1	1	0	0	0	0
7	17	0	0	0	0	2	0	0	0	0	0
0	0	0	0	0	0	19	0	0	0	0	0
1	0	0	0	20	0	0	7	12	0	0	0
0	0	0	0	10	0	0	0	0	0	0	1
12	0	0	0	0	0	0	2	0	0	0	0
10	1	0	0	6	0	0	1	2	1	0	0
13	0	4	0	0	0	0	2	1	1	0	0
1	2	0	0	4	0	0	2	0	0	0	0
0	8	0	0	16	0	0	0	0	0	0	0
0	0	0	0	4	0	0	0	0	0	0	35
11	5	0	0	0	0	3	16	0	0	0	1
0	0	0	0	0	0	24	8	0	0	0	0
12	4	0	0	3	0	8	6	1	0	0	0
0	0	0	0	0	0	1	0	0	0	0	0
1	6	0	0	11	0	2	1	5	0	0	0
0	0	0	0	0	0	0	0	0	0	0	39

Cell M -30.00% accuracy
Cell N -02.50% accuracy
Cell O -10.00% accuracy
Cell P -00.00% accuracy
Cell Q -40.00% accuracy
Cell R -0.00% accuracy
Cell S -7.50% accuracy
Cell T -20.00% accuracy
Cell U -2.50% accuracy
Cell V -0.00% accuracy
Cell W -0.00% accuracy
Cell X -97.5% accuracy

Percent Accurate = 18.1250%

FIGURE 7-6: (B) CONFUSION MATRIX 24-CELL LOCALIZATION RESOLUTION, NON-CENTERED LOCATIONS

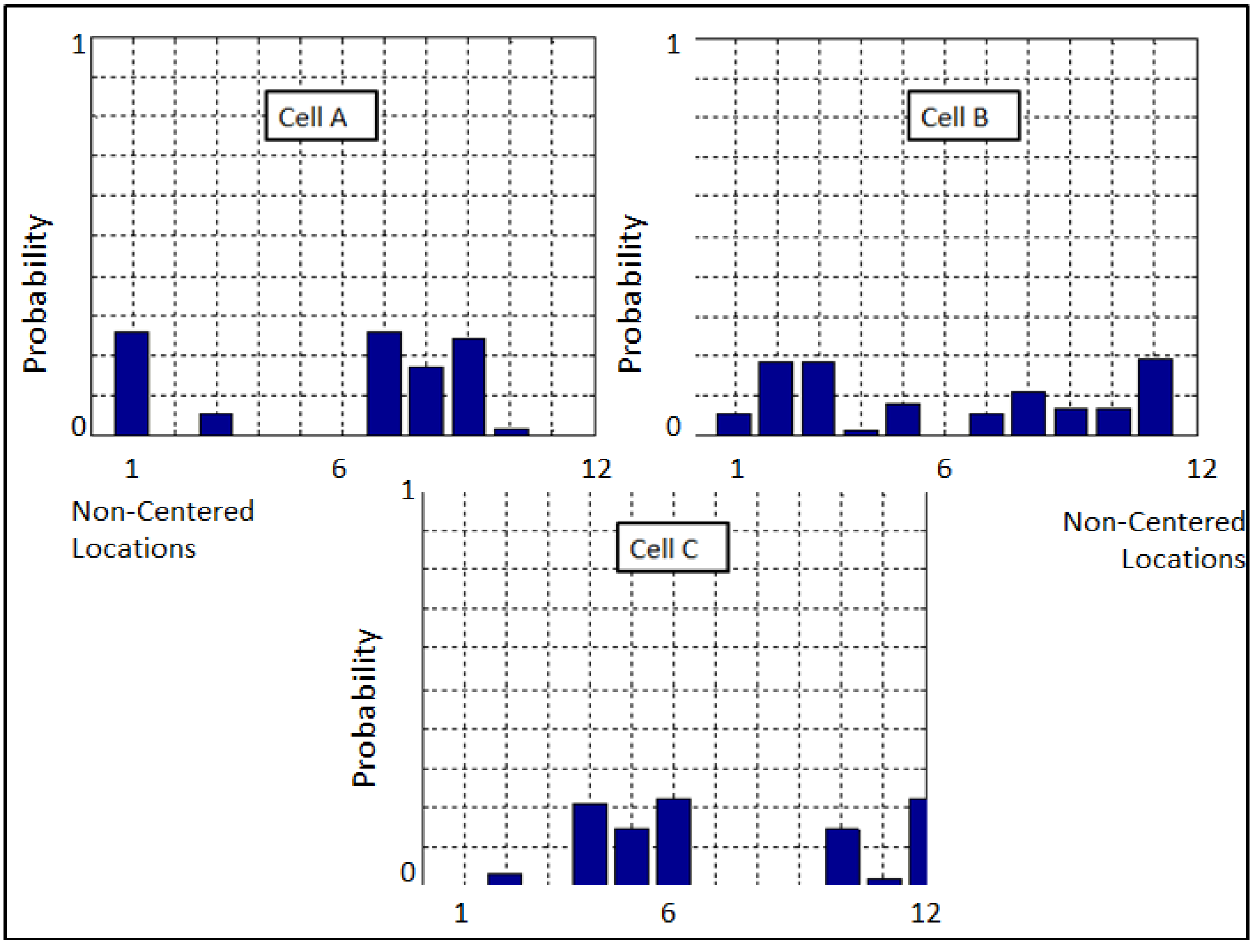

FIGURE 7-7: INDIVIDUAL ACCURACY OF NON-CENTERED LOCATIONS FOR 3-CELL LOCALIZATION RESOLUTION

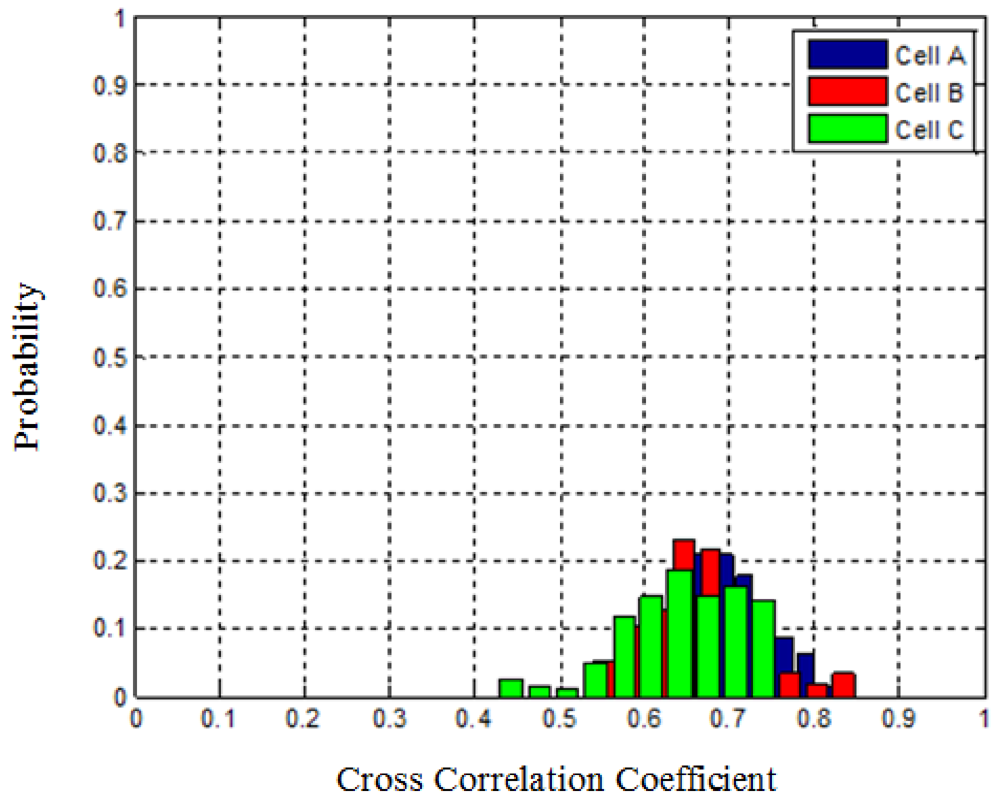

FIGURE 7-8: CROSS CORRELATION DISTRIBUTION FOR NON-CENTERED LOCATION 2, 3CLR

Using Weka in conjunction with the features extracted, provided an increase in the poor classification rate given by using only the MACC algorithm. For all the cell resolutions, the overall accuracy yielded an increase. Figure 7-9 and Table 7-1 show a graph depicting the increasing trend in the overall classification accuracy and a table of the classification accuracies from the 8 classifiers used on the entire feature set respectively (3CLR). The best classifier for this experiment was the Multilayer Perceptron, with an accuracy of 92.08%. For the 12CLR case, figure 7-10 and Table 7-2 depict the same information for the results showcased for 3CLR using Weka. The best classifier for this case was Simple Logistic Regression, with 97.29%. Lastly, figure 7-11 and Table 7-3 for the 24CLR case show a maximum classification accuracy of 96.25% under Logistic Regression. It is important to note that note all classifiers resulted in a similar trend of increasing accuracy. It is also important to note that in Weka, each resolution, existing with a different number of features, counts as a different experiment and does not follow the decreasing trend in accuracy as the number of cells increase. However, the statement can be made that with the addition of each feature, an improvement in the overall accuracy of classifying the non-centered locations into their respective cell of origin is present.

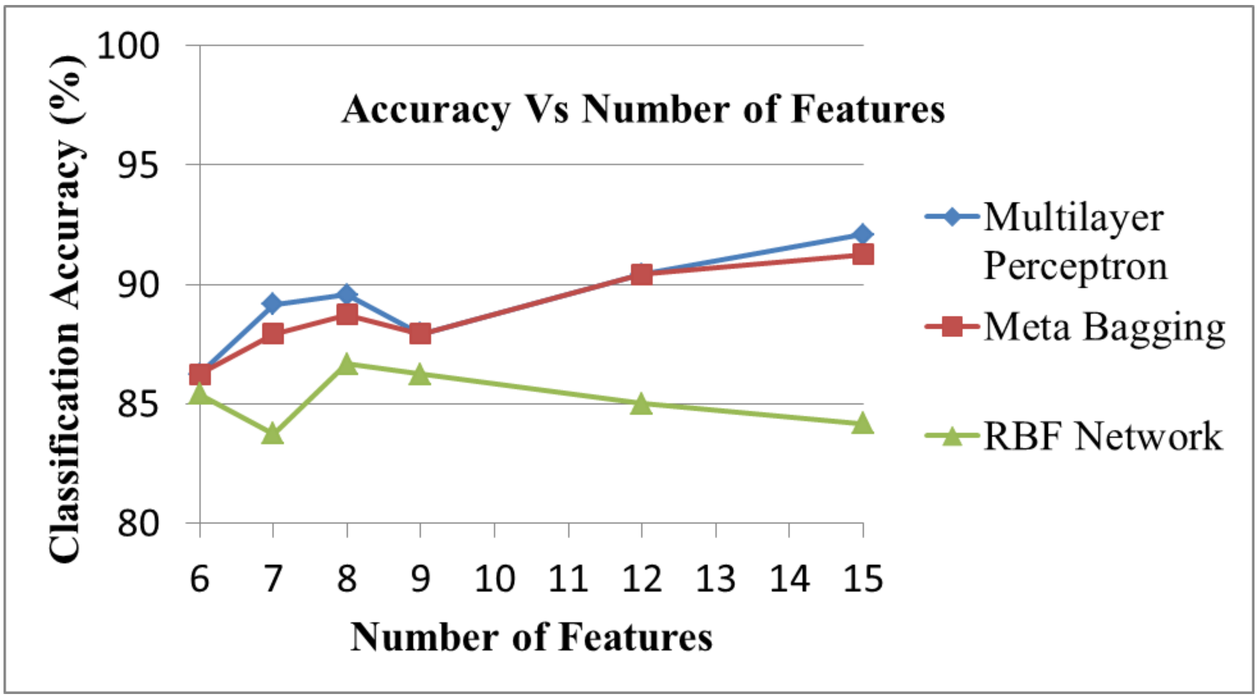

FIGURE 7-9: TREND IN CLASSIFICATION ACCURACY FOR 3CLR, NON-CENTERED LOCATIONS

Features:
Correlation Coefficient
Signal Length
Number of peaks above Threshold
Number of samples from start of wave to max peak
Standard Deviation
Kurtosis
Skewness

Classifier	Accuracy
Multilayer Perceptron	92.08%
Meta Bagging	91.25%
RBF Network	84.17%
J48 Decision Tree	89.17%
Logistic Regression	82.92%
Simple Logistic Regression	84.58%
SMO	86.67%
Naïve Bayes	78.75%

TABLE 7-1: LIST OF CLASSIFIERS AND THEIR ACCURACY FOR THE ENTIRE FEATURE SET FOR 3CLR, NON-CENTERED LOCATIONS

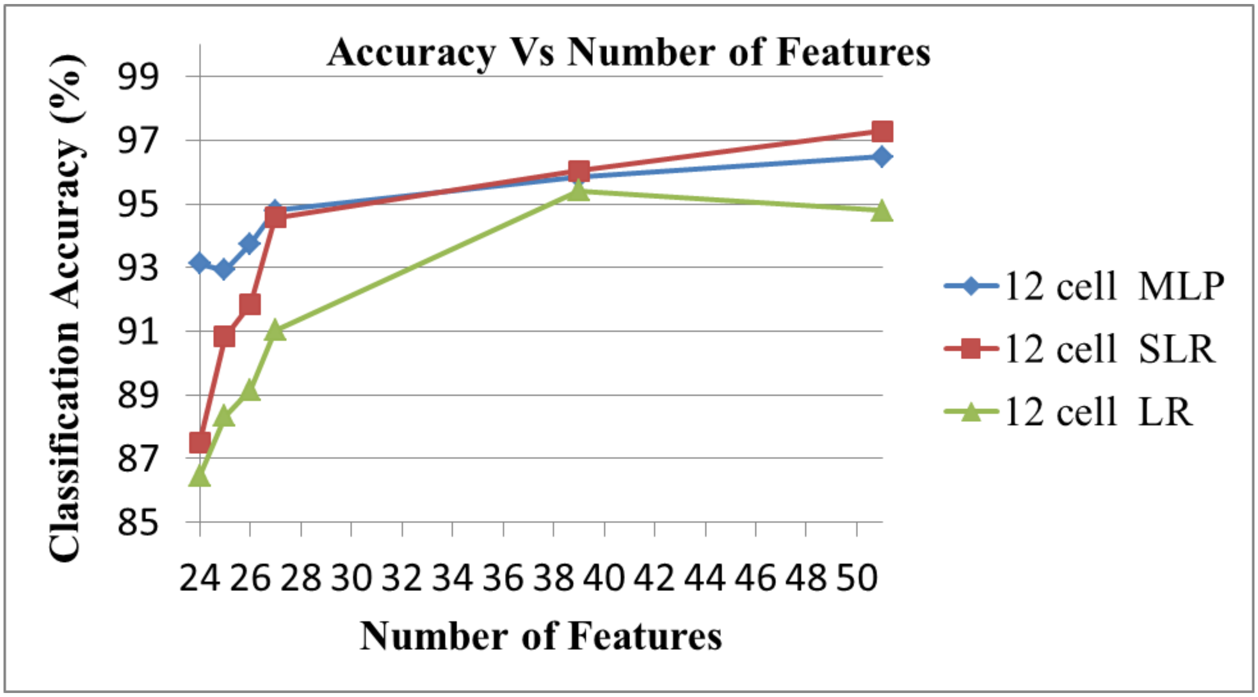

FIGURE 7-10: TREND IN CLASSIFICATION ACCURACY FOR 12CLR, NON-CENTERED LOCATIONS

Features:
Correlation Coefficient
Signal Length
Number of peaks above Threshold
Number of samples from start of wave to max peak
Standard Deviation
Kurtosis
Skewness

Classifier	Accuracy
Multilayer Perceptron	96.46%
Meta Bagging	89.58%
RBF Network	95.83%
J48 Decision Tree	84.17%
Logistic Regression	94.79%
Simple Logistic Regression	97.29%
SMO	95.42%
Naïve Bayes	87.08%

TABLE 7-2: LIST OF CLASSIFIERS AND THEIR ACCURACY FOR THE ENTIRE FEATURE SET FOR 12CLR, NON-CENTERED LOCATIONS

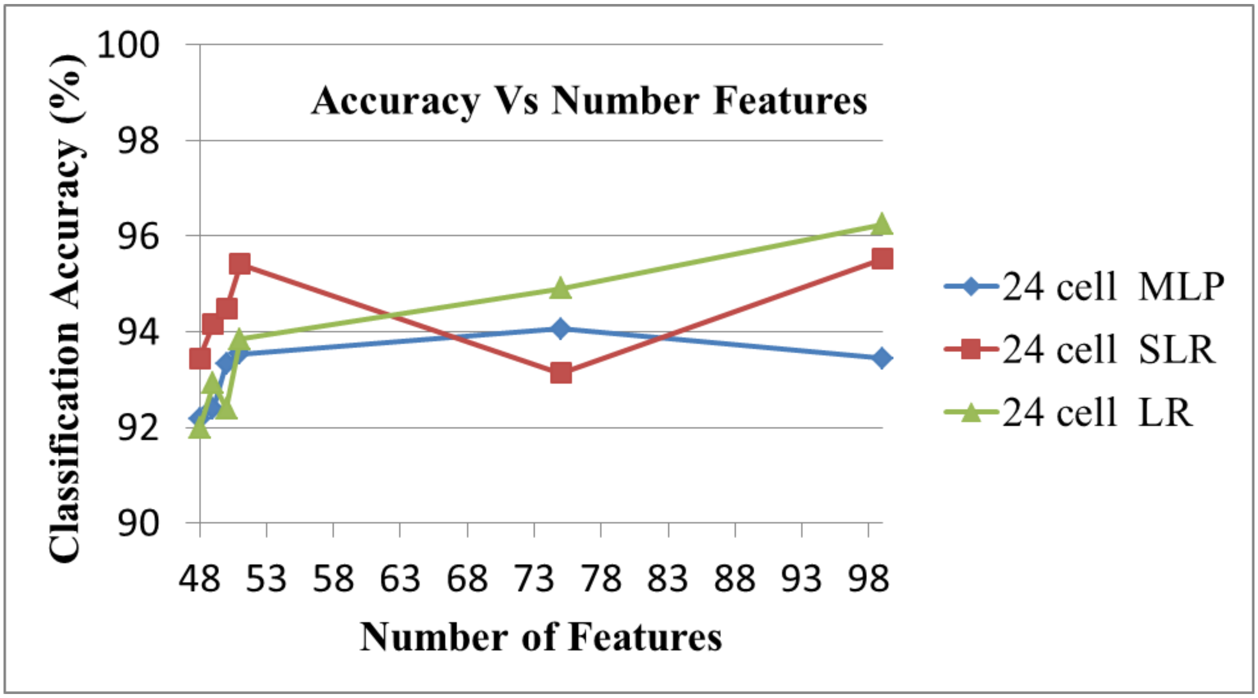

FIGURE 7-11: TREND IN CLASSIFICATION ACCURACY FOR 24CLR, NON-CENTERED LOCATIONS

Features:
Correlation Coefficient
Signal Length
Number of peaks above Threshold
Number of samples from start of wave to max peak
Standard Deviation
Kurtosis
Skewness

Classifier	Accuracy
Multilayer Perceptron	93.44%
Meta Bagging	90.00%
RBF Network	Lab machine
J48 Decision Tree	78.65%
Logistic Regression	96.25%
Simple Logistic Regression	95.52%
SMO	90.63%
Naïve Bayes	75.21%

TABLE 7-3: LIST OF CLASSIFIERS AND THEIR ACCURACY FOR THE ENTIRE FEATURE SET FOR 24CLR, NON-CENTERED LOCATIONS

7.4. Performance under Feature Reduction

In addition to assessing whether the feature set chosen for this thesis would be suitable enough to obtain high classification accuracy, other usefulness's can be found in optimizing a set of features that yield the best performance. Although that was not achieved in the scope of work within this thesis, Weka's feature reduction software proved helpful in the determination of the highest accuracy possible, using the smallest set of features possible. This tradeoff produced results that were able to lie close in value to the results using the entire feature set, and in the cases where a large amount of features are used, a drastic reduction in the size of the feature set became achievable. Figures 7-12, 7-13, and 7-14 show the results for feature reduction experiments performed on non-centered locations for 3, 12 and 24 cell localization resolutions respectively. Each experiment was conducted under the classifier in Weka in which the highest accuracy was given. For 3CLR, a combination of 8 features (Table 7-4) was chosen that resulted in an accuracy of 90.5%. In 12CLR and 24CLR, combinations of 11 (Table 7-5 & Table 7-6) different features were used, yielding accuracies of 93.55% and 90.72% respectively. This is of course, a large reduction in comparison to the total amount of features used (52 for 12CLR and 99 for 24CLR). Even with the occurrence of this phenomenon, high accuracy is still able to be obtained for localization classification.

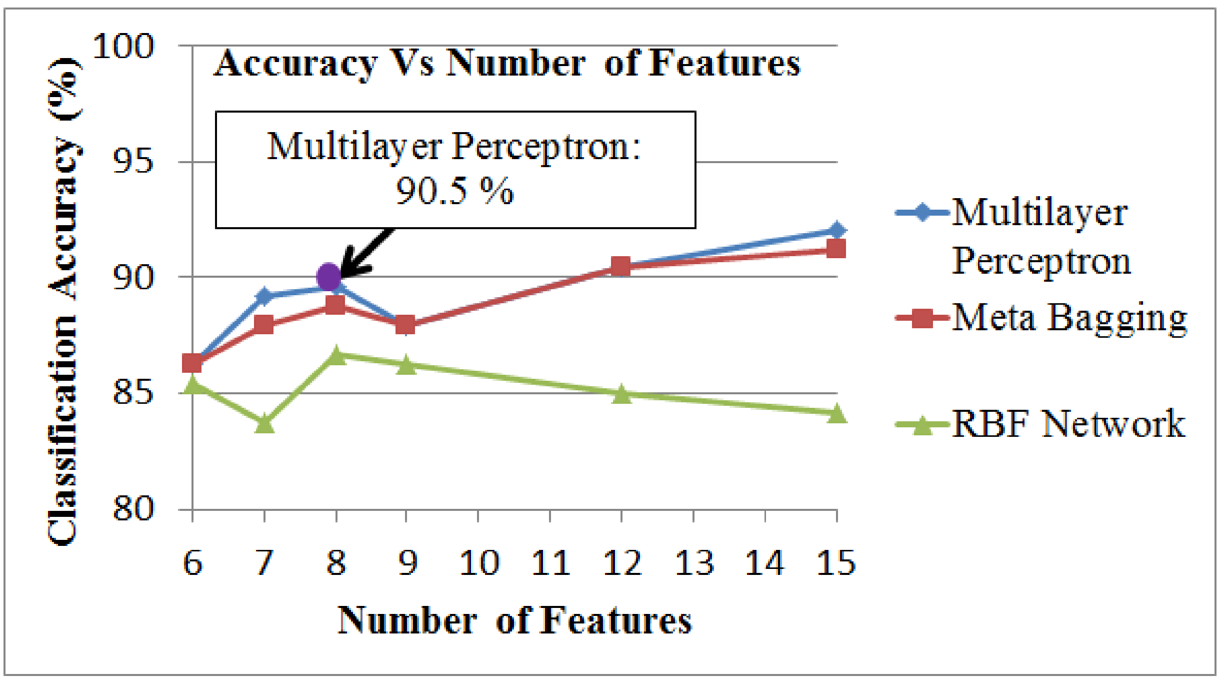

FIGURE 7-12: FEATURE REDUCTION PERFORMANCE FOR 3CLR, NON-CENTERED LOCATIONS

Reduced Feature Set for 3CLR
Signal Length with Respect to Cell A
Correlation Coefficient with Respect to Cell A
Correlation Coefficient with Respect to Cell B
Correlation Coefficient with Respect to Cell C
Number of Peaks Above Threshold
Standard Deviation
Kurtosis with Respect to Cell C
Skewnesss with Respect to Cell C

TABLE 7-4: REDUCED FEATURE SET FOR 3CLR

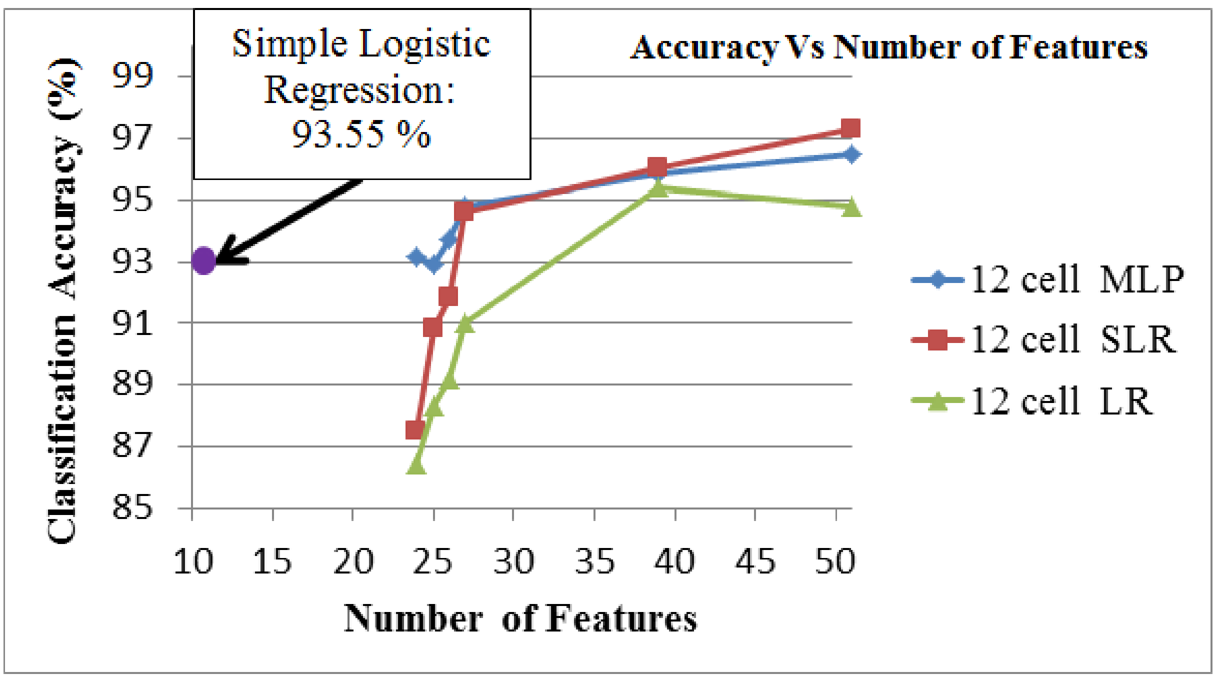

FIGURE 7-13: FEATURE REDUCTION PERFORMANCE FOR 12CLR, NON-CENTERED LOCATIONS

Reduced Feature Set for 12CLR
Signal Length with Respect to Cell A
Correlation Coefficient with Respect to Cell D
Correlation Coefficient with Respect to Cell F
Correlation Coefficient with Respect to Cell H
Correlation Coefficient with Respect to Cell I
Correlation Coefficient with Respect to Cell J
Standard Deviation
Kurtosis with Respect to Cell D
Kurtosis with Respect to Cell G
Skewnesss with Respect to Cell F
Skewnesss with Respect to Cell L

TABLE 7-5: REDUCED FEATURE SET FOR 12CLR

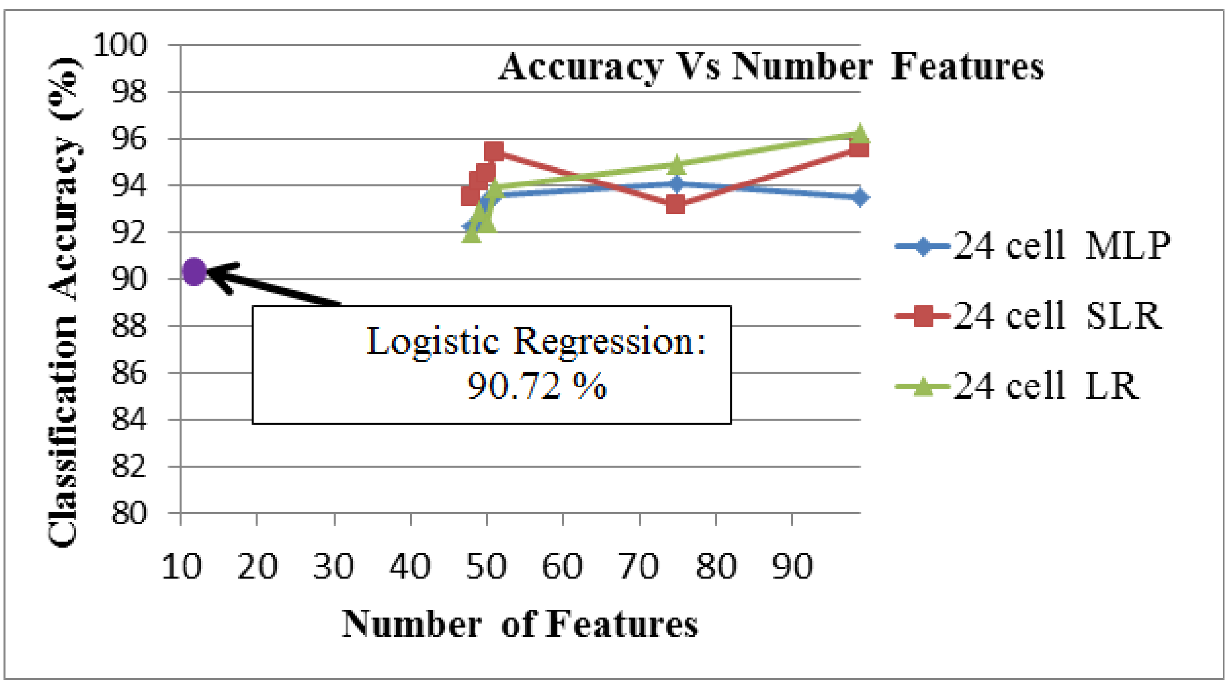

FIGURE 7-14: FEATURE REDUCTION PERFORMANCE FOR 24CLR, NON-CENTERED LOCATIONS

Reduced Feature Set for 24CLR
Correlation Coefficient with Respect to Cell A
Correlation Coefficient with Respect to Cell C
Correlation Coefficient with Respect to Cell D
Correlation Coefficient with Respect to Cell F
Correlation Coefficient with Respect to Cell G
Correlation Coefficient with Respect to Cell N
Correlation Coefficient with Respect to Cell O
Correlation Coefficient with Respect to Cell V
Number of Samples from start of wave to max peak
Standard Deviation
Kurtosis with Respect to Cell X

TABLE 7-6: REDUCED FEATURE SET FOR 24CLR

7.5. Summary

The results presented in this chapter lead way to a few key points and the understanding behind what governs their occurrence. It is essential to get a view of the feasibility of the approaches presented in this thesis for the purpose of ultrasound localization on a metal substrate. The accuracy for center of cell cases is extremely high using only the MACC algorithm to classify cells positions. As the cell resolution increases, the accuracy decreases, but not enough to bring about substantial change in the way the center of cell cases are classified. Using the same method for non-centered locations does not yield the same results, but worsens the classification accuracy drastically, due to immense overlap within the regions of the correlation coefficient distribution. Weka is then used in conjunction with the features previously extracted, to increase the accuracy to more desirable results. With the use of Weka for non-centered locations and the MACC algorithm for centered locations, it can be seen that this attempt at ultrasound localization was quite successful for the system implemented in software, producing classification accuracies above 90% for all cases.

CHAPTER 8: RUN-TIME LOCALIZATION

Thus far, any attempts presented in this thesis for successful ultrasound localization have all been implemented via MATLAB, with previously collected data, and have had very little consideration for real world constraints that are always present in the creation of a real system. This and the following chapters leading up to the conclusion of this thesis, shall all involve the implementation of a run-time localization system, with the intent of generating localization accuracy similar to what has been achieved and presented in Chapter 7.

8.1. Motivation

Producing a run-time system capable of ultrasound localization on a metal substrate is essential for applications of Structural Health Monitoring. The presence of a system in which normal areas of constraints such as energy efficiency, storage capacity, sampling rate and processing power don't exist or are ignored, would be overlooking some of the fundamental areas of research in terms of applications for wireless sensor networks. Therefore, it is most useful to be able to begin to introduce these constraints in the form of a run-time system, and evaluate the minimum requirements needed to achieve successful implementation of a localization system in an ultrasonic sensor network.

8.1.1. Hardware Constraints

The localization system implemented in MATLAB relies on a few key factors that contribute to its performance. For ultrasound pulse transmission, a constant 6V power source is applied to the transmitter. For data collection via the stand-alone piezo, an oscilloscope with an extremely high sampling rate is used to reconstruct the signal. For processing and storing, a desktop machine is used in combination with powerful software such as MATLAB and Weka to perform the classification directly on the host machine. Unfortunately, some of these elaborate approaches prove infeasible for a run-time system. As a result, the areas mentioned will now become constraints for the development of the system. The transmission power of 6V will now be used as an upper bound for all power delivered to the run-time system. Data collection will be no longer done at high sampling rates. Instead, an approach at uncovering a lower bound on the sampling rate needed to maintain high localization accuracy will be determined. Processing of the signal to produce an envelope will need to be accomplished in hardware, to alleviate the level of computational complexity needed in the use of a commercial microcontroller, which will also be used to sample the signal and send the processed data to a base station like machine. Utilization of such a method, allows for the host machine to be alleviated of all the tasks for localization, as performed thus far in this thesis. Lastly, it is important to note that the introduction of passive and/or active circuit elements will also bring more real world issues into the development phase. More of these issues will be discussed during the explanation of the proposed system design in the upcoming chapter.

8.2. Down Sampling Experimentation

Before continuing further with any step in the implementation of a run-time system, the minimum sampling rate needed to reconstruct an envelope signal is crucial to the performance of the new system. Without proper reconstruction, the basis of all the classification algorithms becomes null and void. Therefore, experiments were done in MATLAB to determine such a value. By examining the cutoff frequency of FFT of the envelope produced in MATLAB, the minimum sampling frequency needed to reconstruct the envelope can be determined by observing twice the value of the cutoff frequency, satisfying the commonly known sampling theorem. Figure 8-1 shows the frequency domain of the envelope signal. The entire sets of envelopes generated are down sampled and ran through the MACC algorithm just as before. The newly down sampled envelope then has its FFT examined to acquire the cutoff frequency. A script is written in MATLAB that continues to perform the down sampling and records the cutoff frequency value associated with it. From here, Figures 8-2 through 8-4 are produced for each cell resolution, which shows the relationship between localization accuracy and the sampling rate. From these figures, it can be observed that for the 3CLR case, a sampling frequency of approximately 25 kHz is needed to maintain previous results of localization accuracy, and for 12CLR and 24CLR, approximately 50 kHz.

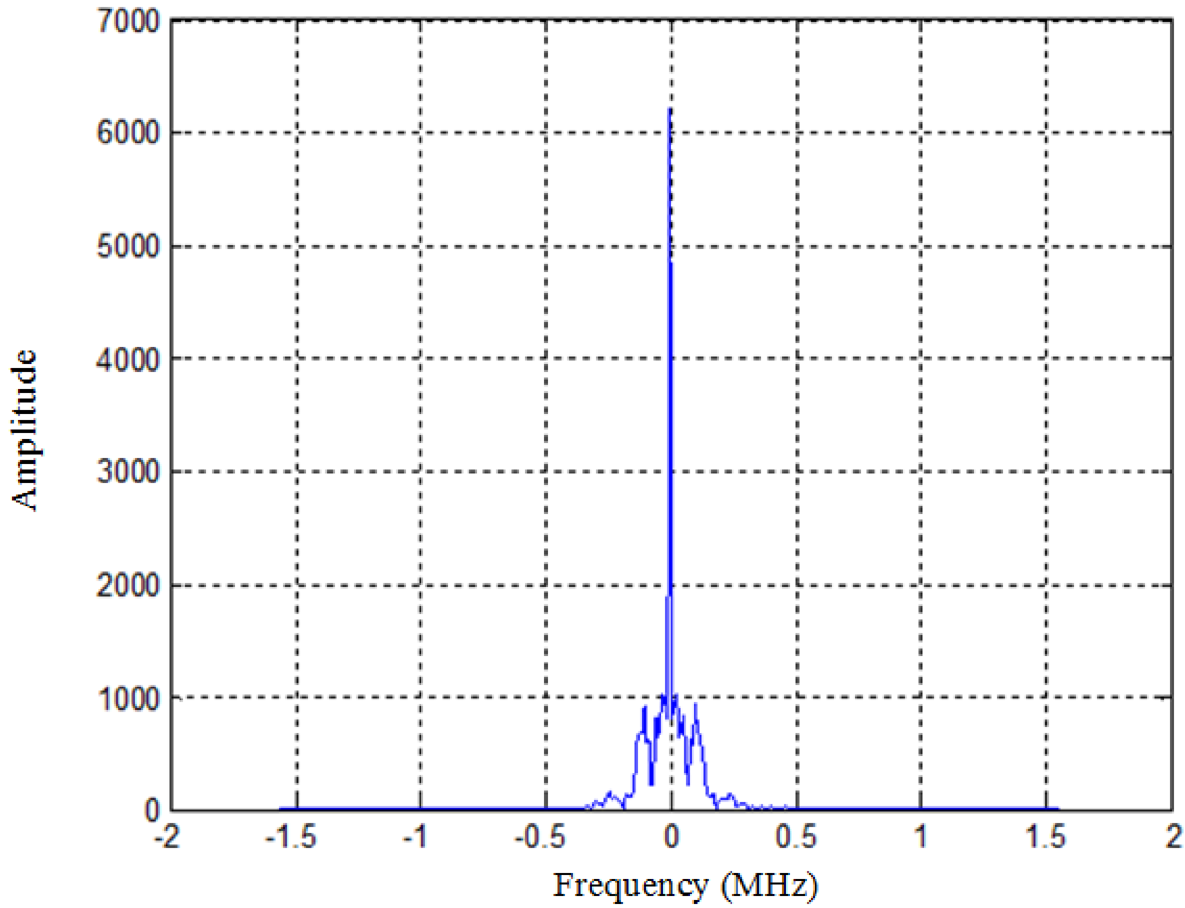

FIGURE 8-1: FREQUENCY DOMAIN PLOT OF RECEIVED ENVELOPE SIGNAL

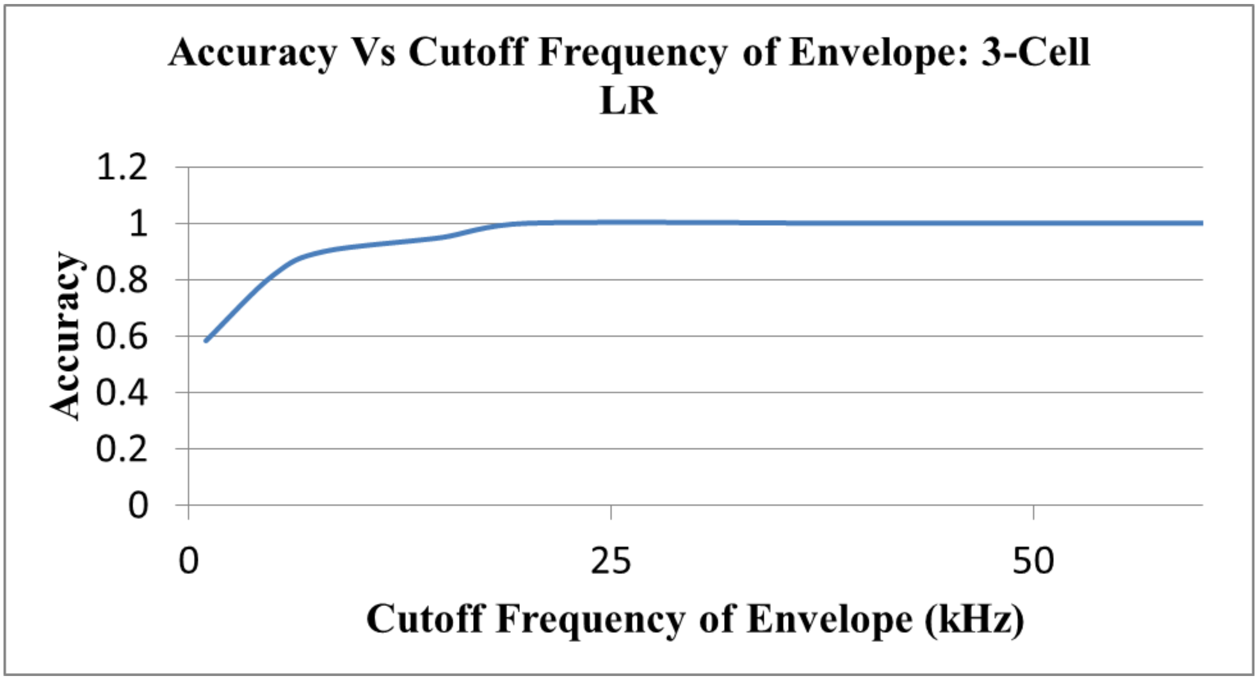

FIGURE 8-2: ACCURACY VS. CUTOFF FREQUENCY OF ENVELOPE FOR 3CLR

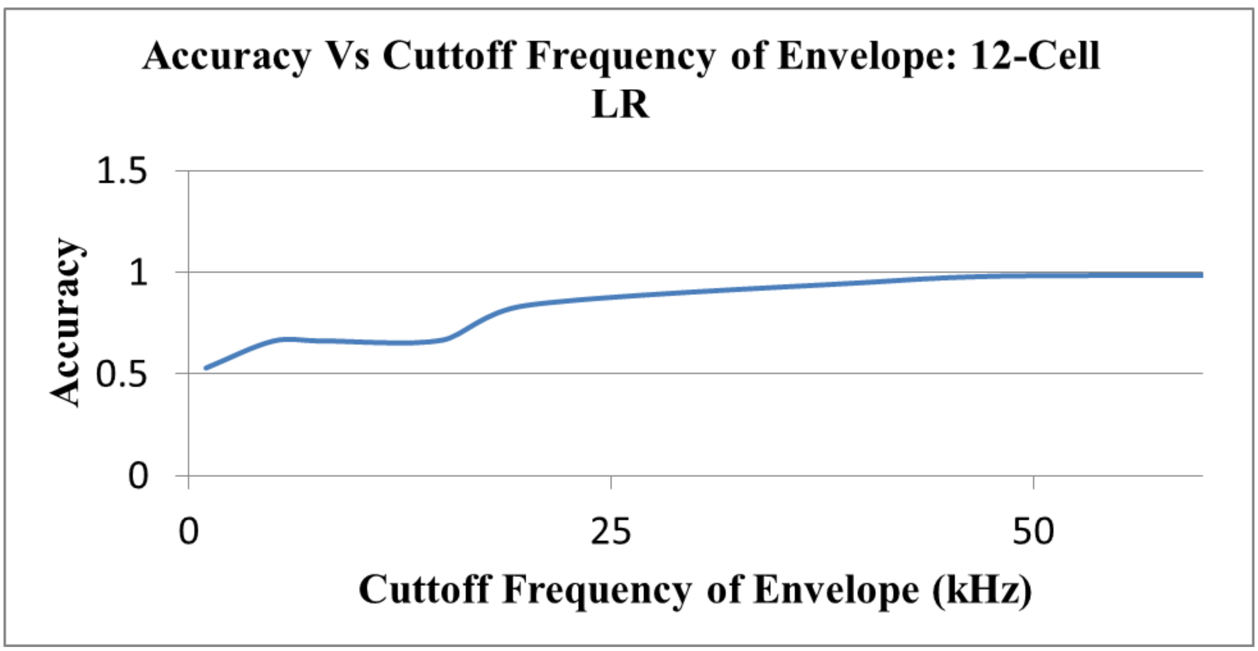

FIGURE 8-3: ACCURACY VS. CUTOFF FREQUENCY OF ENVELOPE FOR 12CLR

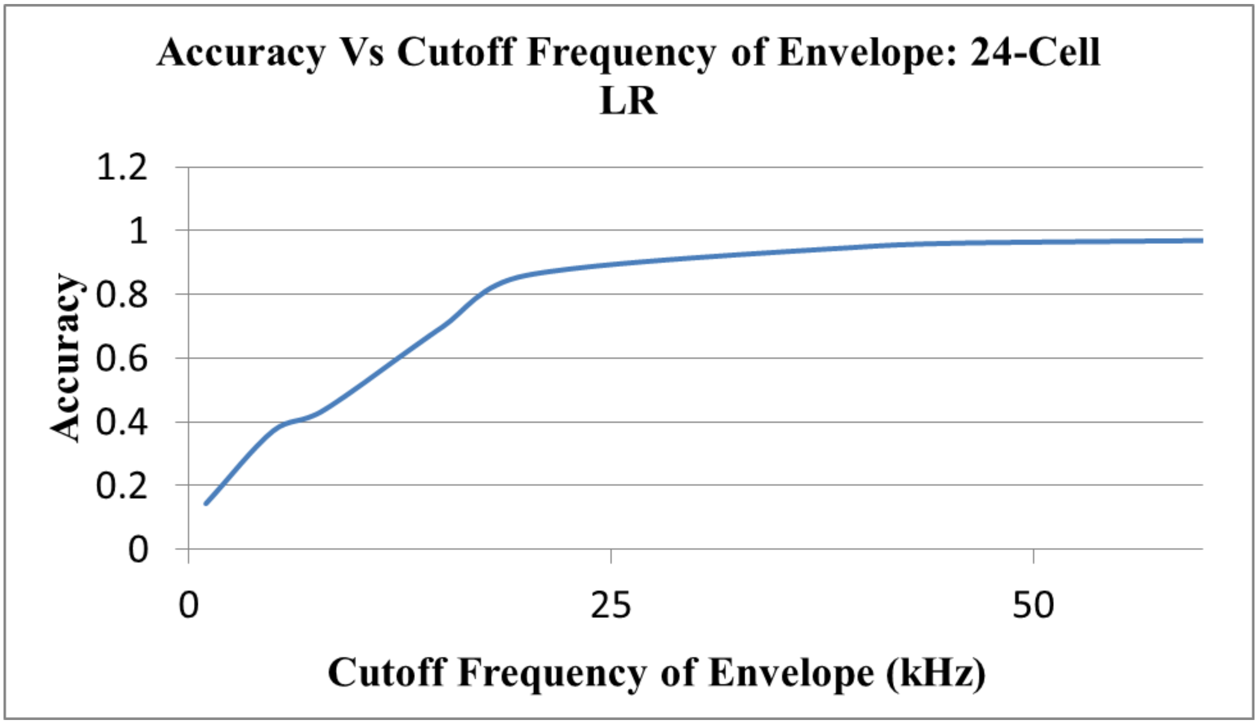

FIGURE 8-4: ACCURACY VS. CUTOFF FREQUENCY OF ENVELOPE FOR 24CLR

8.3. Summary

The results presented in this chapter show that many real world constraints will exist during the implementation of a run-time system for ultrasound localization on metal substrate. One of the main constraints lies in the area of the sampling frequency. Previously being sampled at a higher rate, the signal of use must now be sampled at a rate that is low enough to be achieved through a commercial microcontroller, but high enough to properly reconstruct the envelope and provide reasonable localization accuracy. From the set of figures presented in this chapter, and performing research on the sampling rates capable by common microcontrollers, it can be seen that it in theory it is possible to maintain a good degree of accuracy comparable to the system implemented via MATLAB.

CHAPTER 9: SYSTEM DESIGN AND EXPERIMENTAL LOCALIZATION PERFORMANCE

Taking into consideration the constraints mentioned in Chapter 8, a run-time system that operates on 3.57 Volts (Vcc of the microcontroller), was designed for the purpose of ultrasound localization on a metal substrate. The performance of each stage of the system is heavily evaluated, and when applicable, will be compared with the system implemented via MATLAB. The overall performance of the entire system will also be evaluated with respect to the results obtained from earlier work in this thesis. Figure 9-1 depicts the end-to-end block diagram for the entire system, beginning with the input of the raw signal. The amplifiers are used to increase the signal amplitude to a voltage level suitable enough to be detected by the envelope circuit, and to be able to compensate for the attenuation that it will present. The low pass filters are placed in a position to remove any unwanted higher frequencies that may cause aliasing to occur before the sampling done by the Analog-to-Digital Conversion (ADC) Channel used by the microcontroller (MSP430). Lastly the comparator and IRIS mote work in conjunction with one another to act as a timer triggered switch that is used to inform the microcontroller to sample the received envelope on its rising edge. This sampled data is then sent to the PC to calculate and display the classification of cell positions in run-time. The overall goal of developing such a chain in hardware is to evaluate the performance of localization system, undertaking the real world constraints that may follow. Under the presence of such real world constraints, the performance of the run-time system is expected to be comparable with the system in which those same constraints were not present. In this chapter, the experimental localization results of the run-time system will also be presented, and for the center-of-cell case.

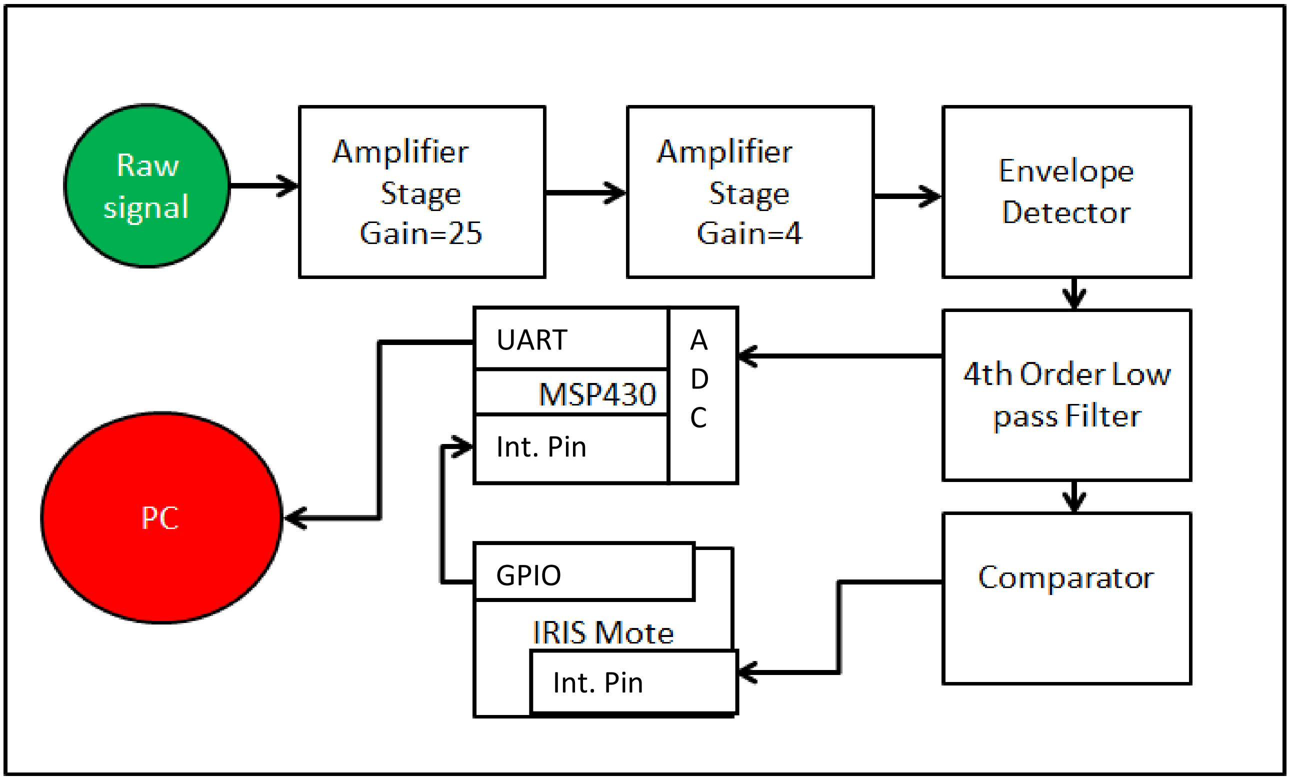

FIGURE 9- 1: RUN-TIME SYSTEM BLOCK DIAGRAM

9.1. Amplifier Design

From early observation of the peak-to-peak voltage of the raw signal, it has been deemed too low to perform the filtering needed in subsequent operations of the system. As a result, a stage of amplification was determined to be the first initial step necessary in the chain of stages for the run-time system. In order to design an amplifier with a gain capable of providing sufficient amplification of the signal throughout the entire plate, experiments were conducted to measure the received voltage level of the ultrasound signal at maximum plate distances (i.e., the 3 remaining corners of the plate). Figure 9-2 shows the raw signal measurements obtained from the previously mentioned experiments. Based on these measurements, conventional a non-inverting amplifier was designed and implemented in two stages with a gain of 25 and a gain of 4, via the MAX4488 operational amplifier, provided by Maxim Integrated Circuits. The parameters that control the gain were varied to provide the best coverage possible, while staying in line with the minimum requirements for input voltage levels for the subsequent components in the system chain. Figure 9-3 illustrates the regions in which the amplification exists in the usable boundaries (component dependent), without the loss of signal data in the form of peaks (through the effects of saturation or attenuation). The red areas outline the regions in which there is saturation and signal data is lost, the yellow areas depict possible areas of saturation (PZT coupling dependent), and the green areas show the regions in which the amplification does not cause the loss of ultrasound waveform information. Overall, the results here indicate that it is possible to cover a large area of the plate and not lose drastic amounts of signal integrity.

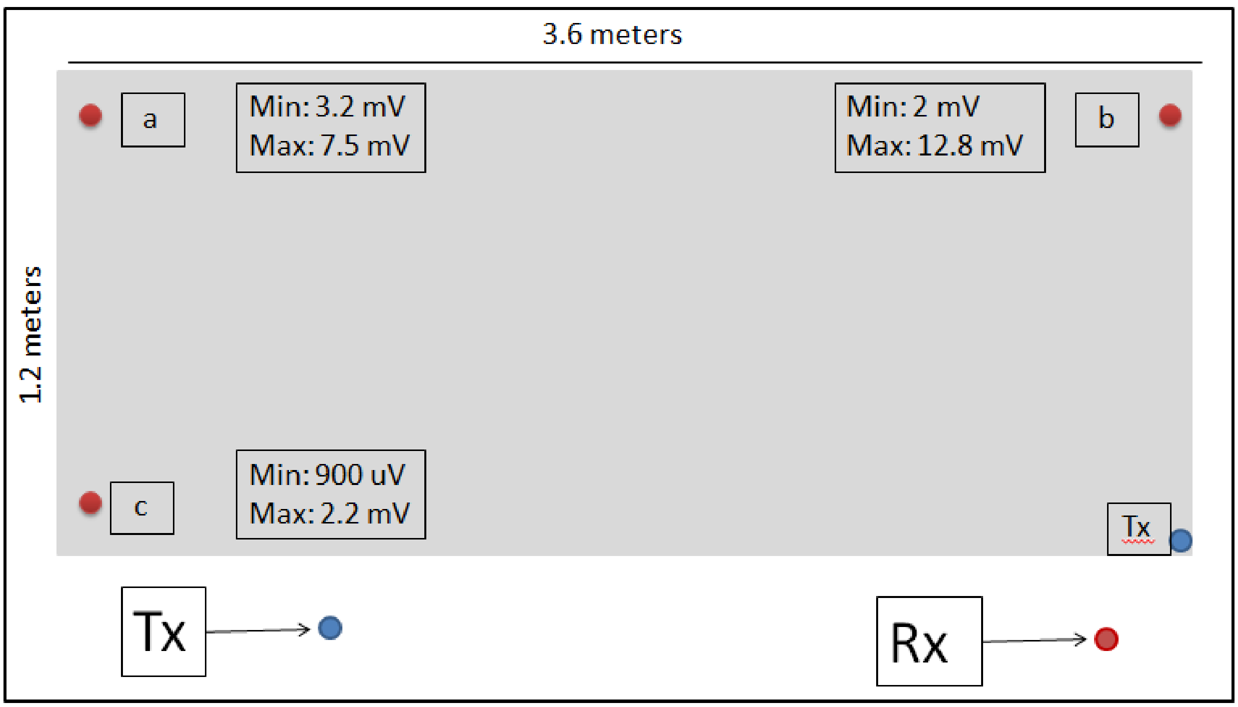

FIGURE 9-2: MEASUREMENTS OF RAW SIGNAL AT MAX PLATE DISTANCES

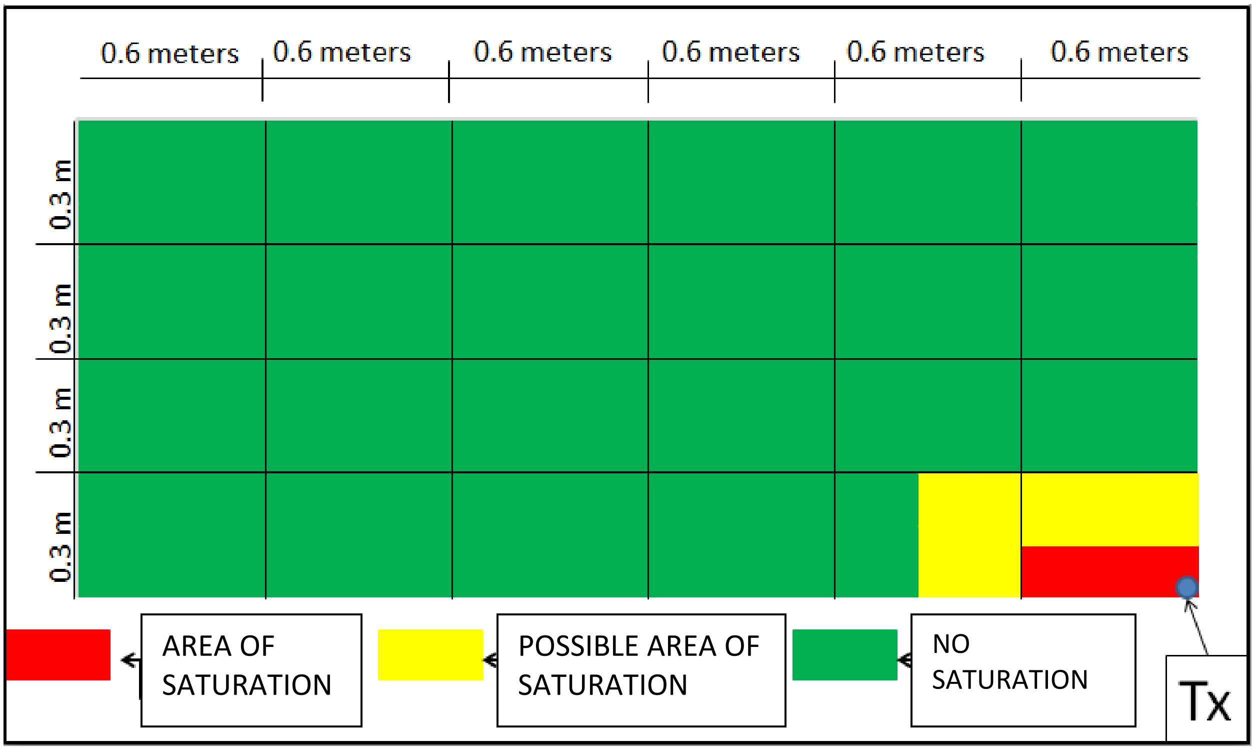

FIGURE 9-3: AMPLIFIER REGIONS OF OPERATION

9.2. Envelope Detector

The creation of the envelope signal is produced in hardware by utilizing a germanium diode in series with a resistor and capacitor in parallel. Figure 9-4 shows the schematic diagram represented by circuit elements. The performance of the envelope detector is showcased in figure 9-5, comparing the output of the two amplifier stages to the envelope produced. From this figure, it can be shown that the performance overall is visually good in terms of the overall shape similarity between the two waveforms. However, it is noted and exemplified in Figure 9-6, that there are high frequency components that are still present, that could alter the performance of the overall system if they are not properly dealt with. Under a closer inspection, it can be seen that the frequency components that are unwanted lie in the 245 kHz range and the harmonics associated with it. The dominant frequency components of the envelope do not exceed 25 kHz. Depending on the sampling frequency limitations of the microcontroller that will be used (discussed later), there can be many implications of attempting to sample this signal, one being a potential aliasing problem. Therefore, to produce an envelope signal comparable to those created in MATLAB, an RC Low Pass Filter was implemented to remove the higher frequencies and smoothen out the signal.

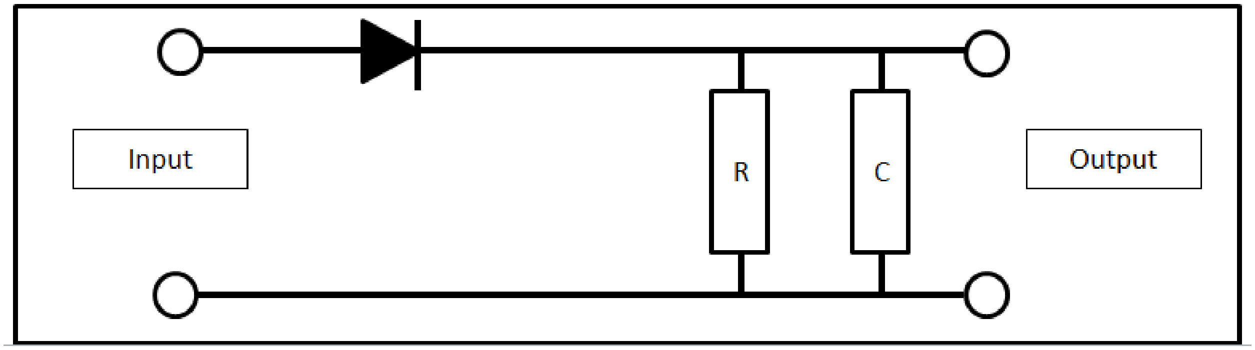

FIGURE 9-4: SCHEMATIC OF ENVELOPE DETECTOR CIRCUIT

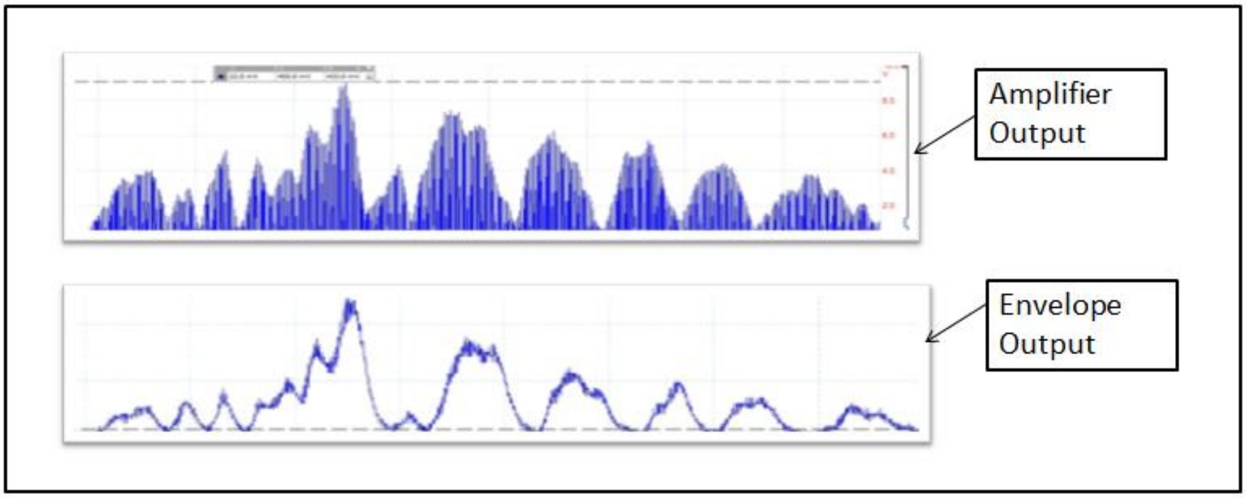

FIGURE 9- 5: PERFORMANCE OF ENVELOPE DETECTOR CIRCUIT

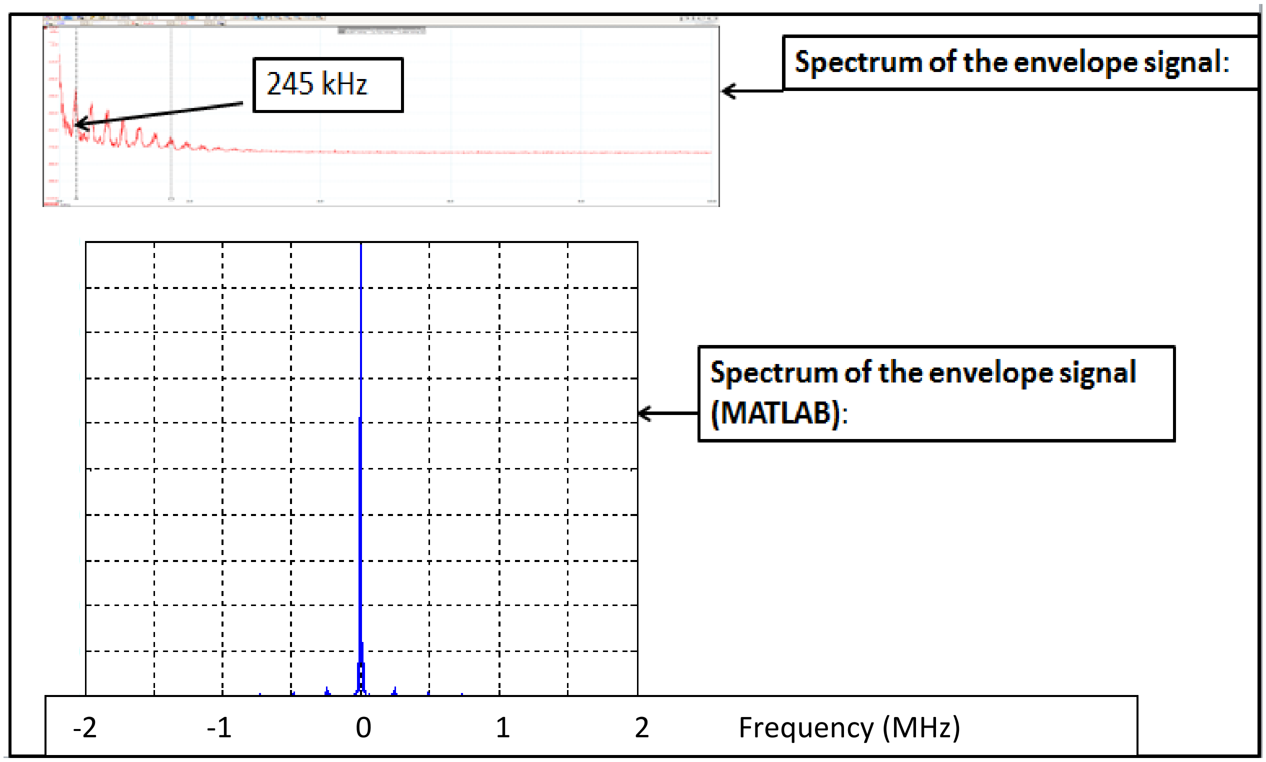

FIGURE 9-6: FREQUENCY DOMAIN OF THE ENVELOPE SIGNAL IN HARDWARE

9.3. Low Pass Filter

In order to verify that a filtering process would prove useful, the envelope produced in hardware was sampled via the Picoscope and filtered via a 4th Order Butterworth Filter in MATLAB. Figure 9-7 shows the results of the filtering process. The left graph shows before the filtering took place and the right graph is the envelope after the filtering has taken place. From this, it can be concluded that in theory, a low pass filter should be sufficient in removing the unwanted frequency components. As a result of the preliminary tests done in MATLAB, a traditional 3rd RC low pass filter was implemented to remove the frequency components that are unwanted in the newly produced envelope signal. The cutoff frequency is designed to reach a theoretical value of 50 kHz. The performance of each order is evaluated by observing its effect on the removal of the high frequency components of the envelope signal. Figure 9-8 is the bode plot of the magnitude portion of each order of the low pass filter, indeed verifying that the design and functionality is correct. This figure was produced by using a function generator to vary the frequency of an input signal while using an oscilloscope to measure the received signal strength. Figure 9-9 (a&b) shows how the low pass filter behaves. The addition of each cascaded stage continues to remove higher frequencies and smoothen out the envelope. The left graphs represent the envelope signal in the time domain, while the right set of graphs are in the frequency domain. These figures make it known that exceeding the implementation of a third order passive low pass filter is unnecessary and any further filtering will simply cause more attenuation in the envelope.

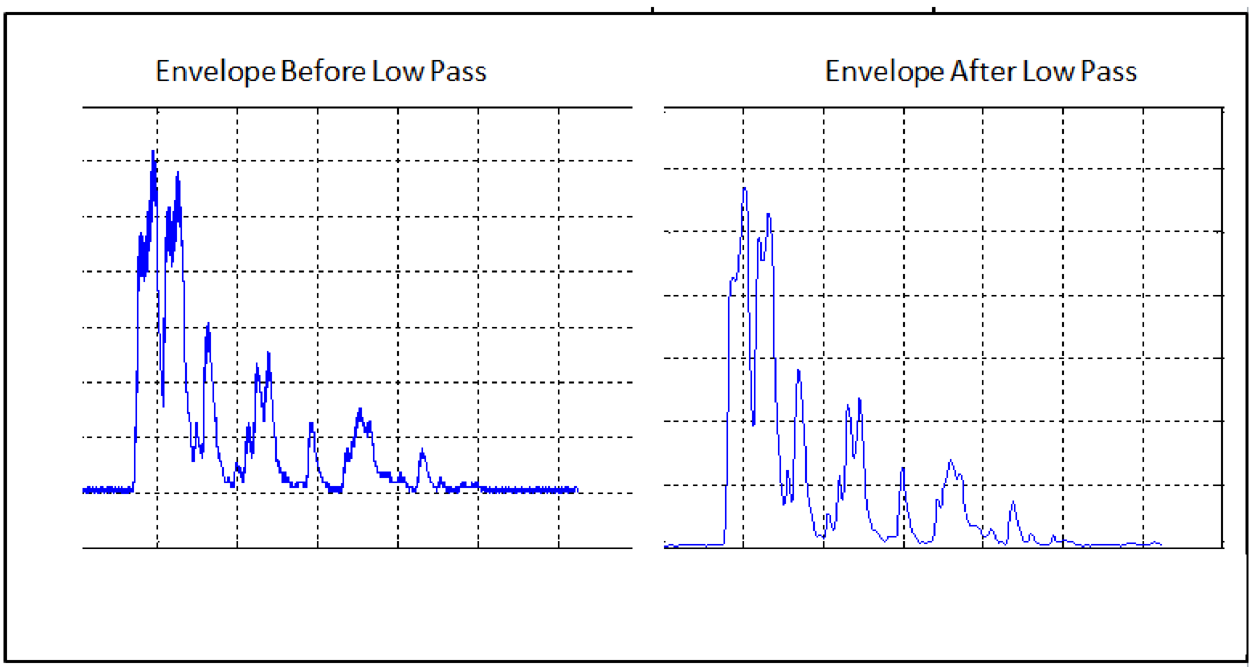

FIGURE 9-7: EVALUATION OF FILTERING PROCESS IN MATLAB

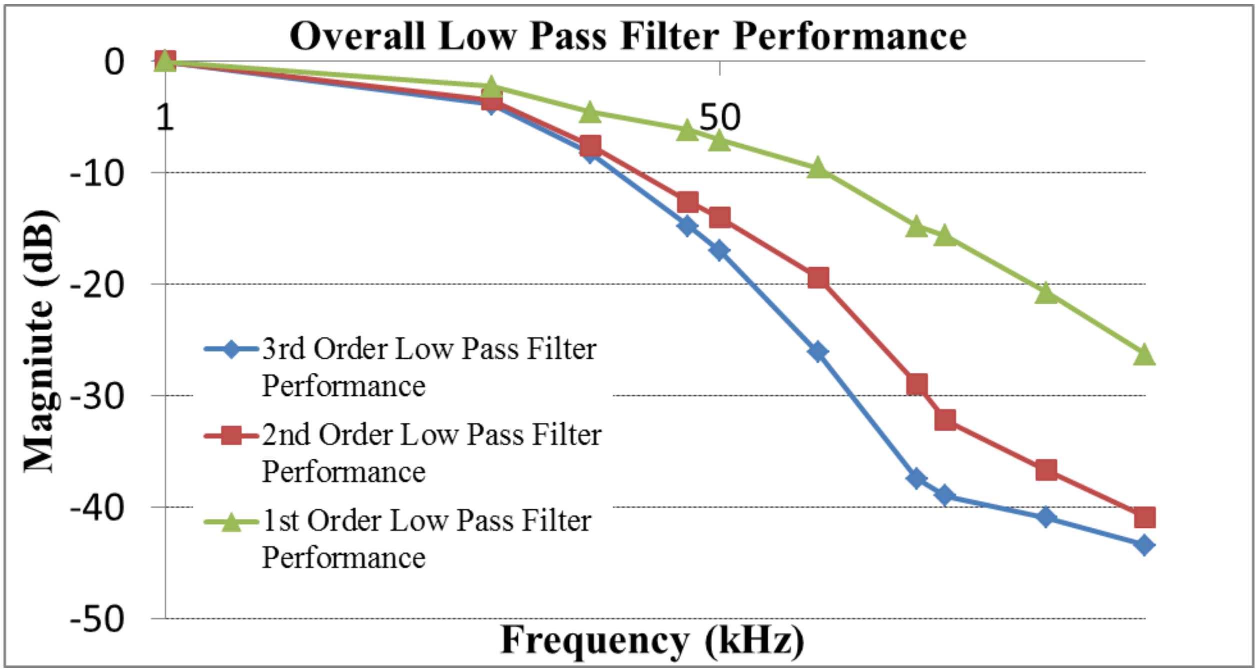

FIGURE 9-8: MAGNITUDE BODE PLOT OF PASSIVE LOW PASS FILTER

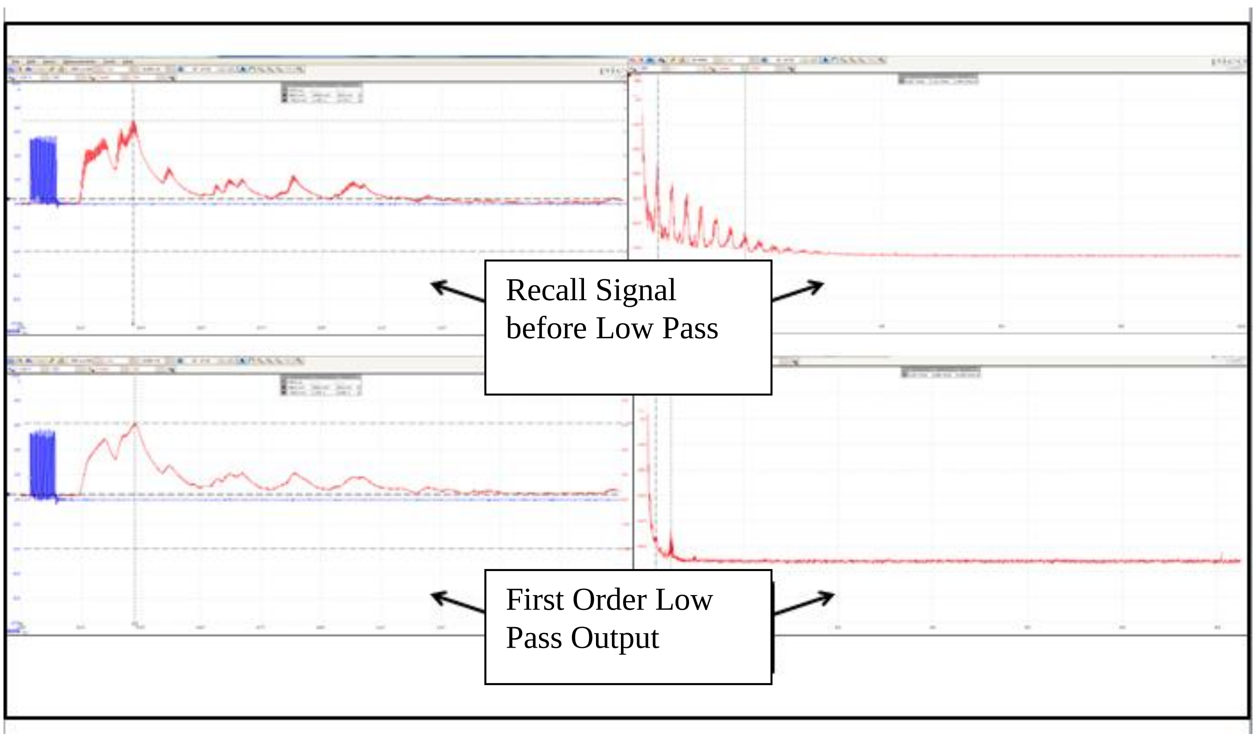

FIGURE 9-9: (A) PERFORMANCE OF LOW PASS FILTER IN SYSTEM

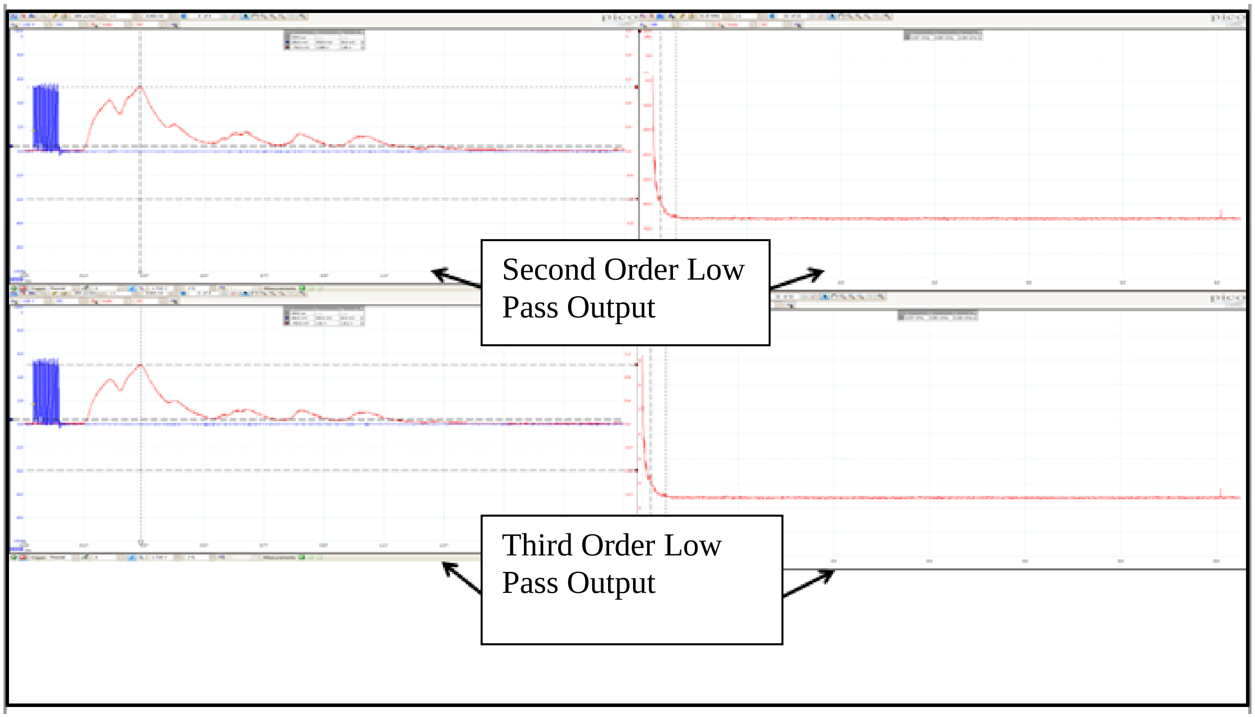

FIGURE 9-9: (B) PERFORMANCE OF LOW PASS FILTER IN SYSTEM

9.4. Comparator Circuit

As mentioned briefly in the beginning of this chapter, a basic comparator is implemented. Using the MAX4488 used to create the non-inverting amplifier stages; the insertion of a comparator circuit is made possible. The comparator is fed the signal output from the low pass filter, and it operates under a threshold of 50 mV, set through experimental observations of the envelope signal. Similar to the tests done to set the amplifier gain, the envelope amplitude was measured at maximum plate distances. These results led to the configuration of the threshold value for the comparator circuit. Figure 9-10 depicts these values for the three remaining corners on the metal substrate. This triggering from a low to high state of the comparator enables the microcontroller (discussed in detail in a later section of this chapter), to be able to sample on the rising edge of the envelope signal. Recall that the original signal is continuous, but there are periods of inactivity, due to the time (30 milliseconds) in between each transmission pulse. As a result, it is difficult for the ADC Channel of the microcontroller to sample the envelope at the proper moment. Figure 9-11 depicts the output of the comparator function and the envelope detector, comparing the rising edge time between the two. From this figure, it can be seen that its performance is a bit inaccurate in terms of the timing between when the envelope signal does occur and when the comparator threshold detects it. There is approximately 60 microseconds of difference between the signals. The loss of potentially 60 microseconds of data in stored in the microcontroller will not cause a drastic effect in the performance of the system, which will be discussed in a later section of this chapter.

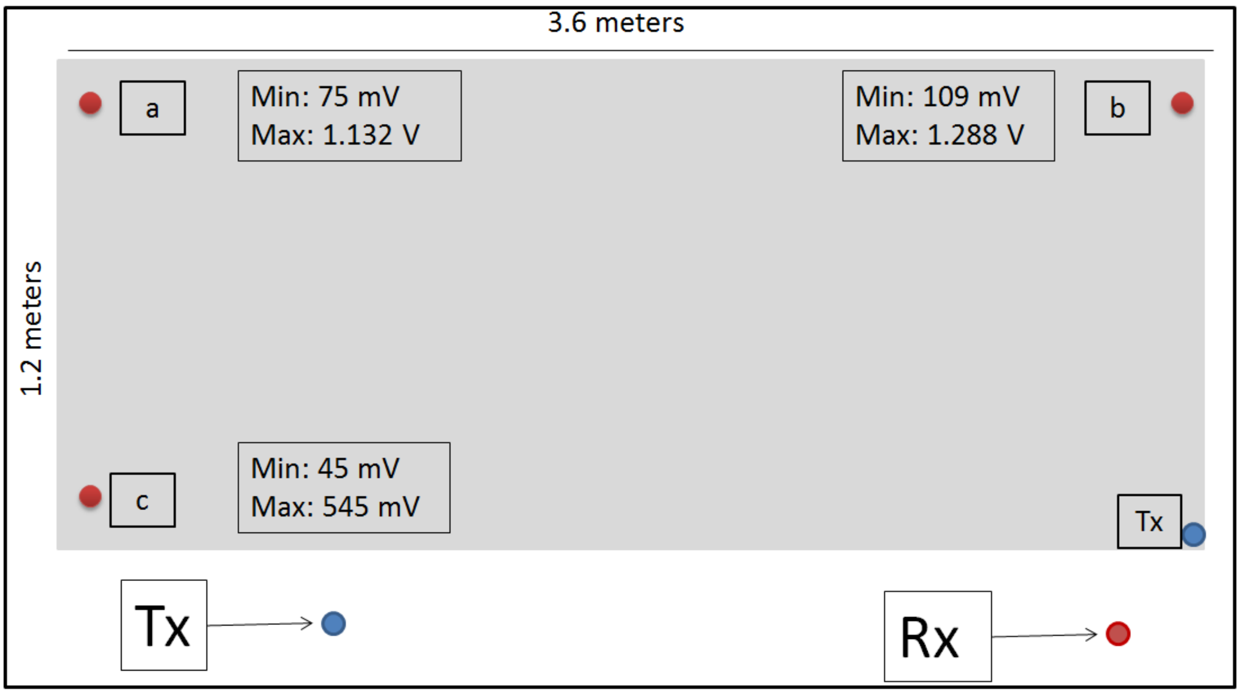

FIGURE 9-10: MEASUREMENTS OF THE ENVELOPE SIGNAL AT MAX PLATE DISTANCES

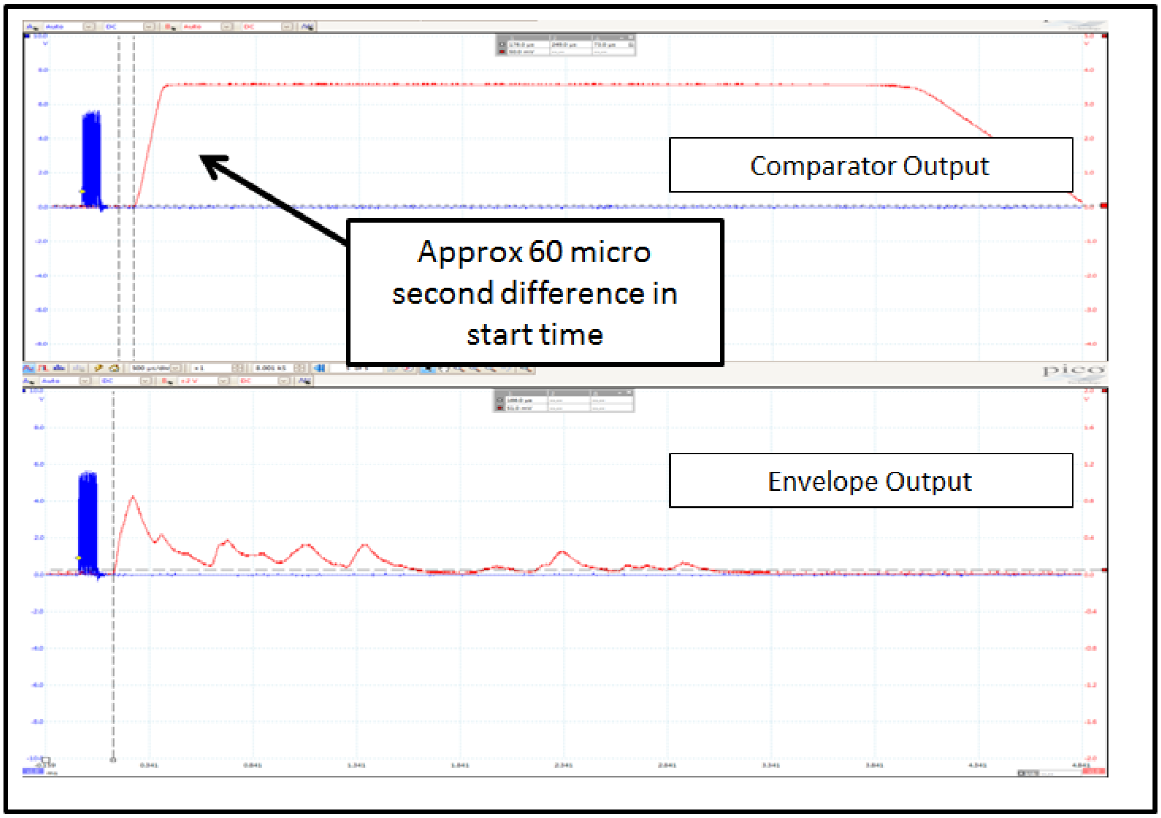

FIGURE 9-11: TIMING COMPARISON BETWEEN COMPARATOR OUTPUT AND ENVELOPE CIRCUIT OUTPUT

9.5. IRIS Mote

The IRIS Wireless Sensor Network Module (IRIS mote), provided by Memsic, Powerful Sensor Solutions, is used to aid in the successful sampling of the entire envelope waveform. It is important to note, that the system can function properly with the use of only the comparator acting as a switch, but the addition of the IRIS mote (pictured in Figure 9-12) provides more reliability in terms of signal capturing. One addition was made to the system in the form of a simple voltage divider circuit, placed in between the comparator output and the interrupt pin on the IRIS mote. This is due to the limitation of the interrupt pin, being restricted to no greater than 3 Volts input. The interrupt pin on the IRIS is rising edge sensitive. When an interrupt is received via the comparator circuit, the GPIO is toggled 29 milliseconds later. This timer triggered GPIO is configured as such to account for the time duration of the entire envelope signal, in addition to 30 millisecond transmission of the next incoming ultrasonic pulse (80 microsecond duration) used to generate the following envelope. The GPIO feeds a signal to a push button interrupt pin that was modified on the microcontroller for any generic interrupt. Once the interrupt is received by the microcontroller, the sampling of the envelope begins. It will be proven later in this chapter that the addition of this mechanism has improved the overall signal capturing capability of the microcontroller.

FIGURE 9-12: PICTURE OF THE IRIS WIRELESS SENSOR NETWORKING PLATFORM

9.6. MSP430

More properly named the MSP-EXP430G2 (pictured in Figure 9-13); the Launchpad provided by Texas Instruments, is a microcontroller platform, flash programmer and debugging tool for the MSP430G2553 microcontroller that is used to perform the sampling of the envelope signal and the sending of the data to a personal computer. This device is equipped with up to 16kB Flash, 512B RAM, 16MHz CPU speed, 10-bit ADC, timers and serial communication functionality. The 10-bit ADC channel can provide sampling rates up to 200 kHz while being sourced by a 1 MHz clock, more than enough to provide the proper envelope resolution needed for high localization accuracy. For the sake of attempting to provide the best tradeoff between sampling rate and localization accuracy, the sampling rate of the MSP430 will be configured to approximately 68 kHz. Even in the presence of the limitation in the size of the ADC conversion buffer (400 bytes), the entire envelope is able to be sampled and stored on the device. Once stored on the device, the data is sent to the PC to obtain the classification results. Sending is done through the use of the UART module, sending at a rate of 9600 baud.

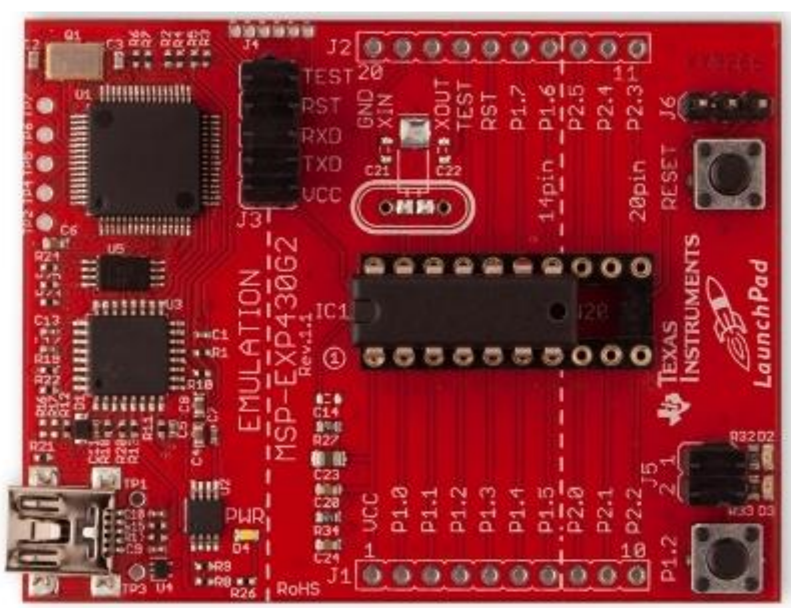

FIGURE 9-13: PICTURE OF THE MSP-EXP430G2

9.7. PC

Once the data is received on the serial port of the PC, a terminal program equipped with a plot function is used to verify the correctness of the data sent, but MATLAB is once again used for the classification. Figure 9-14 illustrates the mini-system implemented in MATLAB that handles the pre-processing of the sampled data leading up to cell classification. MATLAB serial port functions are used to bring in the data from the MSP430. Once acquired, any additional noise that may be present is also removed through the use of a second order Butterworth low pass filter with a cutoff of 45 kHz, implemented in software. The filtered envelope signal is then down sampled to the appropriate length of sample points needed to give the signal equal length to the software produced envelopes previously generated. This length requirement is essential for the computation of the cross correlation coefficient between envelopes. The software produced envelopes will now serve as a basis for comparison between ech of the hardware produced envelopes, in order to run the MACC algorithm for the center-of-cell case. Figure 9-15 shows the comparison between the Picoscope view of the hardware created envelope and the envelope signal after it has been sent and processed in MATLAB. This figure proves that the envelope has indeed been reconstructed and can now be used for cell localization.

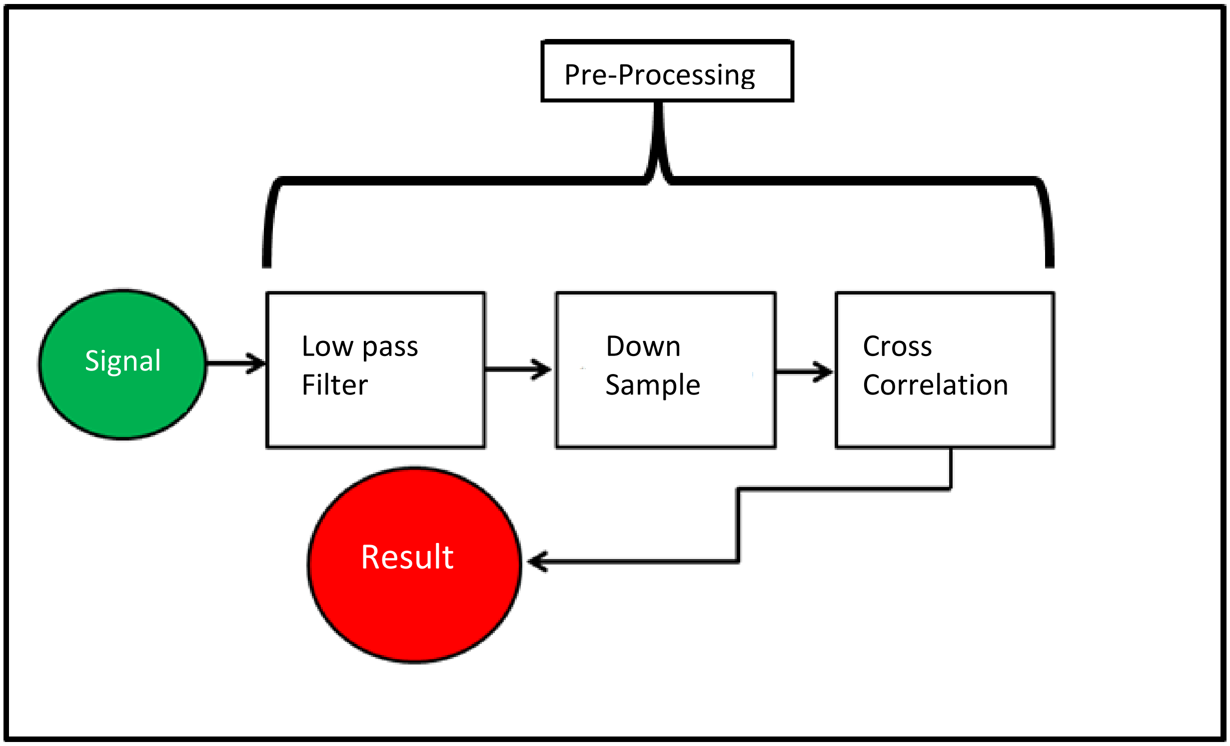

FIGURE 9-14: BLOCK DIAGRAM OF THE MINI-SYSTEM IMPLEMENTED IN MATLAB

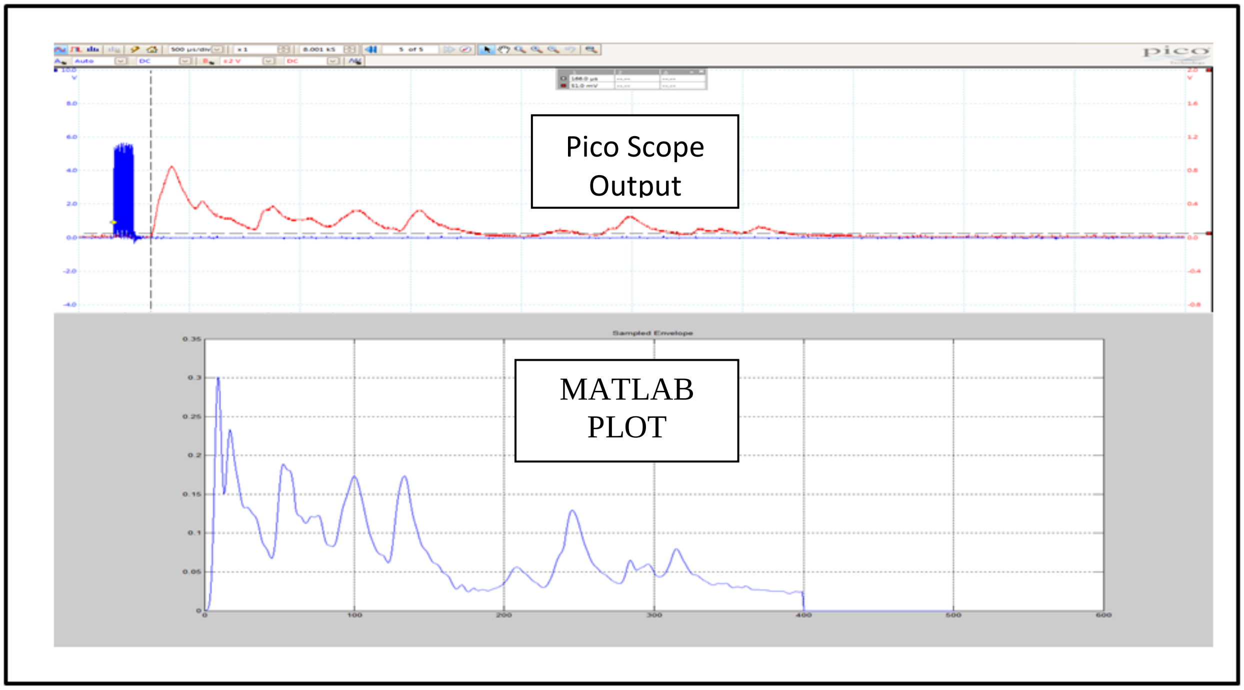

FIGURE 9-15: PERFORMANCE OF ENVELOPE RECONSTRUCTION

9.8. Experimental Localization Performance

Using the set of the envelopes generated in software as a reference, the envelope data retrieved by the PC will be used to run the MACC Algorithm to compute the localization result. Procedures for gathering results are done in a similar manner in which they were presented earlier in this thesis for the center-of-cell case. For each of the twenty coupling trials done for each cell, the triggering of a push button on the MSP430 device initializes the transition from a sleep state to an active state, the MSP430 then receives the necessary interrupts for sampling, and then sends the sampled data for the localization results to be displayed via MATLAB.

9.8.1. Center-of-Cell Performance

The performance for 3-Cell Localization Resolution is obtained for two cases, (1) with the absence of the IRIS mote providing the functionality of time-triggered signal capturing, and (2) with the IRIS mote inserted into the chain of the system. Figure 9-16 depicts the confusion matrix from case (1), while figure 9-17 applies to case (2). Case (1) instead feeds the comparator output directly to the interrupt pin on the MSP430 device, triggering the sampling. Sending is done in the normal fashion. The addition of the IRIS mote resulted in an increase in accuracy from 80% to 98.33%. It is evident that the localization results from case (2) are more comparable with the results achieved from the system implemented in software for the 3CLR case (100% Localization Accuracy).

Cell A	Cell B	Cell C	
19	0	1	Cell A – Accuracy = 95%
0	11	10	Cell B – Accuracy = 55%
0	2	18	Cell C – Accuracy = 90%
Percent Accurate = 80%			

FIGURE 9-16: EXPERIMENTAL LOCALIZATION ACCURACY WITHOUT THE IRIS MOTE

Cell A	Cell B	Cell C	
20	0	0	Cell A – Accuracy = 100%
0	19	1	Cell B – Accuracy = 95%
0	0	20	Cell C – Accuracy = 100%
Percent Accurate = 98.33%			

FIGURE 9-17: EXPERIMENTAL LOCALIZATION ACCURACY WITH THE IRIS MOTE

9.9. Summary

The results presented in this chapter show that the entire chain of the system is fully functional. The hardware components designed are capable of producing an envelope of the raw ultrasound signal that is very comparable from a visual point of view. The sampling and sending mechanisms are also able to reproduce the signal and send the data of the sampled signal to a PC, where additional processing is also done for the purpose of run-time classification. Following the results presented in this chapter, the evaluation of actual run-time localization will take place for center of cell cases. In addition, it can be seen that the findings for the 3CLR case come very close to achieving the performance marks of the localization system implemented via software. This high localization accuracy is even obtainable by using data collected at a much higher resolution as a reference. An intelligent assumption can be made, that if initial stages of data collection are conducted with the run-time system itself that localization error would decrease.

CHAPTER 10: CONCLUSION

10.1. Conclusion

In this thesis, a localization system for the discovery of the cell-based position of a single unknown node using ultrasound communication on a metal substrate (2024 Aluminum Plate) is introduced. The traditional functionality of localization in the context of wireless sensor networking involves using time of arrival (TOA) family based techniques to accurately estimate the position of an unknown network node in a particular environment, with high accuracy and precision. The use of these hardware and software systems opens up the avenue to many real life constraints during its implementation phase. In the work presented in this thesis, the basic properties that govern mechanical carrier waves (lamb waves) are used to aid in the problem of solving localization in an ultrasonic sensor network, without the use of traditional techniques Using the boundary dependent multipath reflections of the lamb waves, the position of a single node is achieved in a cell-based manner on a metal substrate. Using MATLAB, the raw received waveforms of the ultrasound signal are pre-processed to produce an envelope of that signal that which was discovered to be both location and multipath reflection dependent. Through extensive amounts of data collection and signal processing, the study of the waveform produced on the receiving end of ultrasound communication was conducted. As a result, features were determined, extracted and evaluated using pattern classification techniques to provide distinguishability among received envelopes. Utilizing these features, and varying complexity levels of classification algorithms and techniques, center-of-cell and non-center-of-cell localization is performed on the data collected from all possible cells mapped out on the aluminum plate. This set of experiments deemed it possible to achieve localization using a less understood concept in relation to widely known and used time of flight based approaches. As a result, it yielded the implementation of a run-time system capable of achieving similar localization results. The run-time system generates the envelope of the received waveform purely through hardware and utilizes a microcontroller in conjunction with a popular sensor networking platform to intelligently sample the envelope signal at its correct start time. This sampled data is sent to a base station like device where the localization results are computed in run-time, using the same set of features extracted previously. Final results prove that it is possible to achieve high localization accuracy while removing some of the limitations placed upon traditional approaches of localization in WSNs, both in theory and in a practical implementation.

10.2. Future Work

Future work in regards to this topic will include the evaluation of the localization accuracy in run-time of higher cell resolutions, increasing the number of cells while still using the same pool of data collected in initial experiments as a basis for cell localization. In addition to this, the use of the machine learning software Weka will be extended to localize the non-center-of-cell locations in the presence of the run-time localization system. The future results stemming from this extension will also be compared to the results generated in the theoretical system. Lastly, an important area of future work lies in attempting to optimize the operation of the run-time system, in the hopes of achieving high cell based localization accuracy with the most minimal of hardware and software requirements for the different stages of the system.

BIBLIOGRAPHY

BIBLIOGRAPHY

[1] S. Lorenz, B. Dong, Q. Huo, W. J. Tomlinson, and S. Biswas, “Pulse based sensor networking using mechanical waves through metal substrates,” in *Proceedings of the SPIE*, vol. 8753, pp. 8, May 2013.

[2] D. Zhang, F. Xia, Z. Yang, L. Yao, and W. Zhao, "Localization Technologies for Indoor Human Tracking," in *Future Information Technology (FutureTech), 2010 5th International Conference*, vol., no., pp.1-6, May 2010.

[3] S. Guowei, R. Zetik, and R. S. Thoma, "Performance comparison of TOA and TDOA based location estimation algorithms in LOS environment," in *Positioning, Navigation and Communication, 5th Workshop*, *March* 2008.

[4] H.Noh, A. C. Young, and G. Daxia, "Solving the Damage Localization Problem in Structural Health Monitoring Using Techniques in Pattern Classification," 2007.

[5] E. Baravelli, M. Senesi, M. Ruzzene, and L. De Marchi, "Fabrication and Characterization of a Wavenumber-Spiral Frequency-Steerable Acoustic Transducer for Source Localization in Plate Structures," in *Instrumentation and Measurement, IEEE Transactions*, vol. 62, no. 8, pp. 2197-2204, Aug. 2013.

[6] R. Demirli, and J. Saniie, "Asymmetric Gaussian Chirplet model for ultrasonic echo analysis," in *Ultrasonics Symposium (IUS), 2010 IEEE* , vol., no., pp.124,128, 11-14, Oct. 2010.

[7] E. O. Dijk, C. H. Van Berkel, R. M. Aarts, and E. J. Van Loenen, "3-D indoor positioning method using a single compact base station," in *Pervasive Computing and Communications, Proceedings of the Second IEEE Annual Conference*, vol., no., pp.101-110, March 2004.

[8] A.A. Anastassopoulos, V. N. Nikolaidis, and T. P. Philippidis. "A comparative study of pattern recognition algorithms for classification of ultrasonic signals," in *Neural Computing & Applications*, vol. 8.1, pp. 53-66, 1999.

[9] L. Kyungmi, "Feature extraction schemes for ultrasonic signal processing," in *Computer Sciences and Convergence Information Technology (ICCIT), 2010 5th International Conference*, pp.366-372, Nov. 2010.

[10] X. Zhao, et al., "Active health monitoring of an aircraft wing with embedded piezoelectric sensor/actuator network: I. Defect detection, localization and growth monitoring." in *Smart materials and structures*, vol. 16.4, pp. 1208, 2007.

[11] A. Mal, F. Ricci, S. Banerjee, and F. Shih, "A conceptual structural health monitoring system based on vibration and wave propagation," in *Structural Health Monitoring* , 2005.

[12] E. H. Clayton, S. J. Dyke, and C. Lu. "Monitoring Infrastructural Health: In-situ Damage Detection and Localization Utilizing Distributed Smart Sensor Technology." in *4th World Conference on Structural Control and Monitoring*, 2006.

[13] H. Schau, and A. Robinson, "Passive source localization employing intersecting spherical surfaces from time-of-arrival differences," in *Acoustics, Speech and Signal Processing, IEEE Transactions*, vol.35, no.8, pp. 1223-1225, Aug. 1987.

[14] P. S. Tua, S. T. Quek, and Q. Wang, "Detection of cracks in plates using piezo-actuated Lamb waves," in *Smart Materials and Structures*, 2004.

[15] Z. Su, Y. Lin, and L. Ye, "Guided Lamb waves for identification of damage in composite structures: A review," in *Journal of sound and vibration*, 2006.

[16] V. Giurgiutiu, and C. Soutis. "Enhanced composites integrity through structural health monitoring," in *Applied Composite Materials*, pp. 813-829, 2012.

[17] Ultrasonic Testing, "PART 6. Lamb Waves," in *Generation and Detection of Ultrasound*, pp. 103.

[18] L. Bin,V. Giurgiutiu, and M.K. Ayman, "The use of exact Lamb waves modes for modeling the power and energy transduction of structurally bonded piezoelectric wafer active sensors," in *Proceedings of the SPIE, Sensors and Smart Structures Technologies for Civil, Mechanical, and Aerospace* Systems, vol 8345, April 2012.

[19] X. Buli, “Structural health monitoring instrumentation, Signal Processing and interpretation with piezoelectric Wafer Active Sensor”, in *Partial Fulfillment of the Requirements For the Degree of Doctor of Philosophy in Department of Mechanical Engineering College of Engineering & Computing University of South Carolina*, 2009.

[20] B. Ayrulu, and B. Barshan, "Comparative analysis of different approaches to target classification and localization with sonar," in *Multisensor Fusion and Integration for Intelligent Systems International Conference,* vol., no., pp.25-30, 2001.

[21] L. Sangho, K. Eunchan, K. Chungsan, and K. Kiseon, "Localization with a Mobile Beacon based on Geometric Constraints in Wireless Sensor Networks," in *Intelligent Sensors, Sensor Networks and Information, 3rd International Conference*, pp.61-65, Dec. 2007.

[22] N. Patwari, J. N. Ash, S. Kyperountas, A. O. Hero, R.L. Moses, and N.S. Correal, "Locating the nodes: cooperative localization in wireless sensor networks," in *Signal Processing Magazine, IEEE* , vol.22, no.4, pp. 54-69, July 2005.

[23] R. Hajrya, M. Verge, and N. Mechbal, "Active damage detection and localization applied to a composite structure using piezoceramic patches," in *Control and Fault-Tolerant Systems (SysTol), 2010 Conference*, vol., no., pp.849-854, Oct. 2010.

[24] L. Wang, and F. G. Yuan, "Lamb wave propagation in composite laminates using a higher-order plate theory." in *The 14th International Symposium on: Smart Structures and Materials & Nondestructive Evaluation and Health Monitoring*. *International Society for Optics and Photonics*, 2007.

[25] S. S. Kessler, S. M. Spearing, and C. Soutis, "Damage detection in composite materials using Lamb wave methods," in *Smart Materials and* Structure, 2002.

[26] V. Giurgiutiu, and C. Soutis. "Enhanced composites integrity through structural health monitoring." in *Applied Composite Materials*, 2012.

[27] Q. Ling, Z. Tian, Y. Yin, and Y. Li, "Localized Structural Health Monitoring Using Energy-Efficient Wireless Sensor Networks," in *Sensors Journal, IEEE*, vol.9, no.11, pp.1596-1604, Nov. 2009.

[28] Perioperative Ultrasound, “Workshop Notes,” in *AACA Pre-conference Workshop*, Nov. 2006.

[29] M. Bocca, J. Toivola, L.M. Eriksson, J. Hollmén, and H. Koivo, "Structural Health Monitoring in Wireless Sensor Networks by the Embedded Goertzel Algorithm," in *Cyber-Physical Systems (ICCPS), 2011 IEEE/ACM International Conference*, vol., no., pp. 206-214, April 2011.

[30] A. Cuc, et al, "Structural health monitoring with piezoelectric wafer active sensors for space applications," in *AIAA journal*, 2007.

[31] V.Giurgiutiu, and G. Santoni-Bottai. "Structural Health Monitoring of Composite Structures with Piezoelectric-Wafer Active Sensors," in *AIAA journal*, 2011.

[32] M. Hall, E. Frank, G. Holmes, B. Pfahringer, P. Reutemann, and I. H. Witten, “The WEKA Data Mining Software: An Update,” in *SIGKDD Explorations*, vol. 11, 2009.